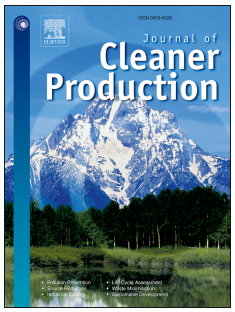

6E analyses of a new solar energy-driven polygeneration system integrating CO_2 capture, organic Rankine cycle, and humidification-dehumidification desalination

N. Khani, M.H. Khoshgoftar Manesh, V.C. Onishi

PII: S0959-6526(22)04050-1

DOI: https://doi.org/10.1016/j.jclepro.2022.134478

Reference: JCLP 134478

To appear in: *Journal of Cleaner Production*

Received Date: 11 June 2022

Revised Date: 21 September 2022

Accepted Date: 30 September 2022

Please cite this article as: Khani N, Khoshgoftar Manesh MH, Onishi VC, 6E analyses of a new solar energy-driven polygeneration system integrating CO_2 capture, organic Rankine cycle, and humidification-dehumidification desalination, *Journal of Cleaner Production* (2022), doi: https://doi.org/10.1016/j.jclepro.2022.134478.

CRediT authorship contribution statement

Nastaran Khani: Investigation, Data curation, Formal analysis, Visualization, Software, Writing – original draft.

Mohammad H. Khoshgoftar Manesh: Conceptualization, Methodology, Supervision, Writing – review & editing.

Viviani C. Onishi: Methodology, Formal analysis, Visualization, Writing – review & editing.

6E analyses of a new solar energy-driven polygeneration system integrating CO_2 capture, Organic Rankine cycle, and humidification-dehumidification desalination

N. Khani [a], M. H. Khoshgoftar Manesh [a], V. C. Onishi [b, *]

[a] *Energy, Environmental and Biological Systems Research Lab (EEBRlab), Division of Thermal Sciences and Energy Systems, Department of Mechanical Engineering, Faculty of Technology & Engineering, University of Qom, Qom, Iran; Mh.Khoshgoftar@gmail.com, M.Khoshgoftar@qom.ac.ir*

[b] *School of Computing, Engineering and the Built Environment, Edinburgh Napier University, Merchiston Campus, 10 Colinton Road, Edinburgh EH10 5DT, UK; V.Onishi@napier.ac.uk*

[*] Corresponding author. Edinburgh Napier University, UK. *Email address:* V.Onishi@napier.ac.uk (V.C. Onishi).

ABSTRACT

Integrated solar-assisted polygeneration systems have emerged as an effective and sustainable alternative for meeting thermal, power and freshwater demands through decentralized generation. In this framework, this study introduces a new design and dynamic simulation approach to a solar energy-driven polygeneration system integrating gas and steam turbine cycles, organic Rankine cycle (ORC), CO_2 capture, and humidification-dehumidification (HDH) desalination. The integrated system is designed to supply a greenhouse's power, freshwater and carbon needs. The proposed system is modelled and dynamically simulated via MATLAB software, and the results are validated by literature data and THERMOFLEX software with high accuracy. A comparative study is conducted to evaluate the feasibility of integrating solar thermal energy, in which process simulations are carried out with and without the solar energy field composed of parabolic trough collectors. Sensitivity analysis is used to determine the optimal operating conditions of the HDH system and the ideal ORC working fluid. Furthermore, comprehensive Energy, Exergy, Exergoeconomic, Exergoenvironmental, Emergoeconomic, and Emergoenvironmental (6E)

analyses are performed for scenarios with and without the solar energy field. The results reveal that solar energy integration boosts ORC's power generation from 37.3% (winter) to 59.41% (summer), while the overall power production increases 18 kW compared to the base case scenario. Finally, the system revenues and the payback period are estimated at 50k US$/year and 4.67 years, respectively.

Keywords: 6E analysis; Polygeneration; Solar thermal energy; Dynamic analysis; CO_2 capture; Desalination.

Nomenclature

Roman letters

A	Specific area (m^2/m^3)
A	Area (m^2)
B	Environmental impact per exergy unit (mPts/kJ)
$\dot{\boldsymbol{B}}$	Environmental impact rate (mPts/s)
$\boldsymbol{b_m}$	Environmental impact per mass unit
C	Cost per exergy unit (US$/kJ)
$\dot{\boldsymbol{C}}$	Cost rate (US$/s)
$\boldsymbol{C_p}$	Specific heat at constant pressure (kJ/kg K)
EL	Electricity consumption of CO_2 capture (kJ)
$\dot{\boldsymbol{E}}\boldsymbol{x}$	Exergy rate (kJ/s)
f	Exergoeconomic factor
$\boldsymbol{f_b}$	Exergoenvironmental factor
$\boldsymbol{f_m}$	Emergy-based exergoeconomic factor
$\boldsymbol{f_n}$	Emergy-based exergoenvironmental factor
G	Mass flowrate of air per area in HDH ($kg/s.m^2$)
H	Specific enthalpy (kJ/kg)
$\boldsymbol{h_g}$	Convective heat transfer coefficient (W/m^2 °C)
$\boldsymbol{k_g}$	Mass transfer coefficient of air/water mixture (kg/m^2 s)
L	Mass flowrate of water per area in HDH ($kg/s.m^2$)
M	Specific economic emergy (sej/J)
$\dot{\boldsymbol{m}}$	Mass flowrate (kg/s)
$\dot{\boldsymbol{M}}$	Economic emergy rate (sej/s or sej/h)
N	Specific environmental emergy (sej/J)
$\dot{\boldsymbol{N}}$	Environmental emergy rate (sej/s or sej/h)
$\boldsymbol{n_{mirror}}$	Number of mirrors
P	Pressure (kPa)
R	Relative cost difference
$\boldsymbol{r_m}$	Relative economic emergy difference
$\boldsymbol{r_n}$	Relative difference of environmental emergy
$\boldsymbol{r_p}$	Pressure ratio
sej	Scale factor coefficient
T	Temperature (K)
TIP	Turbine inlet pressure (K)
TIT	Turbine inlet temperature (K)

Acronyms

AC	Air compressor
ARC	Absorption refrigeration cycle
CCS	Carbon capture and storage
CC	Combustion chamber
Cond	Condenser
DHW	Domestic hot water
DNI	Direct normal irradiance
GT	Gas turbine
HDH	Humidification-dehumidification
HPP	High-pressure pump
HRSG	Heat recovery steam generator
HTF	Heat transfer fluid
HX	Heat exchanger
ECO	Economizer
EVA	Evaporator
GWP	Global warming potential
LCA	Life cycle assessment
MED	Multi-effect distillation
MOGA	Multi-objective genetic algorithm
MOWCA	Multi-objective water cycle algorithm
MSF	Multi-stage flash
NGCC	Natural gas combined cycle
ORCP	Organic Rankine cycle pump
ORCT	Organic Rankine cycle turbine
PEC	Purchased equipment cost
PCC	Post-combustion carbon capture
PRO	Pressure retarded osmosis
RO	Reverse osmosis
S-CO_2	Supercritical carbon dioxide
SF	Solar fraction
SFHX	Solar field heat exchanger
SFP	Solar field pump
SPECO	Specific exergy costing
ST	Steam turbine

$\dot{\boldsymbol{U}}$	Component-related economic emergy rate (sej/s or sej/h)	SUP	Superheater
$\dot{\boldsymbol{V}}$	Component-related environmental emergy rate (sej/s or sej/h)		
W	Work (kJ)	*Subscripts*	
x	Mole fraction	*0*	Ambient conditions
X	Packing length (m)	*c*	Collector
Y	Environmental impact of components (mPts)	*d*	Dehumidifier
y	Packing width (m)	*D*	Destruction
$\dot{\boldsymbol{Y}}$	Environmental impact rate of equipment (mPts/s)	*F*	Fuel
$\dot{\boldsymbol{Z}}$	Cost rate of equipment (US$/s)	*fg*	Flue gas
		g	Gas-phase (air/water mixture)
Greek letters		*h*	Humidifier
β	Scale factor coefficient	*i*	Interface
γ	Ratio of the specific heats	*k*	Counter of components
$\boldsymbol{\lambda_0}$	Latent heat of vaporization	*P*	Product
Δ	Difference	*q*	Heat
ε	Exergy efficiency	*th*	Therminol
η	Efficiency	*s*	Steam
ν	Specific volume	*sub*	Subcritical
ω	Humidity ratio	*u*	Useful
		w	Work
		wb	Water bulb

1. Introduction

The development of advanced polygeneration plants has been fueled in recent decades by the need to address ever-increasing energy demands, water scarcity, and the environmental impacts related to greenhouse gas emissions. In this way, renewable energy-driven polygeneration systems integrating desalination and other subsystems have attracted increasing attention as an effective and sustainable alternative for meeting several thermal, power, and freshwater demands through decentralized energy generation. Nevertheless, the holistic design of integrated polygeneration systems is a demanding endeavor that requires thorough thermodynamic analyses and cutting-edge computational tools to enhance overall system energy, economic and environmental performances (Manesh and Amidpour, 2020; Khoshgoftar Manesh and Onishi, 2021).

Thermal and membrane desalination technologies have been considered in decentralized polygeneration systems to tackle rising water shortages worldwide. However, among the most

promising alternatives, humidification-dehumidification (HDH) desalination technology is usually adopted in household-scale plants due to its lower running costs at low capacities, effectiveness in moderate operating conditions, and lower sensitivity to the quality of inlet saline water in comparison with membrane-based processes (Ayati et al., 2019). In this context, Ghiasirad et al. (2021) have evaluated the integration of heating, cooling, and power systems with an HDH desalination unit and an absorption heat transformer powered by a 100% geothermal resource. Their results indicate energy and exergy efficiencies of 60.55% and 17.05%, respectively, for summer, and for winter, 70.58% and 43.59%, respectively.

The design and implementation of more cost-efficient and environmental-friendly solar-assisted HDH desalination systems have gained significant traction over the last few years. Zamen et al. (2013) have performed the design and transient analysis of a solar energy-driven HDH desalination system for a greenhouse. The authors proposed using direct contact dehumidification instead of indirect condensers, together with a solar water heater to boost the freshwater production rate. They reported freshwater production rates ranging from 6 and 22 m^3/day/ha. Deniz and Çınar (2016) have conducted energy, exergy, economic, and environmental analyses of a solar-assisted HDH desalination system using data acquired from the experimental results. Their results show peak values for daily energy efficiency and exergy efficiency of 31.54% and 1.87%, respectively. They have also determined a maximum freshwater production rate of 1117.3 g/h. The cost of produced freshwater was estimated at 0.0981 US$/L and the enviro-economic factor at 2.4041 US$/year. Zubair et al. (2017) have assessed the energy and economic performance of a HDH desalination system integrated with solar evacuated tubes. The authors determined the rate of freshwater production and cost per liter for the HDH system operation in different geographical locations. Their results indicate that the productivity of freshwater ranged from 16,430 to 19,445

L, and cost analysis suggested that the price can reach 0.032 to 0.038 US$ per liter depending on the location.

Applying simultaneous energy, exergy, exergoeconomic, and exergoenvironmental analysis can provide a better understanding of the system irreversibilities, energy and exergy efficiencies, costs and environmental impacts. Anvari et al. (2020) have employed energy, exergy, exergoeconomic, and exergoeconomic (4E) analyses to evaluate a polygeneration system to yield power, heating, cooling, and desalinated water. As a result, the cycle's total cost and total CO_2 emissions were estimated at 1943.5 US$/h and 0.163 kg/kWh, respectively. Moreover, enhancement of the pre-heater outlet temperature led to a 26% reduction in CO_2 emissions. Ehyaei et al. (2021) have conducted energy, exergy, economic, exergoenvironmental, and environmental analysis (5E) analyses on a polygeneration system composed of geothermal energy, RO, and electrolysis. The proposed system yielded 1.751 GJ/year of electricity, 1.04 GJ/year of cooling, 18,106.8 m^3/year of potable water, 7.396 ton/year of hydrogen, and 3.838 ton/year of sodium-hypochlorite. In addition, the results show that energy and exergy efficiencies are 12.25% and 19.6%, respectively. Khoshgoftar Manesh and Onishi (2021) have reviewed energy, exergy, and exergoeconomic analyses of renewable energy-based polygeneration systems for sustainable desalination, including systems operated via solar, biomass, geothermal, ocean, wind, and hybrid renewable sources.

Given the high temperature it can provide, solar energy is one of the most practical solutions to decrease the usage of fossil fuels and deal with related greenhouse gas pollution. Therefore, several authors have attempted integrating different concentrated solar thermal power technologies with combined power cycles and polygeneration plants. El-Emam and Dincer (2018) have assessed the energy and exergy efficiencies of a solar heliostat-based polygeneration system

comprising a steam turbine, seawater RO desalination unit, and absorption cooling system. The proposed polygeneration system provided cooling, heating, freshwater, and hydrogen through electrolysis. Ghorbani et al. (2020b) have considered a polygeneration system integrated with a solar parabolic dish collector to deliver 4.36 MW power, 1.65 MW cooling, and 2026 kg/h hydrogen. Furthermore, the authors have performed energy and exergy analyses and reported system energy and exergy efficiencies of 90.77% and 92.19%, respectively. Nouri et al. (2020) have evaluated a hybrid cogeneration system's exergy and economic performances to produce 300 kg/s liquid hydrogen and 10.04 kg/s liquid CO_2 by utilizing solar energy as a renewable source. The total reported exergy efficiency and specific energy consumption of the hydrogen liquefaction system are 94.87% and 3.368 kWh/kg, respectively.

Mouaky and Rachek (2020) have performed thermodynamic and thermo-economic analyses on a trigeneration system used to produce electricity, freshwater, and domestic hot water (DHW). The proposed solar-biomass trigeneration system is located in a semi-arid region of Benguerir, Morocco. Their results exhibit monthly overall energy efficiencies varying between 11.35% and 16.32%, while exergy efficiency ranged from 5.33 to 5.96%. They also found that the proposed trigeneration system can reach production costs of 0.231 €/kWh electricity, 0.86 €/m^3 freshwater, and 0.047 €/kWh DHW. Ghorbani et al. (2020a) have conducted energy, exergy, and economic (3E) analyses of a solar energy-driven polygeneration system for power and liquid fuels production by employing liquefied natural gas regasification and solar collectors. According to their results, the total energy and exergy efficiencies of the plant are 42.36% and 64.72%, respectively. The capital cost per unit of liquid fuel produced and payback period were estimated at 443.9 US$/$m^3$ and 2.186 years, respectively.

Méndez and Bicer (2021) have proposed an integrated solar-assisted polygeneration system to generate electricity and freshwater using solar chimneys and wind energy. The authors have applied pressure retarded osmosis (PRO) technology using the brine discharged from the reverse osmosis (RO) and multi-stage flash (MSF) desalination units. As a result, they obtained a moderate increase in the overall system energy efficiency (0.44%) compared to a single solar chimney. Tukenmez et al. (2021) have investigated a hybrid solar and biomass-driven polygeneration system to produce hydrogen and ammonia. The authors have conducted energy and exergy analyses, and their results showed plant energy and exergy efficiencies of 58.76% and 55.64%, respectively. Moreover, the authors reported a total electrical energy output of 20,125 kW, with hydrogen and ammonia generation rates of 0.0855 kg/s and 0.3336 kg/s, respectively. Modabber and Khoshgoftar Manesh (2021) have studied the optimal design of a solar-assisted polygeneration system based on exergy, exergoeconomic, and exergoenvironmental analyses. Their optimization approach is grounded on a multi-objective genetic algorithm (MOGA) and a multi-objective water cycle algorithm (MOWCA). The authors reported that adding solar thermal collectors to the polygeneration system increases energy efficiency by 4.77%. Moreover, the optimization results show an exergy efficiency increase of 12.66%, while the system's total cost and environmental impact rate are decreased by 47.4 US$/h and 49.2 pts/h, respectively.

Accounting for about 80% of the enhanced global warming effect, CO_2 is thought to be the main contributor to greenhouse gases. Electric-power generation remains the single largest source of CO_2 emissions, equal to the rest of the industrial sectors combined (Petrakopoulou, 2011). Carbon capture, primarily through absorption, has received considerable attention in recent efforts to limit dangerous and increasing emission trends. Along these lines, integrating CO_2 capture technologies and concentrating solar collectors appears to be a viable solution to further reduce

environmental impacts. In this regard, different investigations have been performed in the literature to analyze and design combined power cycles and polygeneration systems coupled to CO_2 capture. Botero et al. (2009) economically evaluated a 400-MW natural gas combined cycle integrated with the post-combustion CO_2 capture unit. The authors reported that using a post-combustion CO_2 capture unit increases capital costs by 43% compared to a plant without a post-combustion system. Petrakopoulou et al. (2012a) have assessed a combined cycle integrated with post-combustion CO_2 capture from exergy, economic and environmental points of view. Their results reveal that the implementation of the CO_2 capture unit increases the overall cost difference, while the relative total environmental impact has a relatively low increase. Olaleye and Wang (2017) have studied the conventional and advanced exergy analyses of a post-combustion CO_2 capture based on chemical adsorbents integrated with a coal-fired power plant. Their results showed that by reducing the energy required for absorption by 1%, the cost is reduced from 0.7 to 1%.

Integration of ORC as a bottoming cycle has also been proposed in the literature to recover the waste heat of power plants. Cao et al. (2016) have investigated the gas turbine and ORC (GT-ORC) integration with two recuperators. Based on the optimum design and thermodynamic assessment, the ORC's net power and thermal efficiency increased with the ORC turbine inlet pressure. Moreover, their research showed that Toluene is the most suitable working fluid for the GT-ORC combined cycle. Sun et al. (2017) have analyzed an ORC system based on industrial low-temperature waste heat as the energy source by using organic fluids to achieve low temperatures. The authors have evaluated the effects of evaporation and condensation temperatures and the degree of superheat on the thermodynamic system performance. Their results show that increasing the ORC's evaporation temperature reduces system exergy efficiency.

Nami et al. (2018) have conducted energy and exergy analyses of an ORC driven by GT exhaust heat recovery. The authors have compared four working fluids and identified MM and R124 as the best working fluids. Patiño and Rivera (2019) have studied the implementation of the ORC coupled to a natural gas combined cycle (NGCC) and post-combustion CO_2 capture to increase the power output. They found that the reduction of CO_2 emissions led to a 78% reduction in global warming potential. Liu et al. (2020) have carried out 4E analyses of carbon capture and storage (CCS), ORC, and an absorption refrigeration cycle in an integrated system using waste heat as the heat source. Their results indicate an exergy efficiency of 42.88%, while the total annual cost of the combination process is 72% lesser than that of the base CCS system. Khoshgoftar Manesh et al. (2021a) have investigated a polygeneration system composed of a GT, supercritical carbon dioxide (S-CO2) cycle, ORC, and RO desalination. The authors have evaluated the system from exergy, exergoeconomic, and exergoenvironmental perspectives. Their results show an increase of 10.9% in total efficiency by integrating the S-CO_2 and GT cycles.

The pertaining literature shows a lack of research on the energy, exergy, exergoeconomic, exergoenvironmental, emergoeconomic, and exergoenvironmental (6E) analyses of integrated solar energy-driven polygeneration systems. This study addresses shortcomings in preceding research by introducing a new design and dynamic simulation approach to a solar-assisted polygeneration system for meeting 720 kW of power, freshwater and carbon demands of a greenhouse. To the best of knowledge, this is the first study proposing a solar energy-driven polygeneration system to simultaneously produce power, freshwater, and CO_2 for increasing energy efficiency and productivity in greenhouse applications. The innovative polygeneration system integrates gas turbine (GT) and steam turbine (ST) power cycles, organic Rankine cycles (ORCs), a heat recovery steam generator (HRSG), and humidification-dehumidification (HDH)

desalination and post-combustion CO_2 capture units. Furthermore, the proposed integrated system takes advantage of the flue gas from the GT pack to drive the ORC for further enhancing process energy efficiency. The proposed integrated system is mathematically modelled and dynamically simulated via MATLAB, and the results are validated by literature data and via THERMOFLEX software. The feasibility of integrating solar energy to the polygeneration system is evaluated via comparative process simulations with and without a solar energy field composed of parabolic trough collectors. Sensitivity analysis is applied to identify the optimal operating conditions of the HDH desalination system and the ideal ORC working fluid. Finally, comprehensive 6E analyses are performed for scenarios with and without the solar field to further investigate the advantages of integrating solar energy resources.

2. System Description

The layout of the proposed integrated polygeneration system for power, CO_2, and freshwater production in a greenhouse is depicted in **Fig. 1**. For enhancing power generation and overall system performance, two steam turbines (STs) cycles and two organic Rankine cycles (ORCs) are placed downstream of the gas turbine (GT)-pack. This configuration allows to recovery waste heat from the flue gases exhausted from the gas turbine cycle. In addition, the devised polygeneration system comprises a post-combustion CO_2 capture unit, a heat recovery steam generator (HRSG), and a humidification-dehumidification (HDH) desalination unit. The system configuration without the solar energy field, as presented in **Fig. 1**, is used as the base case scenario.

The schematic diagram of the integrated solar energy-driven polygeneration system is displayed in **Fig. 2**. In this configuration, ET-100 solar parabolic-trough collectors are used in the solar energy field. The main technical specifications of the deployed solar energy collectors are

shown in **Table 1**. The polygeneration system integrated with the solar energy field, as depicted in **Fig. 2**, is considered the second comparative case study for the dynamic simulations and 6E analyses to evaluate the benefits of using solar energy.

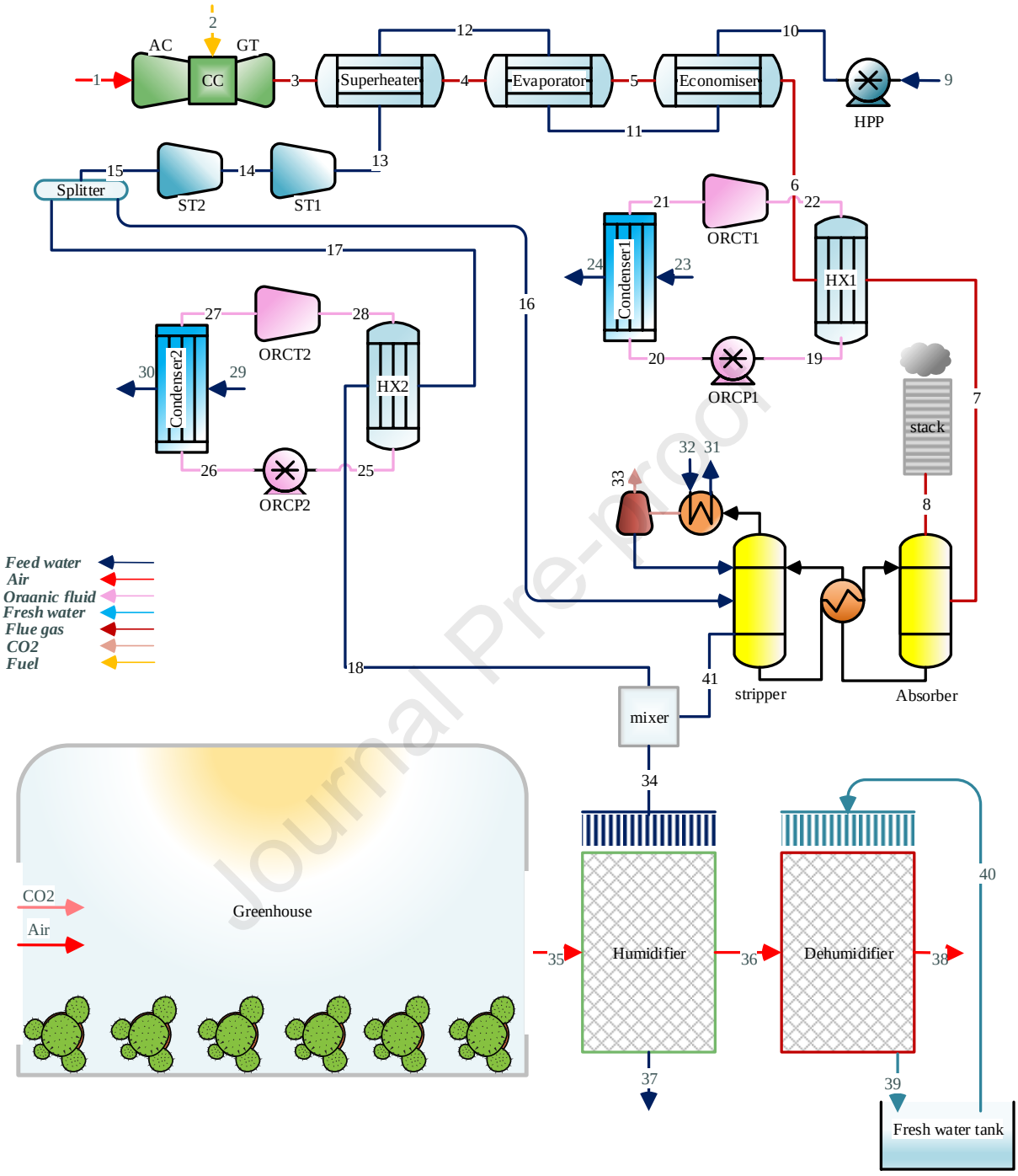

Fig. 1. Polygeneration system configuration without the solar energy field (base case scenario).

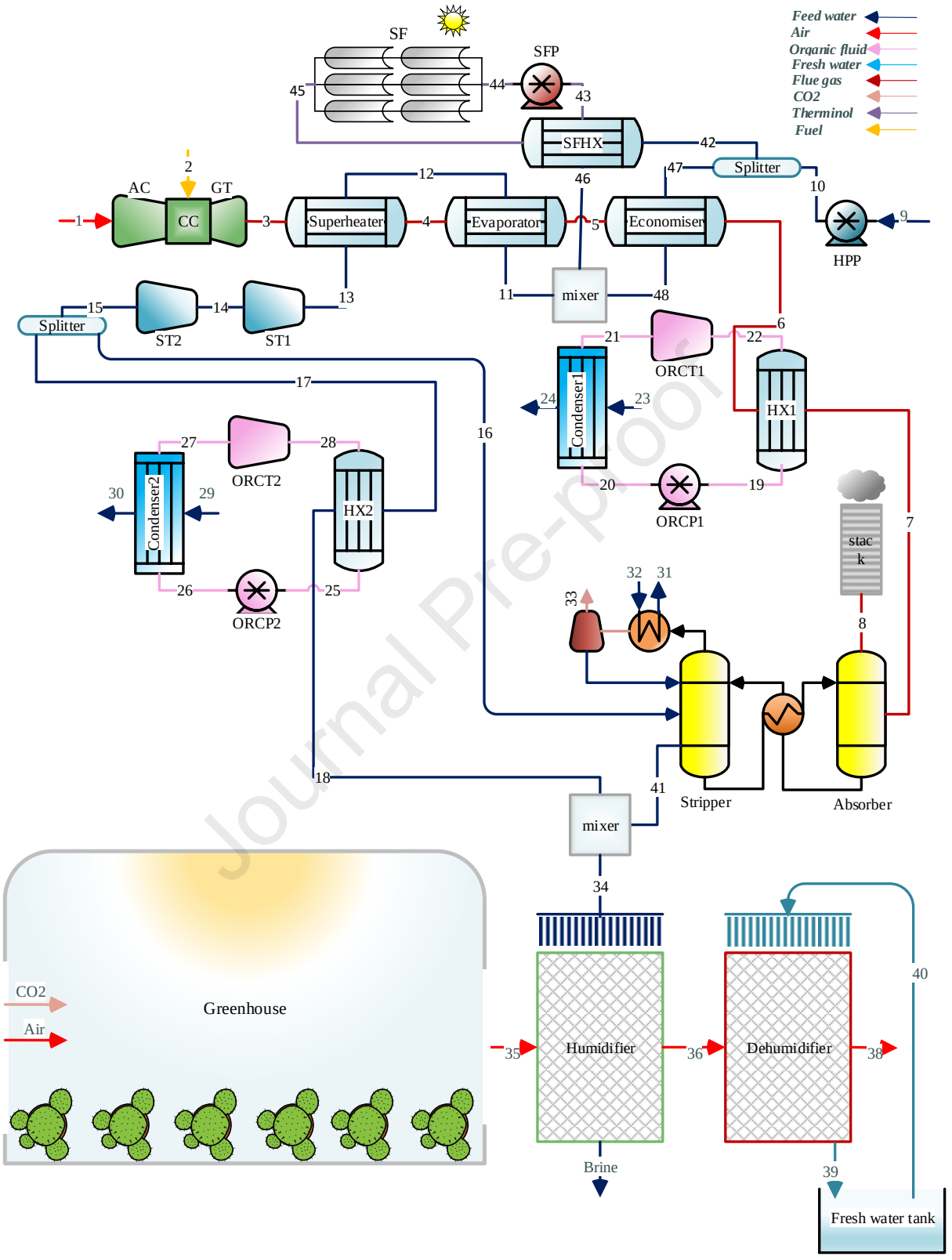

Fig. 2. Polygeneration system configuration integrated with the solar energy field (scenario 2).

Table 1

Main technical specifications of the ET-100 parabolic-trough solar collectors (Lüpfert et al., 2003).

Parameter	Value [Unit]
Focal Length	1.71 [m]
Absorber Radius	35 [mm]
Aperture Width	5.76 [m]
Aperture Area	552 [m²]
Collector Length	99.5 [m]
Collector Modules Length	12 [m]
Parabolic Mirror Panels per Modules (horizontal×vertical)	28 (7 × 4) [-]
Number of Modules per Drive	8 [-]
Number of Glass Facets	224 [-]
Number of Absorber Tubes	24 [-]
Mirror Reflectivity	94 % [-]
Weight of Steel Structure and Pylons, per m^2 aperture	19 [kg]

A brief description of each system subset is given as follows. In this study, the P+W ST6L-721 GT-pack is used for generating power in the proposed polygeneration system. In the GT cycle, compressed air from the air compressor (AC) is mixed with natural gas (fuel) in the combustion chamber (CC). Subsequently, the high-temperature composition of gases is expanded in the GT-pack for power generation. For improving heat recovery, the high temperature flue gases from the GT cycle are utilized as a heat source of the ORC to boost the power generation after passing through the HRSG unit. The latter comprises a superheater, evaporator and economizer units. The outlet flue gas and steam from the two ORC heat exchangers (ORCHXs) are used to supply the required thermal energy of the HDH desalination and CO_2 capture units and address the freshwater and CO_2 greenhouse demands.

The ORCs are composed of a heat exchanger, turbine, condenser, and pump. In the ORC, the working fluid passes through the pump to increase its pressure after being discharged from the condenser. The ORC working fluid then enters the heat exchanger, where it is heated until

changing to a superheated vapor state. Afterwards, it is expanded in the turbine to reach the condenser pressure and restart the cycle. This study compares six different organic working fluids based on their performance to facilitate the selection of the best alternative for the proposed system.

The HDH desalination system consists of open-air, open water, direct contact humidifier and dehumidifier units with packing bed structure to increase the contact surface area between water and air. The distinction between the humidification and dehumidification devices relies in the direction of heat and mass transfer processes. Air from the greenhouse is supplied to the humidifier, while the condensed steam is sprayed onto its structural packing after supplying the heat required for the ORC. As a result, heat and mass transfer occur from water to air direction, increasing the air stream's temperature and humidity. In the dehumidifier, heat and mass transfer are enabled between the heated humid air from the humidifier and the cold water stream, which is sprayed onto the dehumidifier packing bed. Hence, the moist air stream is cooled and condensed, while the water stream is heated due to the difference in the air/water interface humidity ratio. Finally, freshwater is produced and stored in a freshwater tank.

In generating power or heat, CO_2 and other polluting gases are constantly released, which can give rise to the greenhouse effect with adverse effects on the environment. Therefore, deriving electricity, heat, and CO_2 from natural gas by purifying the flue gases will reduce pollution and protect the environment. In this study, a post-combustion CO_2 capture unit is coupled to the system to recover carbon emissions for further reducing environmental impacts. The CO_2 captured and stored is used to maintain the required greenhouse carbon levels and improve the plant productivity. In greenhouse applications, CO_2 supplementation up to 1,000 ppm can increase photosynthesis and plant growth up to 61% (Bao et al., 2018). Additionally, increasing CO_2 concentration reduces transpiration which diminishes water consumption of the crops. **Table 2**

shows the optimal water and CO_2 consumption for three different plant varieties. The flue gas is a combination of NO_x, SO_x, water, and CO_2. Post-combustion amine solvents as considered in this study can capture carbon with up to 90% efficiency (Krishnamurthy et al., 2021).

Table 2

Optimal water and CO_2 consumption of three different plant varieties.

Plant Variety	Water Consumption [Litre/kg]	CO_2 Consumption [ppm]	Reference
Tomato	184	1400	(Li et al., 2017; Lüpfert et al., 2003)
Carrot	131	650	(Wurr et al., 1998)
Strawberry	347	800	(Esmeijer, 1999; Miyoshi et al., 2017)

The following assumptions are required to properly simulate the polygeneration system:

i. Steady-state and steady flow conditions are maintained in equipment units.
ii. The fuel utilized for combustion in the CC consists of pure methane.
iii. The changes in potential and kinetic energy and exergy are negligible.
iv. The ambient temperature and pressure are 25°C and 1.013 bar, respectively, at the compressor inlet.
v. The outlet temperature of the superheater (SUP) is 516°C.
vi. Air and combustion products are operated based on the ideal gas behavior.
vii. The changes in humidity and temperature of air and vapor mix (T_g, ω) occur horizontally.
viii. Water temperature and flowrate (T_L, L) are only changed vertically.
ix. The height of packing in the humidifier and the dehumidifier units is equal.

x. During daylight hours, the temperature (25°C) and humidity ratio (50%) inside the greenhouse will remain virtually stable.

xi. A standard greenhouse with dimensions of 25 m length, 10 m width, and a maximum height of 5 m is assumed.

xii. Structural packing of HDH is made from polypropylene, and specific surface area (a) is 320 m^2/m^3.

xiii. Euro trough ET-100 solar collectors are used in the solar energy field.

xiv. Therminol-VP1 is assumed as the heat transfer fluid (HTF) in the solar energy field.

xv. The percentage of water mass flow which passes through the solar field heat exchanger, known as solar fraction (SF), is equal to 0.8.

xvi. TRNSYS software is used to determine the average Direct Normal Irradiance (DNI) of each month for the specific location (Qom city, Iran).

3. Methodology

3.1. Thermodynamic Analysis

Mass conservation and the first law of thermodynamics, known as thermodynamic analysis, are employed to determine process operating conditions and energy performance at each point of the devised system. The governing thermodynamic equations, input parameters and unknown variables for the different system components are presented in **Table A.1**. The proposed polygeneration systems with/without solar energy integration, i.e., base case scenario and scenario 2, are modelled in MATLAB software. In this approach, the electrical power consumption of the compressor and heat transfer of the CO_2 capture unit are expressed as a function of the energy efficiency, as shown in **Table A.1**. The relations are derived by combining neural network (NN)

and genetic programming (GP) approach in MATLAB software. The resulting dynamic simulation results of thermodynamic properties of the different process streams are validated via THERMOFLEX software and compared to literature data. To model the unit simulation data, 1400 runs are used in the THERMOFLEX software.

The humidification and dehumidification desalination processes are simulated using the modelling equations presented in **Table A.1**. The finite difference method is applied to convert the partial differential governing equations into a system of linear equations. As shown in **Fig. 3**, the humidifier and dehumidifier packing beds are partitioned into small square elements, in which the mesh size can be changed to increase or decrease the accuracy of the results. Heat and mass balance relations are solved for each mesh element. The properties of the inlet air ($\omega_{in,h}$, $T_{g,h,in}$, G) and hot water ($L_{h,in}$, $T_{L,h,in}$) are known for the element number 1 in the humidifier. Therefore, heat and mass balance equations can be solved for this element and the corresponding outputs are taken as input parameters for mesh element 2. In this method, equations are solved for all mesh elements by considering the outlet conditions for air (ω_h, $T_{g,h}$) and water (L_h, $T_{L,h}$) streams from a mesh element n as the input data for solving equations of element number n+1. Similarly, mass and heat balances can be solved for each mesh element in the dehumidifier. In this case, the properties in the element 1 are determined by knowing the inlet conditions of moist air stream from the humidifier and the inlet freshwater properties ($T_{L,d}$, L_d).

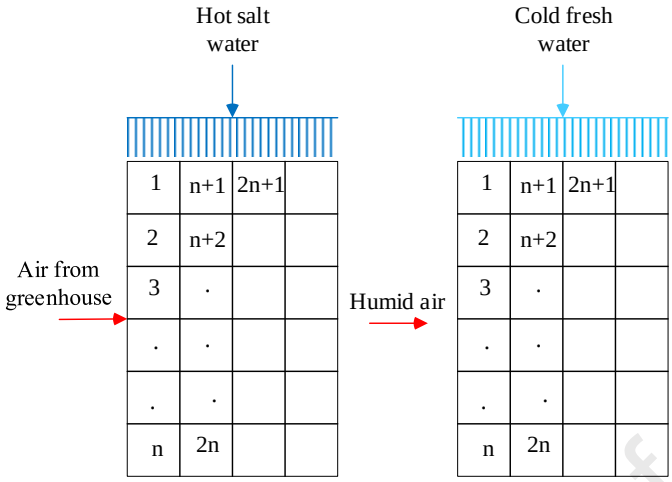

Fig. 3. Square mesh of packing bed for modelling the humidifier and dehumidifier in the desalination unit.

Since the available solar irradiation changes throughout the year, a dynamic approach is considered to accurately model the solar energy field and coupled equipment units. It should be noted that the inlet mass flowrate of the feed water streams passing through the solar thermal collectors and economizer varies as a function of the average solar irradiation per month. Hence, the simulation approach is modified by employing a loop in MATLAB code accounting for the average solar irradiation variation in each month of the year. The DNI of each month is extracted with the help of TRNSYS software. In this way, when solar irradiation is available, the percentage of feed water mass flowrate that splits and enters the solar collectors and economizer can be determined based on the SF calculation in the dynamic loop. Otherwise, steam should be produced via the economizer when solar irradiation is unavailable. **Fig. 4** depicts the programming flowchart for the dynamic simulation approach used to determine thermodynamic properties and monthly SF and model the solar energy field.

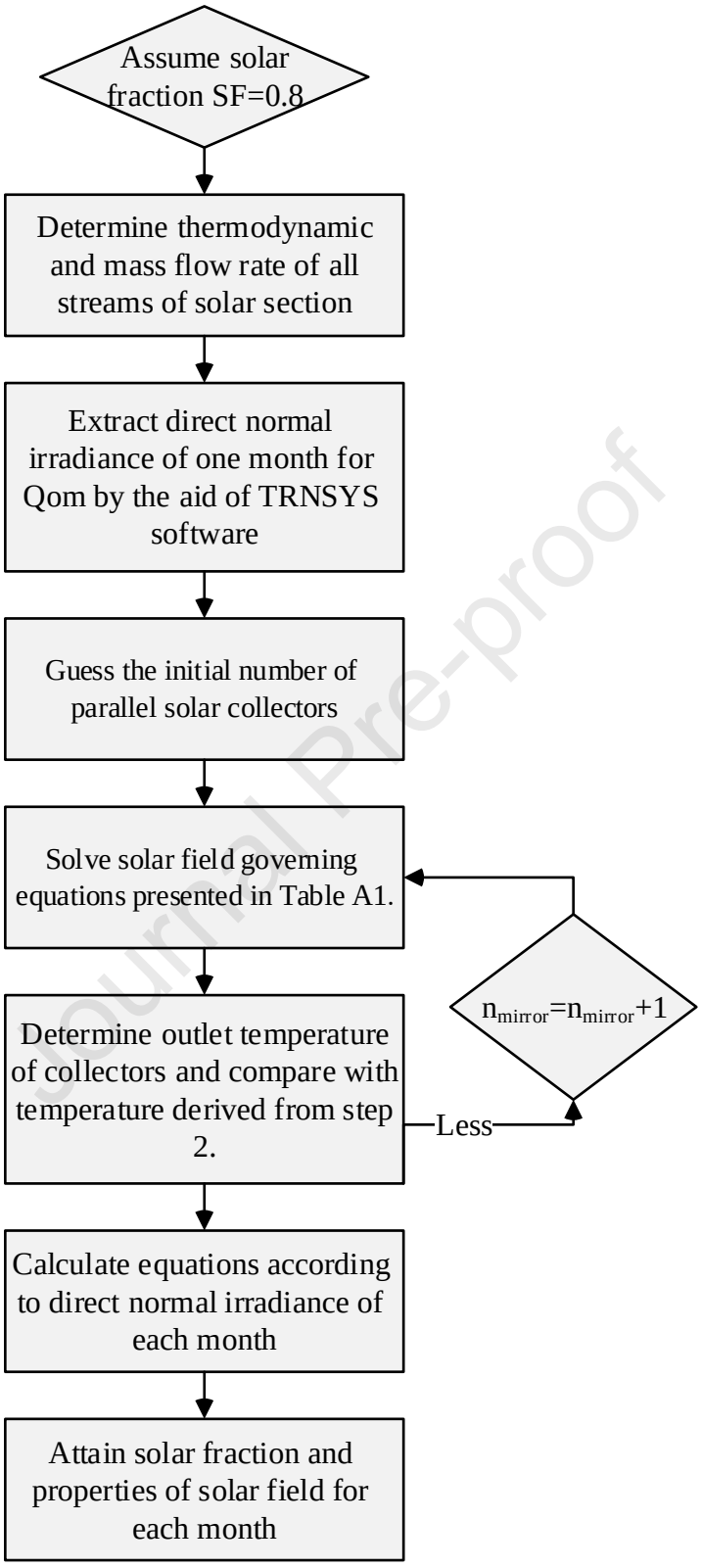

Fig. 4. Programming flowchart for the dynamic simulation of the solar energy field.

Integrating the solar energy field into the polygeneration system increases the flue gas temperature passing through the ORCHX. As a result, the organic fluid mass flowrate increases along with the ORC turbine power generation. The cost of adapting the solar energy field to the plant is determined by calculating the total solar collector area. The energy (in kWh) generated by solar energy field per month can be obtained by the difference in energy generation between the two modes with/without solar collectors and by multiplying it by the average hours of the day, number of days, and the power generated per month of the year. The retail electricity price per plant operating year is calculated by adding up the total power generated per month and multiplying it by operational years and the retail price for electricity per kWh. Finally, the difference between retail electricity price and the cost of collectors allows for estimating the system profit.

Sensitivity analysis is used to determine the optimal operating conditions of the HDH system and the ideal ORC working fluid. Thus, to estimate the impact of the input variables of the HDH unit, a for loop in MATLAB software is utilized, and results are extracted as input variables versus freshwater production rate plots. The latter allows determining the optimal values for the input variables that maximize the freshwater generation. Moreover, different ORC working fluids are considered, and their performance is compared based on the heat source temperature of the ORC heat exchanger.

3.2. Exergy Analysis

Exergy analysis, defined as the maximum possible reversible work, is based on the first and second laws of thermodynamics. Energy analysis alone is insufficient to evaluate the system efficiency since it does not provide an in-depth understanding of integrated power cycles. Therefore, exergy

assessment is employed to accompany energy analysis in this study and provide further insights regarding system energy losses, inefficiencies, irreversibilities, and incurred costs. Exergy transfer to/from an open system at steady-flow conditions must account for mass, work, and heat transfer components as expressed by **Equation (1)** (Nourpour and Khoshgoftar Manesh, 2021).

$$\sum_i^N \left(1 - \frac{T_0}{T}\right) \dot{Q}_k + \sum_i^N \dot{E}_{i.k} = \dot{E}_{w.k} + \sum_e^N \dot{E}_{e.k} + \dot{E}_{D.k} \quad (1)$$

By neglecting kinetic and potential energy changes and assuming steady-state conditions, the physical specific exergy is conducted using the following relation (Bejan et al., 1995; Manesh and Amidpour, 2020).

$$e = (h - h_0) - T_0(s - s_0) \quad (2)$$

The definition of solar exergy differs from previous equation and is given by **Equation (3)** (Dincer and Rosen, 2012).

$$\dot{E}_{solar} = \dot{Q}_{solar}\left(1 - \frac{4}{3}\frac{T_a}{T_{sun}}(1 - 0.28\ln f_{dil})\right) \quad (3)$$

Where f_{dill} indicates the dilution factor (assumed as 1.3×10^{-5}).

The fuel-product-waste (F-P-L) concept proposed by Lozano and Valero (1993) is used, in which an equipment unit (modelled as a control volume) supplies the required resources to generate the product, changes part of the input exergy (fuel exergy) into desired exergy (product exergy) and wastes a part of it to the environment (exergy destruction). Fuel and product exergy relations for different polygeneration system components are shown in **Table 3**. The exergy

destruction for each component of the system is defined as follows (Bejan et al., 1995; Nourpour and Khoshgoftar Manesh, 2021).

$$\dot{E}_D = \dot{E}_F - \dot{E}_P \tag{4}$$

The exergy efficiency for each system component is determined by the following equation (Bejan et al., 1995; Nourpour and Khoshgoftar Manesh, 2021).

$$\varepsilon = \frac{\dot{E}_P}{\dot{E}_F} = 1 - \frac{\dot{E}_D}{\dot{E}_F} \tag{5}$$

Table 3

Fuel-product exergy relations for the different polygeneration system components.

Component	Fuel	Product
AC	$\dot{W}_{AC}$	$\dot{E}_{AC,out} - \dot{E}_1$
CC	$\dot{E}_{fuel}$	$\dot{E}_{CC,out} + \dot{E}_{AC,out}$
GT	$\dot{E}_{CC,out} - \dot{E}_3$	$\dot{W}_{GT}$
ECO	$\dot{E}_5 - \dot{E}_6$	$\dot{E}_{11} - \dot{E}_{10}$
EVA	$\dot{E}_4 - \dot{E}_5$	$\dot{E}_{12} - \dot{E}_{11}$
SUP	$\dot{E}_3 - \dot{E}_4$	$\dot{E}_{13} - \dot{E}_{12}$
HPP	$\dot{W}_{HPP}$	$\dot{E}_{10} - \dot{E}_9$
ST 1	$\dot{E}_{13} - \dot{E}_{14}$	$\dot{W}_{ST1}$
ST 2	$\dot{E}_{14} - \dot{E}_{15}$	$\dot{W}_{ST2}$
HX 2	$\dot{E}_{17} - \dot{E}_{18}$	$\dot{E}_{28} - \dot{E}_{25}$
ORCT 2	$\dot{E}_{28} - \dot{E}_{27}$	$\dot{W}_{ORCT2}$
Cond 2	$\dot{E}_{27} - \dot{E}_{26}$	$\dot{E}_{30} - \dot{E}_{29}$
ORCP 2	$\dot{W}_{ORCP2}$	$\dot{E}_{25} - \dot{E}_{26}$
HX 1	$\dot{E}_6 - \dot{E}_7$	$\dot{E}_{22} - \dot{E}_{19}$
ORCT 1	$\dot{E}_{22} - \dot{E}_{21}$	$\dot{W}_{ORCT1}$
Cond 1	$\dot{E}_{21} - \dot{E}_{20}$	$\dot{E}_{24} - \dot{E}_{23}$
ORCP 1	$\dot{W}_{ORCP1}$	$\dot{E}_{19} - \dot{E}_{20}$
CO_2 capture	$\dot{E}_7 + \dot{E}_{16} + \dot{E}_{32} + \dot{W}_{ORCP1} - \dot{E}_{31} - \dot{E}_{41} - \dot{E}_8$	$\dot{E}_{33}$
Solar energy field	$\dot{E}_{sun}$	$\dot{E}_{45} - \dot{E}_{44}$
SFHX	$\dot{E}_{46} - \dot{E}_{43}$	$\dot{E}_{47} - \dot{E}_{42}$
SFP	$\dot{W}_{solarPump}$	$\dot{E}_{44} - \dot{E}_{43}$
Humidifier	$\dot{E}_{34} - \dot{E}_{37}$	$\dot{E}_{36} - \dot{E}_{35}$
Dehumidifier	$\dot{E}_{36} + \dot{E}_{40} - \dot{E}_{38}$	$\dot{E}_{39}$

3.3. Exergoeconomic Analysis

To evaluate tradeoffs between costs and thermodynamic irreversibilities, the system is evaluated using an exergoeconomic analysis. The exergoeconomic analysis combines the exergy analysis with a detailed economic assessment. Hence, exergoeconomic analysis allows estimating the cost rate of fuel, product, and exergy destruction. The cost balance equation for each system component is based on the Specific Exergy Costing (SPECO) method (Lazzaretto and Tsatsaronis, 2006) as follows.

$$\sum_i^N \left(c_i \dot{E}_i\right)_k + c_{q.k}\dot{E}_{q.k} + \dot{Z}_k = \sum_e^N \left(c_e \dot{E}_e\right)_k + c_{w.k}\dot{W}_{q.k} \quad (6)$$

The associated cost balance equations of different equipment units are presented in **Table A.2** in **Appendix A**. The current cost of the system in dollars per unit of time is estimated by **Equation (7)** (Jadidi et al., 2021).

$$\dot{Z}_k = \frac{Z_k\, CRF\, \varphi}{3600N} \quad (7)$$

Where φ is the maintenance factor (equal to 1.06) and N is the number of operating hours per year (8000 h) (Bejan et al., 1995; Dincer et al., 2017).

The relations of the Purchased Equipment Cost (PEC), Z_k, are given in **Table A.3 (Appendix A)**. The Capital Recovery Factor, *CRF*, is a factor that converts the present capital cost of equipment to an annualized cost, which is determined by the following equation (Smith, 2005).

$$CRF = \frac{i(i+1)^n}{(i+1)^n - 1} \quad (8)$$

Where, i represents the fractional interest rate (10%) per year and n (25 years) indicates the amortization period (plant lifetime) (Dincer and Rosen, 2012; Manesh and Amidpour, 2020).

The cost rate for exergy destruction is given by **Equation (9)** as a product of the specific cost $c_{F.k}$ by the exergy rate $\dot{E}_{D.k}$ (Jadidi et al., 2021).

$$\dot{C}_{D.k} = c_{F.k}\dot{E}_{D.k} \tag{9}$$

The average cost of fuel and product per unit exergy and the relative cost difference, r_k, are defined respectively as follows (Jadidi et al., 2021).

$$c_{f.k} = \frac{\dot{C}_{F.k}}{\dot{E}x_{F.k}} \tag{10}$$

$$c_{p.k} = \frac{\dot{C}_{P.k}}{\dot{E}x_{P.k}} \tag{11}$$

$$r_k = (c_{P.k} - c_{F.k})/c_{P.k} \tag{12}$$

Where the fuel and product cost rates ($\dot{E}x_{F.k}, \dot{E}x_{P.k}$) definitions associated with each system component are presented in **Table A.4**.

Finally, the exergoeconomic factor for each system component, f_k, is given by **Equation (13)** (Bejan et al., 1995; Cao et al., 2016).

$$f_k = \dot{Z}_k/(\dot{Z}_k + \dot{C}_{D.k}) \tag{13}$$

3.4. Exergoenvironmental Analysis

Exergoenvironmental analysis is carried out to assess the environmental performance of the proposed integrated polygeneration system. In this study, the exergoenvironmental analysis is centered on the damage-oriented Eco-indicator 99 methodology which is grounded on life cycle assessment (LCA) principles. In the LCA, environmental impacts related to system components are estimated based on their construction and material weights. The exergoenvironmental analysis combining LCA and exergy analysis is aimed at reducing greenhouse gas emissions via identifying

inefficiencies over the lifetime of components to optimally and ecologically design plants. The exergoenvironmental procedure is analogous to exergoeconomic analysis. The equations of environmental impact balances for various equipment are calculated as follows (Meyer et al., 2009).

$$\sum_i^N \left(b_i \dot{E}_i\right)_k + b_{q.k}\dot{E}_{q.k} + \dot{Y}_k = \sum_e^N \left(b_e \dot{E}_e\right)_k + b_{w.k}\dot{W}_{q.k} \quad (14)$$

Similar to exergoeconomic analysis, cost balance equations of each equipment unit and the rate of environmental effects on fuel and product of the proposed cycle are defined as presented in **Table A.2** and **Table A.4**, respectively. Weight functions of the different system components are shown in **Table 4**.

Table 4

Weight functions of the different system components.

Component	Weight Function (ton)	Reference
AC	$Weight = 0.01.\dot{W}_{net} + (-120.48/(1.23.\dot{W}_{net} - 1484.59))$	*(proposed)*
CC	$Weight = 0.0001 + 0.006.\dot{W}_{net} + (-2.37/(10482.38 - 9.65.\dot{W}_{net}))$	*(proposed)*
GT	$Weight = 0.064.\dot{W}_{net} + 1.13.e^{-8}(\dot{W}_{net})^3 - 17.49 - 4.54e^{-5}.(\dot{W}_{net})^2$	*(proposed)*
ECO	$Weight = 4058.55 + 41.13.(T_{sub})^2 + 2096.16 .log(T_{sub}).\sqrt{(T_{sub})} - 2172.43.T_{sub}$	*(proposed)*
EVA	$Weight = 6948.11 - 1109.97 .log\,\Delta T_{pinch,EVA}$	*(proposed)*
SUP	$Weight = 3511.49 + 0.88.\Delta T_{approch,SUP}$	*(proposed)*
HPP	$Weight = 0.0061.(\dot{W}_{HPP})^{0.95}$	(Manesh et al., 2021b)
ST 1	$Weight = 4.9.(\dot{W}_{ST1})^{0.73}$	(Cavalcanti, 2017)
ST 2	$Weight = 4.9.(\dot{W}_{ST2})^{0.73}$	(Cavalcanti, 2017)
HX 2	$Weight = 2.14.(\dot{Q}_{HX2})^{0.7}$	(Cavalcanti, 2017)
ORCT 2	$Weight = 14.(\dot{W}_{ORCT2})$	*(proposed)*
Cond 2	$Weight = 0.073.(\dot{Q}_{Cond2})^{0.099}$	(Cavalcanti, 2017)
ORCP 2	$Weight = 31.22.(\dot{W}_{ORCP2})$	*(proposed)*
HX 1	$Weight = 2.14.(\dot{Q}_{HX1})^{0.7}$	(Cavalcanti, 2017)
ORCT 1	$Weight = 14.(\dot{W}_{ORCT2})$	*(proposed)*
Cond 1	$Weight = 0.073.(\dot{Q}_{Cond1})^{0.099}$	(Cavalcanti, 2017)
ORCP 1	$Weight = 31.22.(\dot{W}_{ORCP2})$	*(proposed)*
CO_2 Capture	$Weight = 10.(37.27.\dot{m}_g + 0.1312.(\dot{m}_g)^2)$	*(proposed)*

Solar Field	*Weight* = $148.44 + 5550.52.(\dot{m}_{th})$	*(proposed)*
SFHX	*Weight* = $2.14.(\dot{Q}_{SFHX})^{0.7}$	(Cavalcanti, 2017)
SFP	*Weight = 0.0061*$.(\dot{W}_{HPP})^{0.95}$	*(proposed)*
Humidifier	*Weight* = $0.0005.(6.84.L_{h,in}.X.Y)$	*(proposed)*
Dehumidifier	*Weight* = $0.0005.(6.84.L_{D,in}.X.Y)$	*(proposed)*

Still similar to exergoeconomic analysis, the governing equations for environmental analysis are as follows. The environmental impact rate of the equipment unit is defined by **Equation (15)** (Meyer et al., 2009).

$$\dot{Y}_k = \frac{Y_k}{3600Nn} \tag{15}$$

The environmental impact per exergy unit of the fuel and product are given by **Equation (16)** and **Equation (17)**, respectively (Meyer et al., 2009).

$$b_{f.k} = \frac{\dot{B}_{F.k}}{\dot{E}x_{F.k}} \tag{16}$$

$$b_{p.k} = \frac{\dot{B}_{P.k}}{\dot{E}x_{P.k}} \tag{17}$$

The rate of environmental impacts associated with exergy destruction is calculated as follows (Meyer et al., 2009).

$$\dot{B}_{D.k} = b_{f.k} \times \dot{E}_{D.k} \tag{18}$$

The relative environmental impact difference r_b of each system component is estimated by **Equation (19)** (Petrakopoulou et al., 2012b).

$$r_{b.k} = (b_{P.k} - b_{F.k})/b_{P.k} \tag{19}$$

Finally, the environmental exergy factor f_b is defined as follows (Petrakopoulou et al., 2012b).

$$f_{b.k} = \dot{Y}_k / \left(\dot{Y}_k + \dot{B}_{D.k}\right) \tag{20}$$

3.5. Emergy

Emergy is related to macroscopic and microscopic fields. Emergy analysis transfers all input variables of the cycle, energies, and resources into a single unit of solar emergy: Solar Emergy Joule (sej). Emergy analysis, unlike energy analysis, integrates economic and environmental concepts by combining exergoeconomic and exergoenvironmental analyses. In this approach, the scale factor coefficient, β (~0.93), is used to convert all input variables or energy to emergy as given by the following equation (Bastianoni et al., 2007).

$$\beta = 1 + \frac{1}{3}\left(\frac{T_0}{T_S}\right)^4 - \frac{4}{3}\left(\frac{T_0}{T_S}\right) \tag{21}$$

Where T_0 and T_S designate the ambient temperature and the sun temperature, respectively.

3.5.1. Emergoeconomic analysis

The emergoeconomic analysis is grounded on the conventional exergoeconomic assessment. Hence, the SPECO methodology (Lazzaretto and Tsatsaronis, 2006) is employed to each process stream of the proposed integrated system. The emergy cost balance equation for the different system components is given as follows (Aghbashlo and Rosen, 2018).

$$\sum_i^N \left(m_i \dot{E}_i\right)_k + m_{q.k}\dot{E}_{q.k} + \dot{U}_k = \sum_e^N \left(m_e \dot{E}_e\right)_k + m_{w.k}\dot{W}_{q.k} \tag{22}$$

or

$$\dot{M}_{P,k} = \dot{M}_{F,k} + \dot{U}_k \tag{23}$$

Where $\dot{U}_k$ is the component-related emergoeconomic rate defined as the summation of investment and operating and maintenance costs (O&M) as expressed by **Equation (24)** (Aghbashlo and Rosen, 2018).

$$\dot{U}_k = \dot{U}_k^{CI} + \dot{U}_k^{OM} \tag{24}$$

Emergoeconomic balance equations of each equipment unit are presented in **Table A.5 (Appendix A)**. The emergoeconomic rate of the k-th equipment unit is determined based on the exergy destruction as follows (Aghbashlo and Rosen, 2018).

$$\dot{M}_{D.k} = m_{F.k}\dot{E}_{D.k} \tag{25}$$

Where specific emergoeconomic values for fuel ($m_{F,k}$) and product ($m_{P,k}$) of each system component are calculated by **Equation (26)** and **Equation (27)**, respectively (Aghbashlo and Rosen, 2018).

$$m_{P,k} = \frac{\dot{M}_{P,k}}{\dot{E}_{P,k}} \tag{26}$$

$$m_{F,k} = \frac{\dot{M}_{F,k}}{\dot{E}_{F,k}} \tag{27}$$

The total emergoeconomic rate of different system components ($\dot{M}_{TOT,k}$) is given by **Equation (28)** (Aghbashlo and Rosen, 2018).

$$\dot{M}_{TOT,k} = \dot{M}_{D,k} + \dot{U}_k \tag{28}$$

The relative emergy-based cost difference $r_{m,k}$ and emergy-based exergoeconomic factor $f_{m.k}$ are obtained as follows.

$$r_{m.k} = (m_{P.k} - m_{F.k})/m_{P.k} \tag{29}$$

$$f_{m.k} = \dot{U}_k/\left(\dot{U}_k + \dot{M}_{D.k}\right) \quad (30)$$

3.5.2. Emergoenvironmental analysis

The emergy-based exergoenvironmental balance for each system component is defined by **Equation (31)** (Aghbashlo and Rosen, 2018).

$$\sum_i^N \left(n_i \dot{E}_i\right)_k + n_{q.k}\dot{E}_{q.k} + \dot{V}_k = \sum_e^N \left(n_e \dot{E}_e\right)_k + n_{w.k}\dot{W}_{q.k} \quad (31)$$

or

$$\dot{N}_{P,k} = \dot{N}_{F,k} + \dot{V}_k \quad (32)$$

In **Equation (32)**, $\dot{V}_k$ indicates the environmental emergy rate of each system component, which is calculated as follows (Aghbashlo and Rosen, 2018).

$$\dot{V}_k = \dot{V}_k^{CO} + \dot{V}_k^{OM} + \dot{V}_k^{DI} \quad (33)$$

Where $\dot{V}_k^{CO}$, $\dot{V}_k^{OM}$, and $\dot{V}_k^{DI}$ indicate the environmental emergy rates in the construction, operation and maintenance, and disposal phases, respectively. The emergy-based environmental balance equations of various system components are presented in **Table A.5**.

The environmental impact rate associated with the exergy degradation is given by **Equation (34)** (Aghbashlo and Rosen, 2018).

$$\dot{N}_{D.k} = n_{F.k}\dot{E}_{D.k} \quad (34)$$

Where $n_{P,k}$ and $n_{F,k}$ are the specific emergoenvironmental values for product and fuel of the k-th system component, respectively. The previous values are determined as follows (Aghbashlo and Rosen, 2018).

$$n_{P,k} = \frac{\dot{N}_{P,k}}{\dot{E}_{P,k}} \quad (35)$$

$$n_{F,k} = \frac{\dot{N}_{F,k}}{\dot{E}_{F,k}} \quad (36)$$

The total emergoenvironmental rate of each system component can be determined by **Equation (37)** (Aghbashlo and Rosen, 2018).

$$\dot{N}_{TOT,k} = \dot{N}_{D,k} + \dot{V}_k \quad (37)$$

Finally, the relative environmental emergy difference ($r_{n,k}$) and emergy-based exergoenvironmental factor ($f_{n,k}$) are expressed by **Equation (38)** and **Equation (39)**, respectively (Aghbashlo and Rosen, 2018).

$$r_{n.k} = (n_{P.k} - n_{F.k})/n_{P.k} \quad (38)$$

$$f_{n.k} = \frac{\dot{V}_k}{(\dot{V}_k + \dot{N}_{D.k})} \quad (39)$$

4. Results and Discussion

4.1. Energy Analysis

The thermodynamic properties of different process streams obtained from MATLAB and THERMOFLEX software simulations for case studies with/without solar energy are compared in **Table B.1** and **Table B.2 (see Appendix B)**, respectively. The results highlight that the proposed integrated cycle is simulated with high accuracy in both scenarios. Results are reported for June (summer), when the solar energy production is higher.

The validation of the thermodynamic results of the HDH desalination unit is shown in **Table 5**. Sensitivity analysis is used to determine the optimal inputs of the HDH unit. The pressure

of all streams has been assumed to be 1.014 bar. In this case, several references are used to verify the model's accuracy, and most of the results show high accuracy with literature data.

The thermodynamic block diagram of the proposed polygeneration system coupled with the solar energy field is depicted in **Fig. 5**. The figure shows the thermodynamic properties (temperature, pressure, and mass flowrate) of main process streams and power and heat production outputs of system components.

Table 5

Validation of thermodynamic properties obtained for the humidification-dehumidification (HDH) desalination unit.

	$\dot{m}$ (kg/m^{2}s)				T (°C)		
Stream	*Literature Value*	*Reference*	*Code*	*Error (%)*	*Literature Value* (Zamen and Amidpour, 2013)	*Code*	*Error (%)*
34	0.49	(Zamen and Amidpour, 2013)	0.49	0	55	55	0
35	0.28	(Zamen and Amidpour, 2013)	0.28	0	24.1	24.1	0
36	0.28	(Zamen and Amidpour, 2013)	0.28	0	36	38	5.5
37	19.7	(Gholizadeh et al., 2020)	20.1	1.5	45	43	4.4
38	0.28	(Zamen and Amidpour, 2013)	0.28	0	34	33.2	2.4
39	3.612	(Eslamimanesh and Hatamipour, 2010)	3.59	0.4	29.3	26.8	8.4
40	1	(Zamen and Amidpour, 2013)	1	0	20	20	0

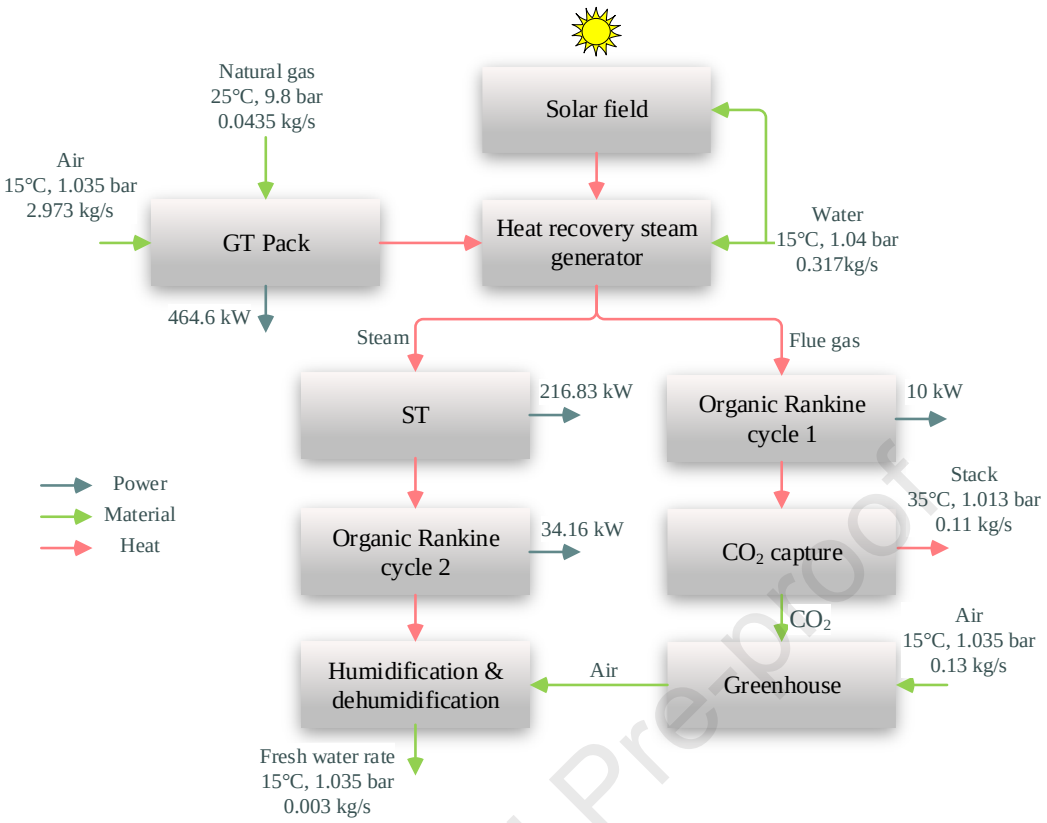

Fig. 5. Block diagram of the proposed integrated solar energy-driven polygeneration system.

Water and air temperature profiles in the humidifier are depicted in **Fig. 6(a)** and **Fig. 6(b)**, respectively. As shown in **Fig. 6(a)**, the water temperature decreases along the humidifier height due to heat transfer from water to airflow. On the contrary, the air stream temperature increases as a result of the increase of its humidity levels while passing along the humidifier. The most significant drop in water temperature occurs in the air entrance section, where the temperature difference is the highest. Water and air temperature profiles in the dehumidifier are shown in **Fig. 7(a)** and **Fig. 7(b)**, respectively. In this case, air and water temperature profiles within the dehumidifier show a more prominent drop and growth, respectively, for lower packing length

values (left-hand side). The intensity of these values decreases in lower sections and the right-hand side of the dehumidifier.

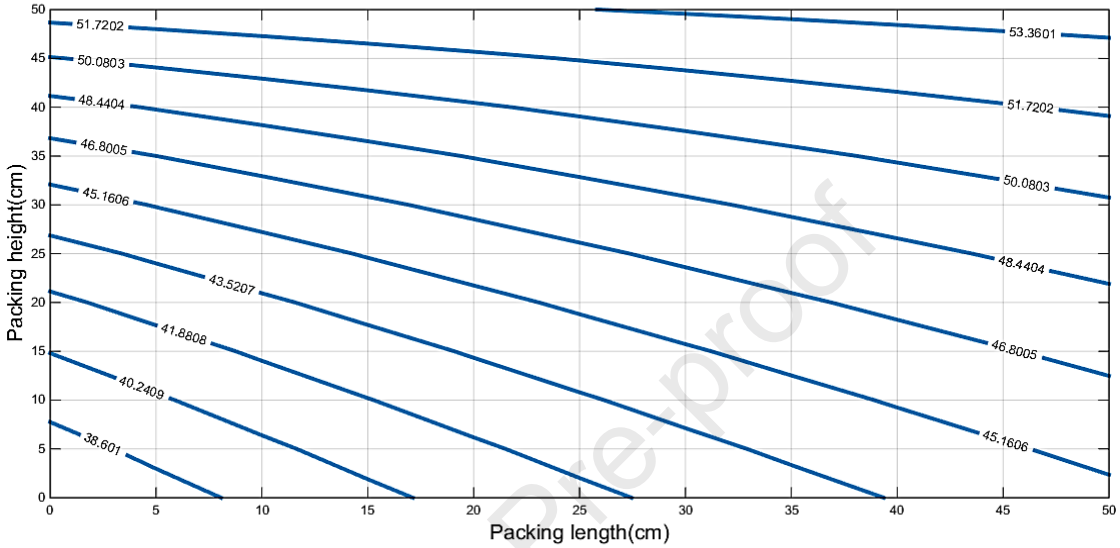

(a)

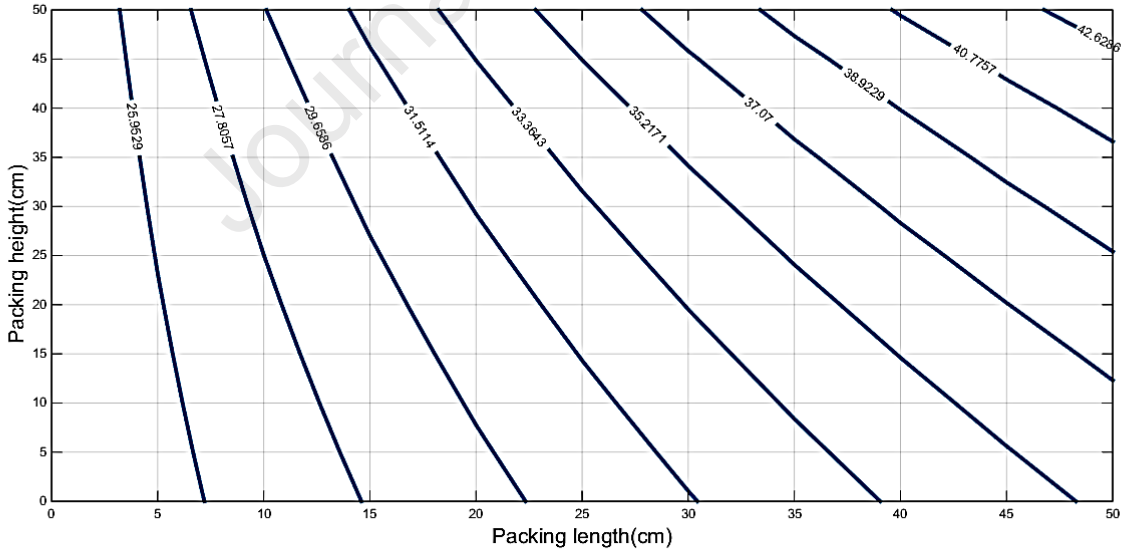

(b)

Fig. 6. Humidifier temperature profiles of (*a*) water and (*b*) air.

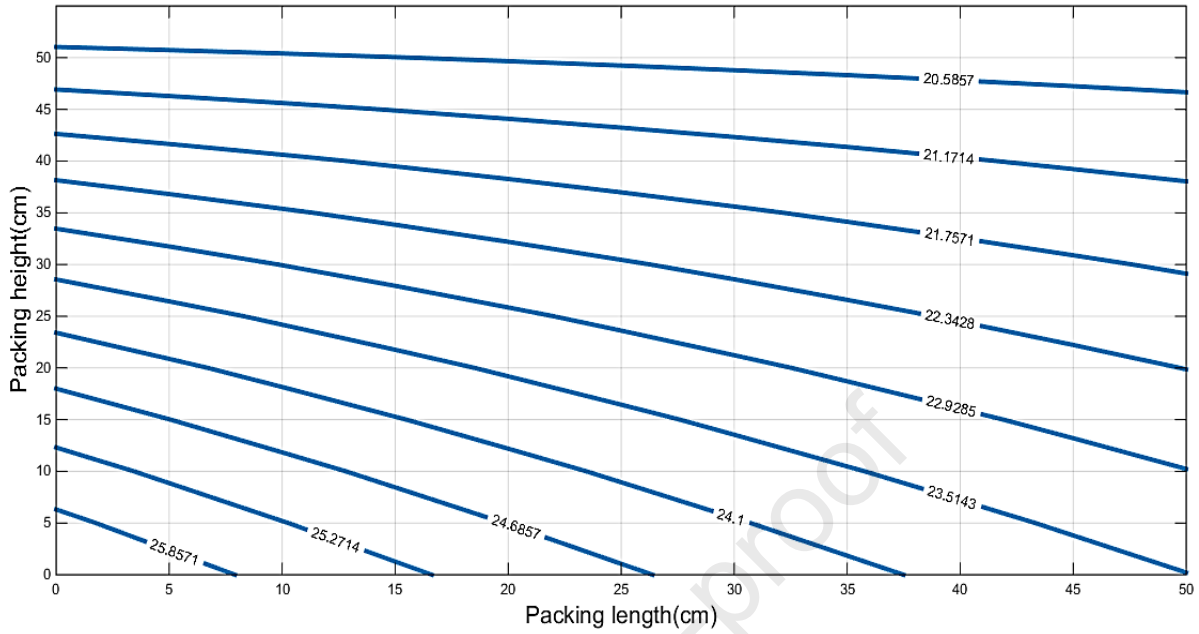

(a)

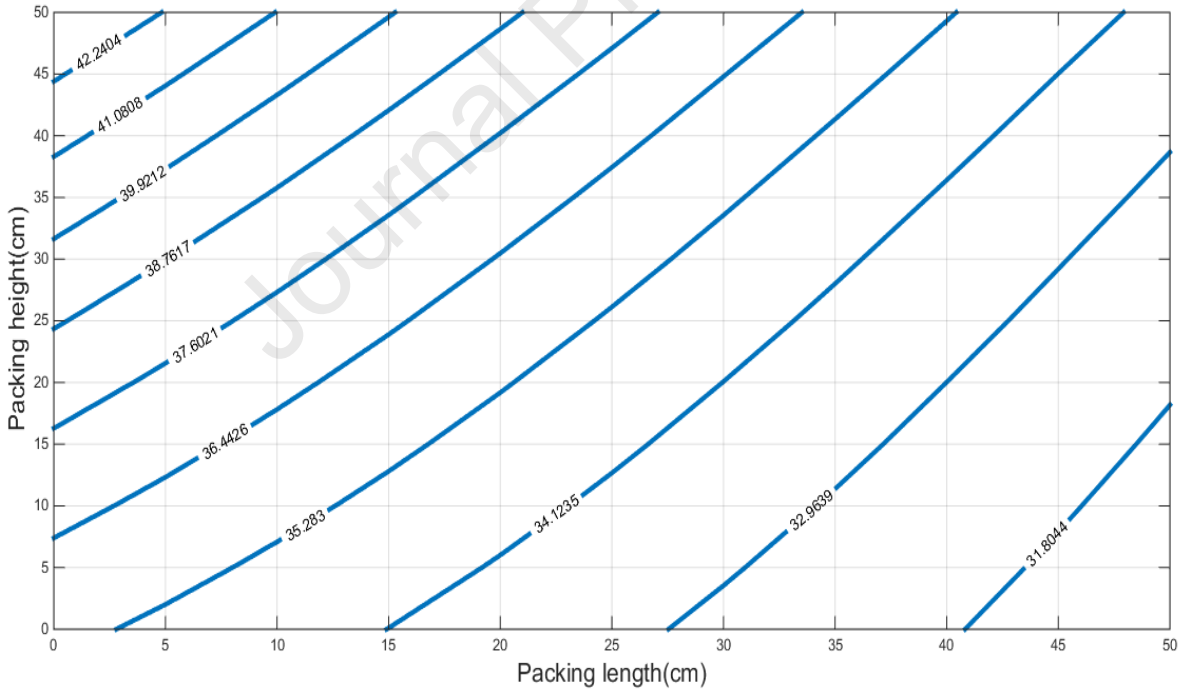

(b)

Fig.7. Dehumidifier temperature profiles of (*a*) water and (*b*) air.

4.2. HDH Operating Parameters

4.2.1 Air mass flowrate

As aforementioned, the greenhouse's desired temperature and humidity ratio are stable and set at 25°C and 50%, respectively. Hence, it is assumed that the airflow enters the humidifier at 25°C and 50% humidity ratio. To determine the optimal air mass flowrate in this unit, the packing size is considered to be constant. The freshwater production ratio in function of the air mass flowrate is displayed in **Fig. B.1** (**Appendix B**). This figure shows that the optimal air mass flowrate that maximizes freshwater production is 0.32 kg/sm^2. It should be noted that increasing the air mass flowrate boosts heat and mass transfer coefficients, but it reduces the temperature of the air leaving the humidifier. Therefore, freshwater production is decreased at higher air mass flowrates.

4.2.2 Packing height

An optimal packing height is required because as the height of the packing increases, the mass flux on the packing decreases. As a result, the heat and mass transfer coefficients will also be reduced at higher packing heights. However, by increasing the packing height, the total heat transfer surface also increases. The effect of packing height on the freshwater production ratio is depicted in **Fig. B.2** (**Appendix B**). Because of the temperature and humidity difference between air and water streams at lower packing heights, an increase in height results in higher production rates. The total output will gradually decrease with further height increases due to reduced heat and mass transfer coefficient and temperature difference. According to **Fig. B.2**, the optimal packing height is determined at 0.7 m.

4.2.3 Cooling water mass flowrate

Fig. 8(a) and **Fig.8(b)** portray the effect of cooling water mass flowrate on freshwater production and energy consumption, respectively. It is observed that the freshwater production ratio decreases with increasing the cooling water flowrate. However, this effect is less pronounced at higher mass flowrate values. As shown in **Fig.8(b)**, the increased cooling water mass flowrate leads to increased energy consumption. The effect of increasing the cooling water mass flowrate decreases at higher values.

A standard greenhouse with 25 meters length, 10 meters width, and 5 meters height is assumed for this design. The average amount of water required for the greenhouse is about 1 L/m^2 per day. Thus, based on the area of the greenhouse, the average volume of water required is 250 liters per day (Zamen and Amidpour, 2013). Therefore, considering the freshwater production rate ($L_{D,out} - L_{D,in}$) of 0.003 kg/s, about 0.1 kg/sm^2 inlet cooling water to the dehumidifier is required in the greenhouse.

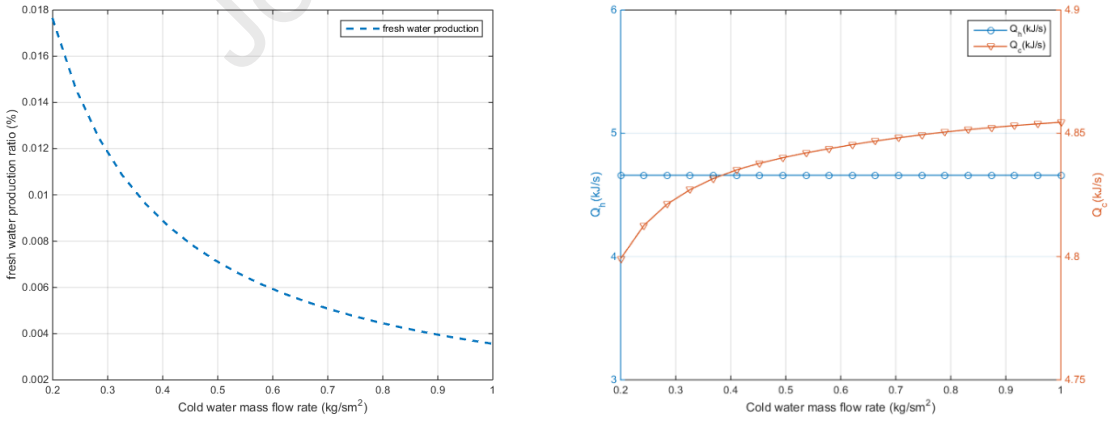

(a) **(b)**

Fig. 8. Effect of the cooling water mass flowrate on the (*a*) HDH freshwater production ratio and the (*b*) HDH energy consumption.

4.2.4 Packing length

The effect of the HDH packing length on the freshwater production ratio is depicted in **Fig. B.3** in **Appendix B**. According to this figure, a value of 0.6 m is chosen due to the low impact of increased packing length on the freshwater production ratio and packing length standard.

4.3. ORC Working Fluid Selection

In taking advantage of low-grade heat sources, ORCs can be used to enhance power production. The effect of working fluids on the system energy conversion efficiency, and economic and environmental performance indicators makes its selection a critical process. Likewise, the selected working fluid should be stable in the heat source temperature range. Regarding the operational temperature, five candidate working fluids are compared from different perspectives and the results as presented in **Table 6**. According to these results, R601 and R365mfc are appropriate fluids from several viewpoints apart from mass flowrate and total environmental impacts. Therefore, R11 is the optimal selection for all parameters considered for this application.

Table 6.

Results of the five recommended ORC working fluids for the proposed integrated cycle.

Parameter	R123	R141b	R365mfc	R601	R11
η_{tot} (%)	36.06	36.14	35.81	36	36.26
ψ_{tot} (%)	31.73	31.81	31.52	31.68	31.91
$W_{tot.net}$ (kW)	715.16	716.84	710.26	713.99	719.22
$W_{ORC.}net$ (kW)	46.32	48.01	41.42	45.15	50.38
$\dot{m}_{ORC}$ (kg/s)	2.29	1.82	1.97	1.05	2.26
$\dot{C}_{tot}$ (US$/s)	0.14	0.14	0.14	0.14	0.14
$\dot{B}_{tot}$ (mPts/s)	15.81	15.72	15.63	15.65	15.86
$\dot{M}_{tot}$ (Gsej/s)	132.25	131.52	133.34	132.79	129.89
$\dot{N}_{tot}$ (Gsej/s)	107.25	107.06	108.2	107.59	106.33

The monthly net power generation of the integrated system is displayed in **Fig. 9**. The highest monthly net power generation occurs in September and the lowest one in April. The monthly net power generation of the power plant varies from 728.3 kW to 737.5 kW.

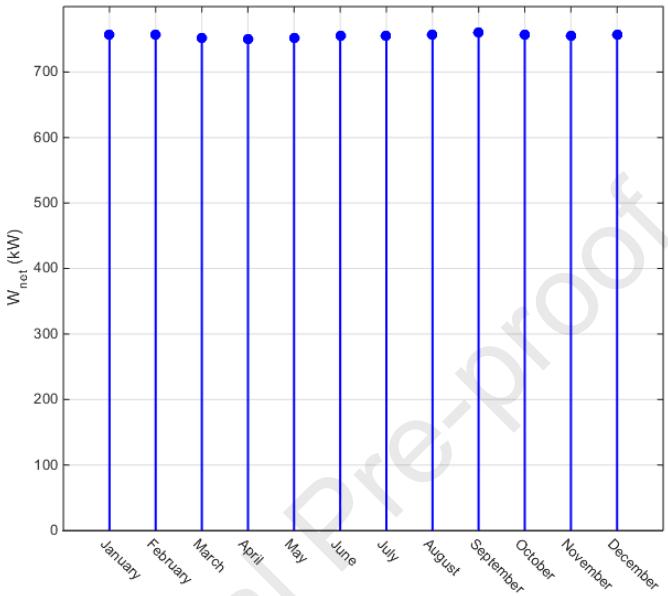

Fig. 9. Monthly net power generation (in kW) of the integrated polygeneration system.

The monthly power generation of the ORCs is shown in **Fig. 10**. The results reveal that the highest ORC power generation occurs in September. The latter is due to Qom's high DNI amount for this month. Therefore, SF increases in this month, and since water is mainly heated by the solar field and the temperature at the outlet flue gas of the economizer increases, the organic fluid mass flow is increased. Consequently, the power generation of ORC is enhanced.

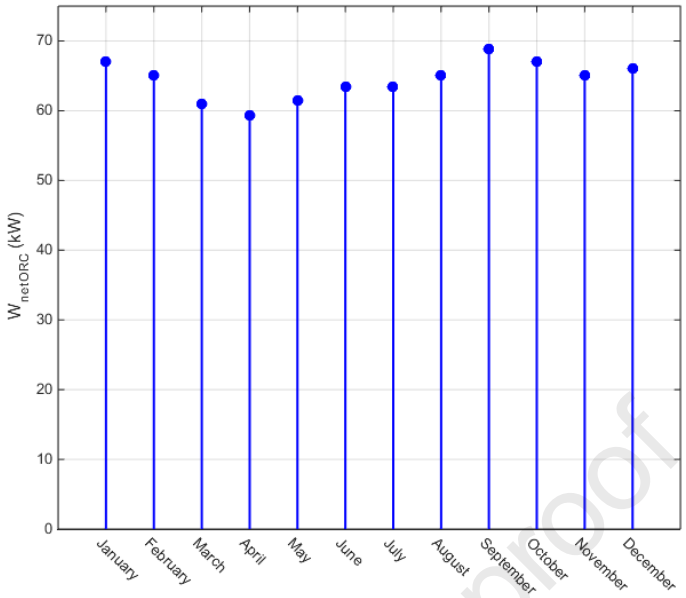

Fig. 10. Monthly power generation (in kW) of the organic Rankine cycles (ORCs).

When the solar energy field is integrated into the polygeneration system, the lowest and the highest ORC power generation values are 59.3 kW in April and 68.85 kW in September, respectively. By contrast, ORCs produce 43.19 kW power in the base case scenario (polygeneration system without solar energy field). Consequently, the solar field unit increases ORC's power production by approximately 37.3% (winter) up to 59.41% (summer) compared to the base case study. The kWh net energy generation difference between the two cases is illustrated in **Fig. 11**. The maximum profit occurs in September due to the highest net energy generation difference.

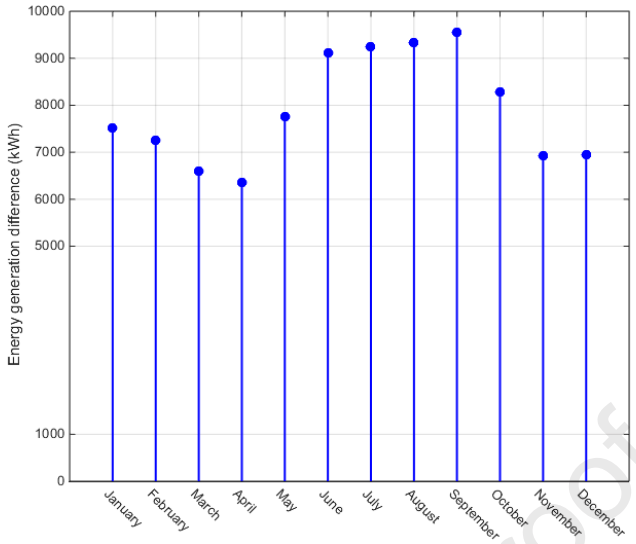

Fig. 11. Net energy generation difference (in kWh) between two case studies (i.e., polygeneration system with and without the solar energy field).

4.4. Exergy Analysis

Table B.3 and **Table B.4** (see **Appendix B**) present the exergy analysis results of each system component for case scenarios with and without the solar energy integration, respectively. In these tables, the integrated solar system results are reported for June. Results reveal that, for both case scenarios, the related cost of exergy destruction of the CC is expressively higher than the other components. Although the solar system integration increases the plant exergy degradation by 18%, it decreases the exergy destruction of the economizer by 76%, and the total power generation of the polygeneration system is increased by approximately 18 kW compared to the base case scenario. The Sankey diagram corresponding to the exergy analysis of the polygeneration plant combined with the solar energy field unit is illustrated in **Fig. 12**.

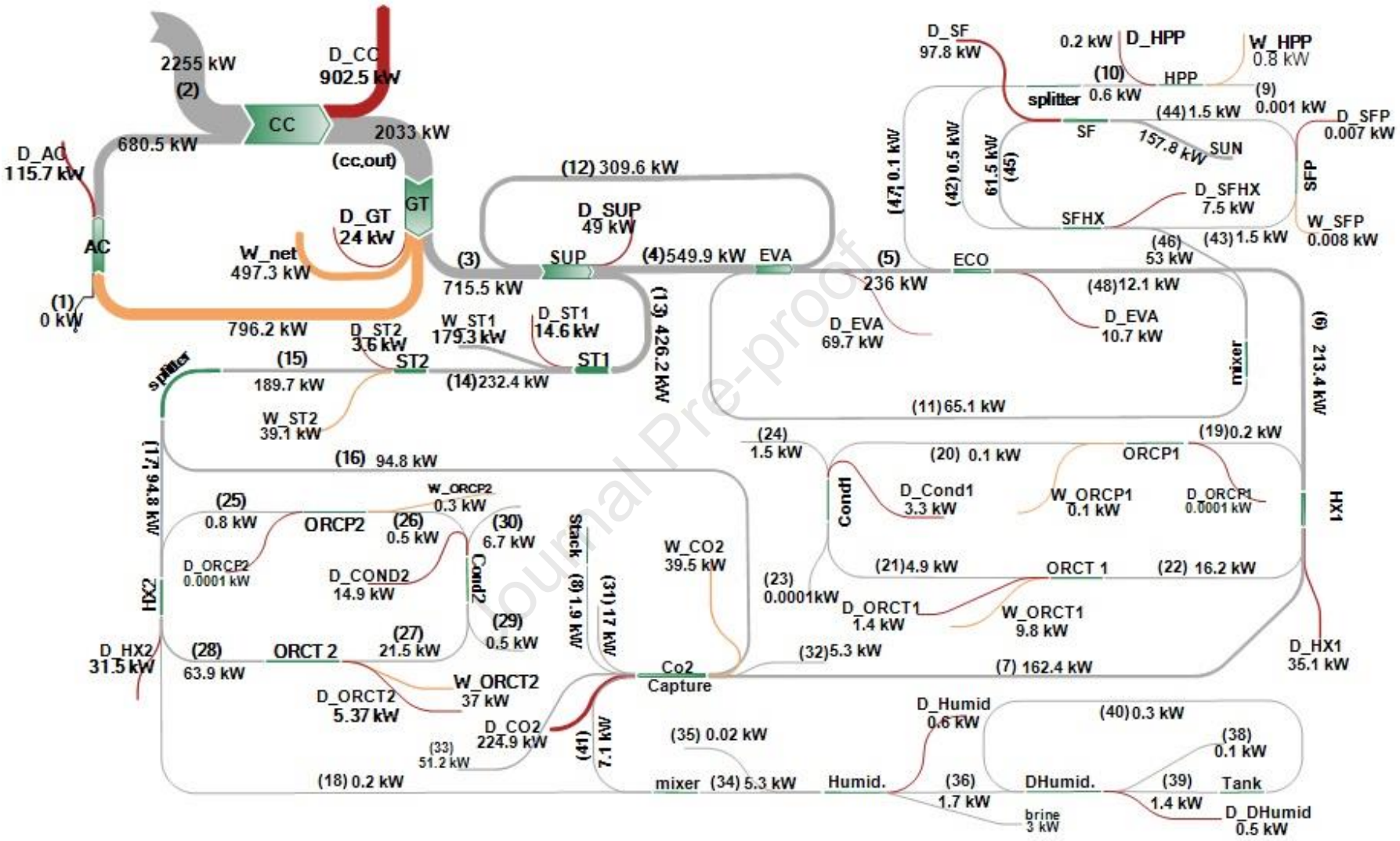

Fig. 12. Sankey diagram of exergy analysis for the polygeneration system integrated with the solar energy field (**Fig. 2**).

Fig. 13 presents the monthly total exergy destruction of the integrated solar energy-driven polygeneration system at each month of the year. The highest monthly total exergy destruction of the power plant occurs in September (2.146 MW), followed by January (2.026 MW), October (2.022 MW), and February (2.021 MW), respectively. The lowest monthly total exergy destruction of the polygeneration system occurs in April (1.84 MW).

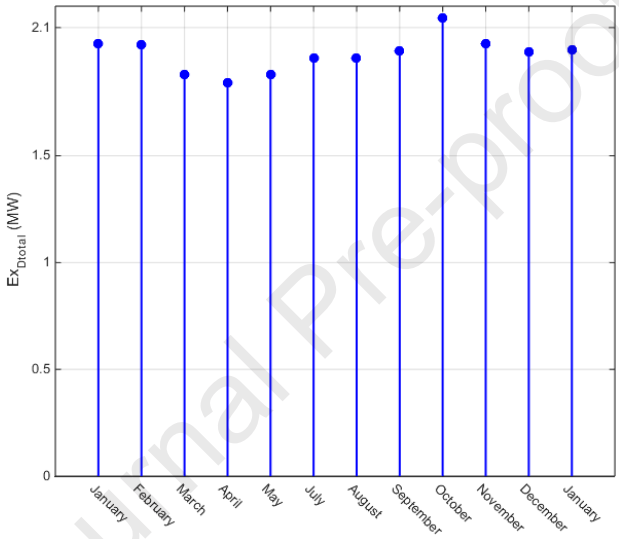

Fig. 13. Monthly total exergy destruction of the polygeneration system integrated with the solar energy field.

The diagrams in **Fig. B.4** (**Appendix B**) display the monthly total exergy destruction of different system components. Except for the economizer, the highest exergy destruction of system units occurs in September. The exception is due to the lower mass flowrate (almost zero) of feed water heated within the economizer, which causes it to remain on standby mode.

4.5. Exergoeconomic Analysis

The cost rate ($\dot{Z}_k$), exergy destruction cost rate ($\dot{C}_{D,k}$), fuel and product cost per exergy unit ($\dot{c}_{F,k}, \dot{c}_{P,k}$), relative cost difference (r_k) and exergoeconomic factor (f_k) for various system components are presented in **Table B.5** and **Table B.6** (**Appendix B**) for both configurations (polygeneration system with and without solar energy field). The results for the integration of the solar system are reported for June.

According to **Table B.5**, the highest cost rate and exergy destruction cost rate given by $\dot{Z}_k + \dot{C}_D$ is associated with the CO_2 capture unit, followed by the CC and ORC heat exchanger 1. The exergoeconomic evaluation presented in **Table B.6** depicts that, similarly to the base case scenario, the CO_2 capture unit, CC, and ORC heat exchanger 1 present higher exergy costs to convert fuel into products. This difference in exergoeconomic values between the two cases is due to the temperature difference between the hot and cold fluids in the ORC heat exchanger 1 and ORC mass flowrate increase due to solar energy integration. Thus, the investment cost of system components with lower exergoeconomic factors needs to be increased to improve the exergy efficiency. However, this enhancement is limited to avoid negative impacts on the exergy destruction and the efficiency of other components.

The maximum relative cost difference r_k is allocated to CO_2 capture unit and ORC heat exchanger 1 in both scenarios (with/without the solar energy field). Therefore, the first candidate for improvement is the ORC heat exchanger 1 with the highest amount of $\dot{Z}_k + \dot{C}_D$ and r_k. Based on the exergoeconomic analysis, it is concluded that integration of solar field increases $\dot{Z}_k + \dot{C}_D$ by 6.6%. The Sankey diagram of exergoeconomic analysis of the solar-assisted polygeneration system is illustrated in **Fig. 14**.

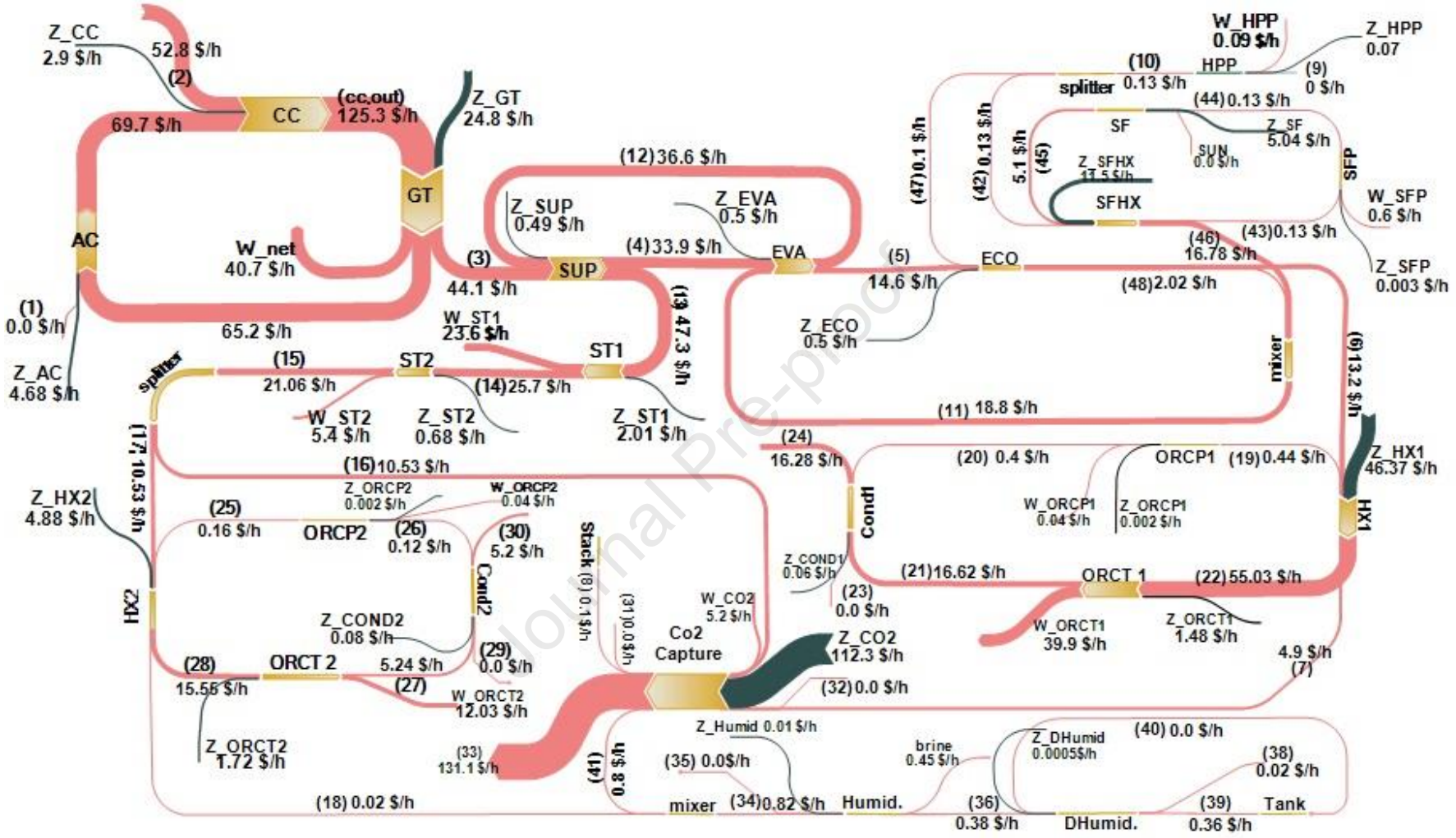

Fig. 14. Sankey diagram of the exergoeconomic analysis for the polygeneration system integrated with the solar energy field (**Fig. 2**).

Fig. B.5 depicts the monthly cost of exergy destruction rates of different dynamic system components. The contribution of the solar energy field to supply the required heating increases in September. Therefore, the temperature of the outlet flue gas from the economizer increases, which increases the organic fluid mass flowrate of the ORC 1. In addition, the monthly cost of exergy destruction rates of components, except for the economizer (standby mode), increases in September due to higher SF values.

Fig. 15 depicts the revenues (in dollars) from selling the generated electricity for each month of the year. The lowest and highest power costs occur in April and September, respectively. Given the difference between the revenues earned by selling the generated power and the annualized investment cost of purchasing solar collectors, the profit of employing the solar field is calculated at 50k US$/year, and the payback period is estimated at 4.76 years.

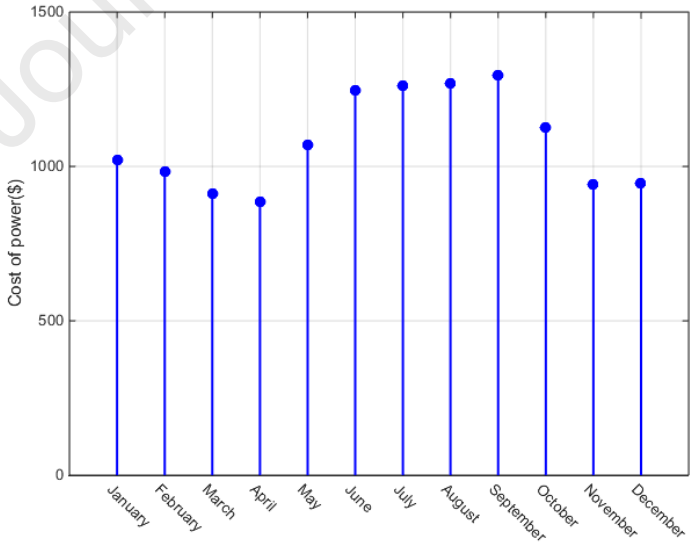

Fig. 15. Monthly selling revenues of the generated electricity.

4.6. Exergoenvironmental Analysis

The exergoenvironmental analysis is performed for both scenarios (with/without solar energy field). The values of environmental impacts ($\dot{Y}_k$), environmental impact rate associated with the exergy destruction ($\dot{B}_{D,k}$), environmental impacts per exergy unit for product and fuel ($\dot{c}_{F,k}, \dot{c}_{P,k}$), exergoenvironmental factor (f_{kb}), and the difference between the relative environmental destructive impacts r_b are listed in **Table B.7** and **Table B.8** (**Appendix B**). The results are reported for June.

According to **Table B.7**, the highest environmental impact rate and exergy destruction expressed by $\dot{Y}_k + \dot{B}_D$ belongs to the CC, followed by the CO_2 capture unit and steam turbine 2. The exergoeconomic evaluation in **Table B.8** reveals that, similar to the base case, the highest $\dot{Y}_k + \dot{B}_D$ is also attributable to the same units. Thus, system components with lower exergoenvironmental factors, such as condensers 1 and 2 and HDH desalination units, require an increase in their exergy efficiency. However, this enhancement is limited to avoid negative impacts on other system components' exergy destruction and efficiency. Still, the CO_2 capture unit and condensers, as components with the highest amount of r_b, are considered to increase their exergy efficiency and reduce the total environmental impact. In the scenario with solar energy integration into the polygeneration system, the solar field heat exchanger stands at the top of the list of the units to be improved with the maximum r_b. Based on the exergoenvironmental analysis, it is concluded that integration of solar field increases $\dot{Y}_k + \dot{B}_D$ by 3.9%.

The Sankey diagram of exergoenvironmental analysis of the polygeneration plant integrated with the solar energy field is illustrated in **Fig. 16**. The total environmental impact rate of system components ($\dot{B}_{TOT}$) –corresponding to the summation of environmental impacts $\dot{Y}_k$ and environmental impact rate associated with the exergy destruction $\dot{B}_{D,k}$– is presented in **Fig. 17**

over the different months of the year for the solar-assisted scenario. The lowest value of $\dot{B}_{TOT}$ occurs in April, and the highest in September. The latter is due to the increase in the contribution of the solar field to supply the required heating demands in this month. Therefore, the temperature of the outlet flue gas from the economizer increases, which leads to a rise of the organic fluid mass flowrate of the ORC1.

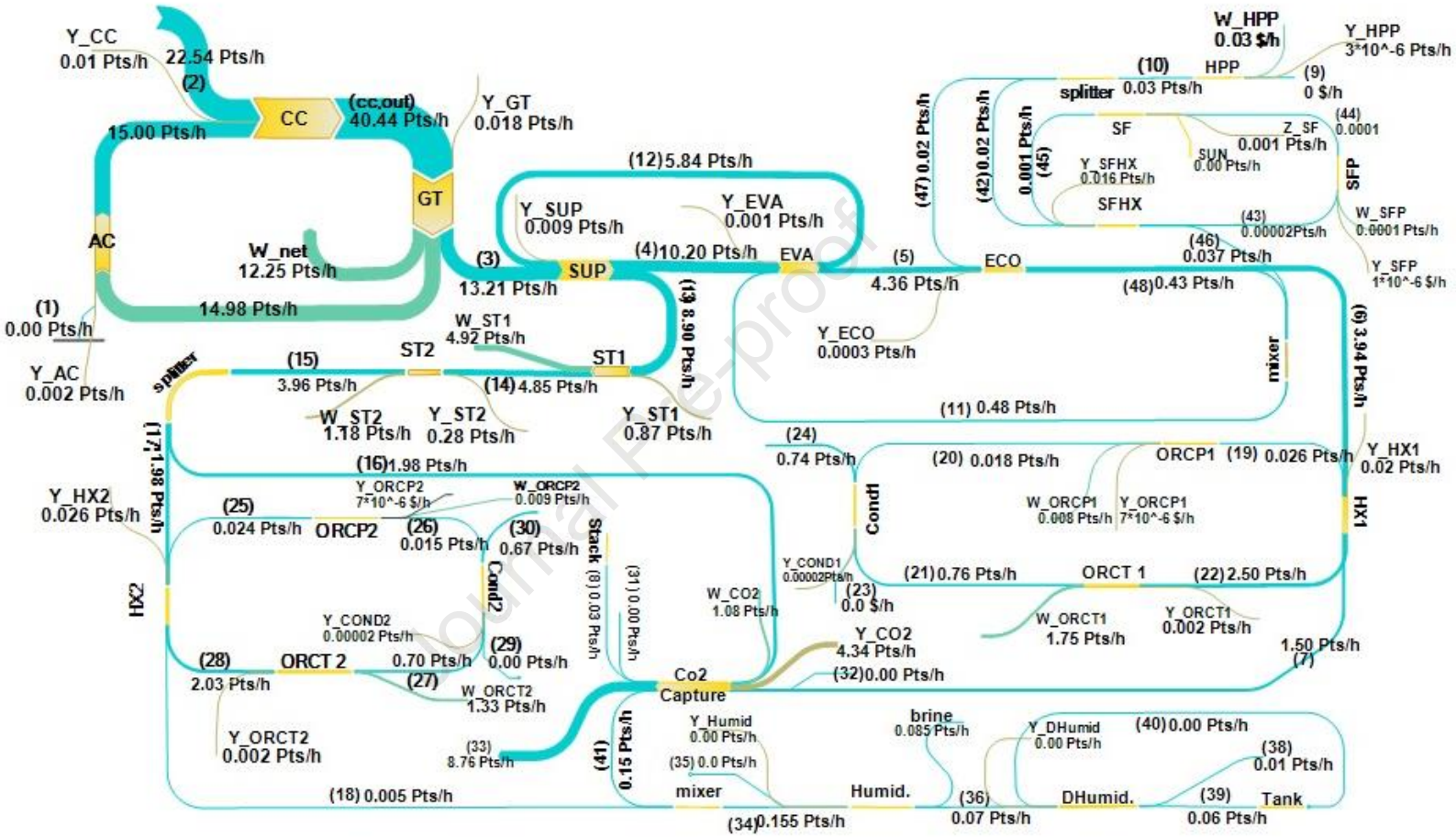

Fig. 16. Sankey diagram of the exergoenvironmental analysis for the polygeneration system integrated with the solar energy field (**Fig. 2**).

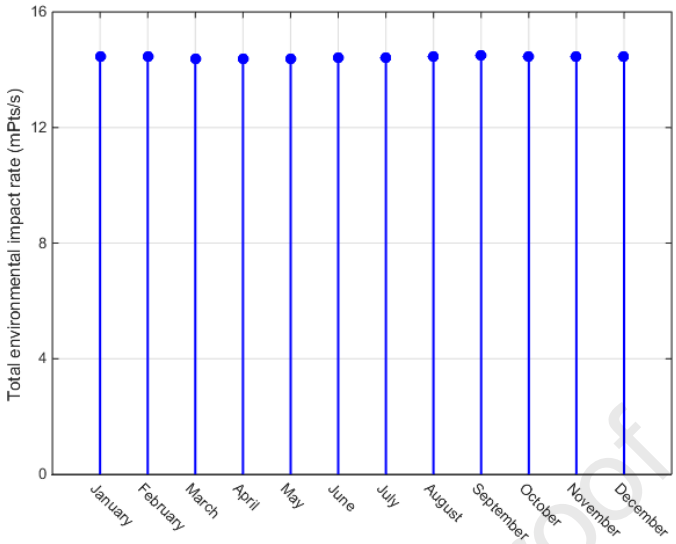

Fig. 17. Monthly rate of overall system environmental impacts.

Finally, the diagrams in **Fig. B.6** (**Appendix B**) display the monthly environmental impact rate associated with the exergy destruction of some dynamic equipment units, which validates the increase of $\dot{B}_{TOT}$ in September according to the previous discussion.

4.7. Emergoeconomic Analysis

The results of emergoeconomic analysis for both proposed system configurations are presented in **Table B.9** (without solar field) and **Table B.10** (with solar field). The results are reported for June. For both scenarios, the maximum summation of economic emergy rate and component-related economic emergy rate given by $\dot{M}_D + \dot{U}$ is attributable to the CO_2 capture unit, followed by the CC and the heat exchanger 1. For exergy analysis of the polygeneration plant without the solar energy system, condensers 1 and 2 as components with lower emergoeconomic factors, and the heat exchanger 1 and CO_2 capture unit as the components with the highest amount of relative monetary emergy difference r_m should be considered to increase their exergy efficiency. On the

other hand, when solar integration is considered, condensers 1 and 2 as components with lower emergoenvironmental factors and solar system pump, CO_2 capture unit, and heat exchanger 1 as the elements with the highest amount of r_m should be considered to increase their exergy efficiency. Based on the emergoeconomic analysis, the integration of solar energy field increases $\dot{U}_k + \dot{M}_D$ by 2.12%.

The total economic emergy rate $\dot{M}_{TOT}$ for the integrated solar-assisted polygeneration system throughout the year is portrayed in **Fig. 18**. In this case, the maximum total economic emergy rate occurs in September and the minimum rate in April.

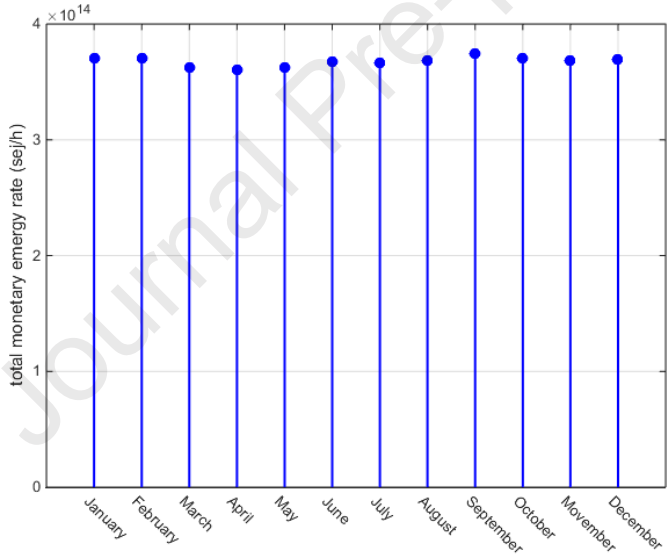

Fig. 18. Monthly total economic emergy rate of the polygeneration system integrated with the solar energy field.

The monthly cost rate based on the emergy associated with the exergy degradation of different system components is shown in **Fig. B.7** (**Appendix B**). As explained previously, the economizer operates in standby mode in September. Consequently, the monthly cost rate based on the emergy associated with the exergy degradation of this device is decreased. On the other hand,

the monthly cost rate based on the emergy associated with the exergy degradation of the ORC components is increased in September due to the organic fluid mass flowrate increase.

4.8. Emergoenvironmental Analysis

The results of emergoenvironmental analysis for both proposed system configurations are shown in **Table B.11** (without solar field) and **Table B.12** (with solar field). The results are reported for June. In this case, the maximum summation of the environmental emergy rate and component-related environmental emergy rate $\dot{N}_D + \dot{V}_k$ is attributable to the CC, followed by the CO_2 capture unit and the heat exchanger 1 when both scenarios are considered. According to the exergy analysis, for the polygeneration system without solar energy integration, the HDH desalination unit as the component with the lowest emergoenvironmental factor and the CO_2 capture unit and condensers 1 and 2 as the components with the highest amount of r_n should be considered to increase their exergy efficiency. While solar integration is studied, the HDH desalination unit, solar field pump, condensers 1 and 2 as components with the lowest emergoenvironmental factors and the solar collectors, solar field heat exchanger, and solar field pump as components with the highest amount of r_n should be considered to increase their exergy efficiency. Based on the emergoenvironmental analysis, the integration of solar energy field increases $\dot{V}_k + \dot{N}_D$ by 1.22%.

The total environmental emergy rate $\dot{N}_{TOT}$ for the integrated solar-assisted polygeneration system throughout the year is depicted in **Fig. 19**. In this case, the maximum total economic emergy rate occurs in September and the minimum amount in April. Finally, the monthly environmental emergy rate related to the exergy degradation of different system components is depicted in **Fig. B.8** (**Appendix B**). Once again, the environmental emergy rate related to the exergy destruction of the economizer is minimal in September due to its standby operation.

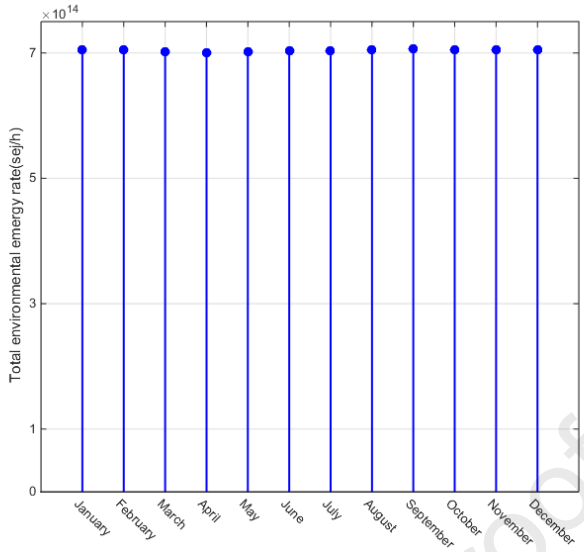

Fig. 19. Monthly total environmental emergy rate of the polygeneration system integrated with the solar energy field.

5. Conclusions

This study introduces a design and dynamic simulation approach of a new integrated solar-assisted polygeneration system to meet the power, freshwater, and CO_2 demands of greenhouse applications. The innovative polygeneration system integrates gas and steam turbine cycles, organic Rankine cycles (ORCs), humidification-dehumidification (HDH) desalination, post-combustion CO_2 capture unit, and parabolic trough collectors. Sensitivity analysis is applied to determine the optimal HDH operating conditions and identify the ideal ORC working fluid. Furthermore, comprehensive energy, exergy, exergoeconomic, exergoenvironmental, emergoeconomic, and emergoenvironmental (6E) analyses are performed on the polygeneration system for scenarios with and without solar energy integration. The main innovative features of this study are as follows:

i. Design of an advanced decentralized solar-assisted polygeneration system coupling ORC, CO_2 capture and HDH technologies to simultaneously meet several demands of greenhouses, which can easily be adapted to other low and large-scale buildings and industrial applications.

ii. Use of detailed 6E analyses allied to a more precise dynamic simulation to further investigate the advantages of using solar energy by evaluating several thermodynamic, economic and environmental performance indicators of the integrated system.

iii. Development of new weight functions and cost relations for several system components to enhance environmental and economic assessments.

Energy analysis results reveal that due to the solar incident angle, the highest monthly net power generation of the solar-assisted polygeneration system occurs in September (737.5 kW), while the lowest amount is in April (728.3 kW). Despite an increase of 18% in the overall plant exergy degradation, the solar energy integration boosts ORCs power generation from 37.3% (winter) to 59.41% (summer) and the overall plant power generation by 18 kW, compared to the base scenario (without solar energy). Exergoeconomic analysis results indicate that for both case scenarios, the CO_2 capture unit, combustion chamber, and ORC heat exchanger 1 present higher exergy costs to convert fuel into products, requiring exergy efficiency enhancement. In addition, solar energy integration increases the sum of cost rate and exergy destruction cost rate by 6.6%. Furthermore, the revenues of using solar energy and the system payback period are estimated at 50k US$/year and 4.67 years, correspondingly.

Exergoenvironmental analysis results show that both scenarios' highest environmental impact and exergy destruction rate is attributable to the combustion chamber, followed by the CO_2 capture unit and steam turbine 2. Moreover, a 3.9% increase is observed in the total environmental impact and exergy rate when the solar energy field is integrated into the polygeneration system.

The emergoeconomic analysis emphasizes that both case scenarios' maximum economic and component-related economic emergy rates are related to CO_2 capture unit, followed by the combustion chamber and heat exchanger 1. The solar energy integration increases the total emergy rates by 2.12%. The emergoenvironmental analysis shows that the maximum sum of environmental emergy and component-related environmental emergy rates is attributable to the combustion chamber, followed by the CO_2 capture unit and the heat exchanger 1 when both case studies are considered. In this case, the emergoenvironmental indicator increases by 1.22% when the solar energy field is integrated into the polygeneration system.

The previous 6E analyses also highlights that the listed system components should receive special attention in reducing irreversibilities and energy degradation to improve the plant's overall economic and environmental performances. Moreover, the price of these equipment units must be reduced as much as possible while their life cycle should be less harmful to the environment. Although additional costs and environmental impacts are related to integrating the solar energy field, it is still a cost-effective and environment-friendly solution for greenhouse applications due to the increase in the overall exergy and energy efficiencies and power generation. Finally, future research will focus on a more effective humidity supply with the aid of the cycle. For example, by designing a fogging system that uses generated freshwater and brings the greenhouse temperature to the optimum in winter using piping supplied from the plant waste heat. Additionally, optimization can be applied to the polygeneration system to further increase the energy efficiency.

Declaration of competing interest

The authors declare that they have no known competing financial interests or personal relationships that could have appeared to influence the work reported in this paper.

Acknowledgments

The authors thank the reviewers and editor for their valuable comments and suggestions.

Appendix A. Additional mathematical formulation and data used for the integrated polygeneration system design and dynamic simulation

Table A.1

Thermodynamic relations, assumptions (input parameters) and unknown variables (output values).

Component	Thermodynamic Relations	Inputs	Outputs
AC	$W_{AC} = \dot{m}_{air}(T_{ac,out}Cp_{ac,out} - T_1 Cp_1)$ $W_{AC} = W_{GT} - W_{net}$ $r_{p,AC} = P_{ac,out}/P_1$ $\eta_{AC} = (r_{p,AC}^{\frac{\gamma_{air}-1}{\gamma_{air}}} - 1)/(T_{ac,out}/T_1 - 1)$	$T_0 = 15℃$ $P_0 = 1.013$ bar $T_1 = T_0$ $P_1 = P_0$ $P_{ac,out} = 6.921$ $\dot{m}_{air} = 2.973$ $W_{net} = 497.3$	W_{AC} η_{AC} $r_{p,AC}$ $T_{ac,out}$
CC	$\dot{m}_{air}h_{ac,out} + \dot{m}_{fuel}LHV_{fuel}\eta_{CC} - \dot{m}_{fg}h_2 = 0$ $\dot{m}_{air} + \dot{m}_{fuel} - \dot{m}_{fg} = 0$ $P_{cc,out} = P_{ac,out}(1 - \Delta P_{CC})$	$LHV_{fuel} = 50047$ kJ /kg T_f, P_f $TIT = 887.2$ $\Delta P_{CC} = 0.04$ $\dot{m}_{fuel} = 0.0435$	$P_{cc,out}$ $\dot{m}_{fg}$ Q_{cc} η_{CC}
GT	$W_{GT} = \dot{m}_{fg}(h_{cc,out} - h_3)$ $P_{23} = P_0 + \sum \Delta P_{HRSG,fg}$ $r_{p,GT}=P_{cc,out}/P_3$ $\eta_{GT} = (1 - T_3/T_{cc,out})/(1 - r_{p,GT}^{\frac{1-\gamma_{fg}}{\gamma_{fg}}})$	$T_3 = TET = 519.8$	W_{GT} P_3 $r_{p,GT}$ η_{GT}
HPP	$v_9 = v_{sat@P_7}$ $h_{10} = h_9 + v_9 \times (P_{10} - P_9)$ $W_P = \dot{m}_s(h_{10} - h_9)$ $T_{10} = T_{@P_{10},h_{10}}$ $h_{10,is} = h_{@P_{10},s_{10,is}}$ $\eta_P = (h_{10,is} - h_9)/(h_{10} - h_9)$	$P_{10} = P_{pump,out}$	T_{10} W_P η_P
SUP	$\dot{m}_{fg}(h_4 - h_3) + \dot{m}_s(h_{13} - h_{12}) = 0$ $P_4 = P_3 - \Delta P_{SH,fg}$ $P_{13} = P_{12} - \Delta P_{SH,s}$ $T_{13} = T_{SH,out}$ $Q_{HPSH} = \dot{m}_s(h_{13} - h_{12})$ $h_{13} = h_{water@T_{13},P_{13}}$	T_3, P_3 $\Delta P_{SH,fg}$ $\Delta P_{SH,s}$ $T_{SH,out}$ T_{12} P_{12} $\dot{m}_s$	Q_{HPSH} T_{10}, P_{10} T_{28}, P_{28}
EVA	$\dot{m}_{fg}(h_5 - h_4) + \dot{m}_s(h_{12} - h_{11}) = 0$ $P_5 = P_4 - \Delta P_{EVA,fg}$ $P_{12} = P_{11} - \Delta P_{EVA,s}$ $Q_{EVA} = \dot{m}_{hp}(h_{28} - h_{22})$	T_4, P_4 $\Delta P_{EVA,fg}$ $\Delta P_{EVA,s}$ T_{11}, P_{11}	Q_{EVA} T_5, P_5 P_{12}
ECO	$\dot{m}_{fg}(h_6 - h_5) + \dot{m}_s(h_{11} - h_{10}) = 0$ $P_6 = P_5 - \Delta P_{ECO,fg}$ $P_{11} = P_{10} - \Delta P_{ECO,s}$ $T_{10} = T_{sat@P_{20}}$ $Q_{ECO} = \dot{m}_s(h_{11} - h_{10})$	T_{10}, P_{10} $\Delta P_{ECO,fg}$ $\Delta P_{ECO,s}$ T_{11}	Q_{ECO} T_6, P_6 P_{11}

ST 1	$\dot{m}_s(h_{13}-h_{14})-W_{ST,1}=0$ $h_{14}=h_{13}-\eta_{ST}(h_{13}-h_{14,is})$ $P_{13}=TIP_{ST1}$ $P_{14}=TIP_{ST2}$	$\eta_{ST}=88\%$ $\dot{m}_s$	W_{ST1} T_{14},P_{14}
ST 2	$\frac{\dot{m}_s}{2}(h_{15}-h_{17})-W_{ST,2}=0$ $h_{17}=h_{15}-\eta_{ST}(h_{15}-h_{17,is})$ $P_{15}=TIP_{ST2}$ $P_{17}=P_{18}\times\Delta P_{HX2,s}$	$\eta_{ST}=88\ \%$ P_{18} $\dot{m}_s$	W_{ST2} T_{17},P_{17}
HX 2	$Q_{HX,2}=\dot{m}_s(h_{17}-h_{18})$ $P_{28}=P_{25}-\Delta P_{HX2,ORC}$	T_{18} T_{28} T_{17} $\Delta P_{HX2,s}$ $\Delta P_{HX2,ORC}$ P_{17}	$Q_{HX,2}$ P_{28}
ORC T 2	$\dot{m}_{ORC,1}(h_{28}-h_{27})-W_{ORCT,2}=0$ $h_{27}=h_{28}-\eta_{ST}(h_{28}-h_{27,is})$	$T_{27},\ P_{27}$ η_{ORC}	$W_{ORCT,2}$
Cond 2	$\dot{m}_{ORC,2}(h_{19}-h_{26})+\dot{m}_{cw}(h_{29}-h_{30})=0$ $Q_{cond,2}=\dot{m}_{ORC,2}(h_{27}-h_{26})$ $T_{30}=T_{29}+\Delta T_{CW}$ $P_{30}=P_{29}-\Delta P_{cond}$ $P_{26}=P_{27}$ $T_{26}=T_{sat@P_{26}}$ $h_{26}=h_{@P_{26},T_{26}},h_{29}=h_{water@T_{39},P_{39}}$	$T_{29},\ P_{29}$ ΔT_{CW}	$Q_{cond,2}$ $\dot{m}_{cw}$ T_{26},P_{26} T_{30},P_{30}
ORCP 2	$P_{25}=P_{26}+\Delta P_{ORCpump,2}$ $v_{26}=v_{sat@P_{26}}$ $h_{25}=h_{26}+v_{26}\times(P_{25}-P_{26})$ $W_{ORC,P2}=\dot{m}_{ORC,2}(h_{25}-h_{26})$ $T_{25}=T_{@P_{25},h_{25}}$ $h_{25,is}=h_{@P_{25},s_{25,is}}$ $\eta_{ORCpump,2}=(h_{25,is}-h_{26})/(h_{25}-h_{26})$	$\Delta P_{ORCpump,2}$ P_{26}	P_{25} $W_{ORC,P2}$ T_{25} $\eta_{ORCpump,2}$ $\dot{m}_{ORC,2}$ h_{25}
HX 1	$P_7=P_6-\Delta P_{HX1,s}$ $Q_{HX,1}=\dot{m}_s(h_6-h_7)$ $P_{22}=P_{19}-\Delta P_{HX1,ORC}$	T_7 T_{22} T_6 $\Delta P_{HX1,s}$ $\Delta P_{HX1,ORC}$ P_6	$Q_{HX,1}$ P_7 P_{22}
ORC T1	$\dot{m}_{ORC,1}(h_{22}-h_{21})-W_{ORCT,1}=0$ $h_{22}=h_{21}-\eta_{ST}(h_{21}-h_{22,is})$	$T_{21},\ P_{21}$ η_{ORC}	$W_{ORCT,1}$
Cond 1	$\dot{m}_{ORC.1}(h_{21}-h_{20})+\dot{m}_{cw}(h_{23}-h_{24})=0$ $Q_{cond,1}=\dot{m}_{ORC,1}(h_{21}-h_{20})$ $T_{24}=T_{23}+\Delta T_{CW}$ $P_{24}=P_{23}-\Delta P_{cond}$ $P_{20}=P_{21}$ $T_{20}=T_{sat@P_{20}}$ $h_{20}=h_{@P_{20},T_{20}},h_{23}=h_{water@T_{23},P_{23}}$	$T_{23},\ P_{23}$ ΔT_{CW}	$Q_{cond,1}$ $\dot{m}_{cw}$ T_{24},P_{24} T_{20},P_{20}

ORCP 1	$P_{19} = P_{20} + \Delta P_{ORCpump,1}$ $v_{20} = v_{sat@P_{20}}$ $h_{19} = h_{20} + v_{20} \times (P_{19} - P_{20})$ $W_{ORC,P1} = \dot{m}_{ORC,2}(h_{19} - h_{20})$ $T_{19} = T_{@P_{19},h_{19}}$ $h_{19,is} = h_{@P_{19},s_{19,is}}$ $\eta_{ORCpump,1} = (h_{19,is} - h_{20})/(h_{19} - h_{20})$	$\Delta P_{ORCpump,1}$ P_{20}	P_{19} $W_{ORC,P1}$ T_{19} $\eta_{ORCpump,1}$ $\dot{m}_{ORC,1}$ h_{19}
CO_2 capture	$\dot{m}_{CO2.in} = \frac{x_{CO2}M_{CO2}}{x_{CO2}M_{CO2} + x_{O2}M_{O2} + x_{H2O}M_{H2O} + x_{N2}M_{N2}} \times m_{fg}$ $\dot{m}_{CO2.out} = \eta_{CO2Capture}\dot{m}_{CO2.in}$ $T_{41} = T_{sat@P_{41}}$ $T_{31} = T_{32} + \Delta T_{cw}$ $Q_{in,CO2Capture} = 4.028024024057373 \times (\eta_{CO2Capture} \times 100 - 0.00178987160251154)$ $EL_{CO2Capture} = 46.9926801139968 + 0.492473855348899 \times \eta_{CO2Capture} \times 100$ $W_{CO2Capture} = 0.438814557877626 \times (\eta_{CO2Capture} \times 100 - 0.000179238981772301)$	$T_8 = T_{stack}$ $P_8 = P_0$ $T_{16} = T_{11}$ $P_{16} = P_{11} = P_{41}$ T_{32}, P_{32} ΔT_{cw} T_{33}, P_{33} $\eta_{CO2Capture}$	$\dot{m}_{CO2.in}$ $\dot{m}_{CO2.out}$ T_{41} T_{22} $Q_{in,CO2Captur}$ $EL_{CO2Capture}$ $W_{CO2Capture}$
Solar Energy Field	$T_{43} = T_{46} + \Delta T_{pinchSFHX}$ $P_{48} = P_{47} + \Delta P_{SFpump}$ $P_{43} = P_{48} - \Delta P_{solarfield}$ $m_{47}C_{p(therminoll)}(T_{43} - T_{47}) = m_{42}(h_{46} - h_{42})$ (Kabiri et al., 2020) $C_{p(therminoll)} = 1.498 + (0.002414)T + (5.9591 \times 10^{-6})T^2 - (2.9879 \times 10^{-8})T^3 + (4.4172 \times 10^{-11})T^4$ $m_{42} = (1 - SF)m_{20}$ $Q_{solar} = A_c.DNI$ (Tzivanidis et al., 2016) $A_c = n_{mirror}.A_{mirror}$ $A_{mirror} = \frac{A_{module}}{7}$ (Lüpfert et al., 2003) $A_{module} = 12 \times 5.77$ (m^2) $Q_u = m_{48}.C_{p(therminoll)}.(T_{out} - T_{in})$ (Tzivanidis et al., 2016) $Q_u = \eta_c.Q_{solar}$ $\eta_c = 0.75 - 0.000045.(T_{in} - T_{am}) - 0.039.\left(\frac{T_{in} - T_{am}}{DNI}\right) - 0.0003.DNI.\left(\frac{T_{in} - T_{am}}{DNI}\right)^2$	ΔP_{SFpump} $\Delta P_{solarfield}$ SF DNI $T_8 = T_{46}$ $\Delta T_{pinchSFHX}$ A_{module} n_{mirror}	m_{47} P_{48} P_{43} T_{43} A_{mirror} m_{42} A_c

Humidifier **(Zamen et al., 2013)**	$dL_h = Gd\omega_h$ $GC_{Pg,h}dT_{g,h} = h_g a(T_{i,h} - T_{g,h})$ $L_h C_{PL,h}dT_{L,h} = (h_{L,h}a + C_{PL,h}dL_h)(T_{L,h} - T_{i,h})$ $Gd\omega_{g,h} = k_{g,h}a(\omega_{i,h} - \omega_{g,h})$ $GC_{Pg,h}dT_{g,h} + C_{PL,h}dT_{L,h}L_h + G(C_{Pv}(T_{g,h} - T_0)$ $- C_{PL,h}(T_{L,h} - T_0) + \lambda_0)d\omega_h$ $\omega_i = 2.19 \times 10^{-6}T_i^3 - 1.85 \times 10^{-4}T_i^2$ $+ 7.06 \times 10^{-2}T_i - 0.077$	$L_{h,in}$ G h_g a $k_{g,h}$ λ_0 $\omega_{in,h}$ $T_{L,h,in}$ $T_{g,h,in}$	L_h $T_{g,h}$ $T_{L,h}$ $T_{i,h}$ $\omega_{g,h}$ $\omega_{i,h}$
Dehumidifier **(Zamen et al., 2013)**	$dL_d = Gd\omega_d$ $GC_{Pg,d}dT_{g,d} = h_g a(T_{g,d} - T_{i,d})$ $L_d C_{PL,d}dT_{L,d} = (h_{L,d}a + C_{PL,d}dL_d)(T_{i,d} - T_{L,d})$ $Gd\omega_{g,d} = k_{g,d}a(\omega_{g,d} - \omega_{i,d})$ $GC_{Pg,d}dT_{g,d} + C_{PL,d}dT_{L,d}L_d + G(C_{Pv}(T_{g,d} - T_0)$ $- C_{PL,d}(T_{L,d} - T_0) + \lambda_0)d\omega_d$ $\omega_i = 2.19 \times 10^{-6}T_i^3 - 1.85 \times 10^{-4}T_i^2$ $+ 7.06 \times 10^{-2}T_i - 0.077$	$L_{d,in}$ G h_g a $k_{g,d}$ λ_0 $\omega_{in,d}$ $T_{g,h}$	L_d $T_{g,d}$ $T_{L,d}$ $T_{i,d}$ $\omega_{g,d}$ $\omega_{i,d}$

Table A.2

Cost relations and auxiliary equations for the different system components.

Component	Cost Equations	Auxiliary Equations
AC	$c_1 \times \dot{E}_1 + c_{w,AC} \times \dot{W}_{AC} + \dot{Z}_{AC} = c_{AC,out} \times \dot{E}_{AC,out}$	$c_1 = 0$
CC	$c_{AC,out} \times \dot{E}_{AC,out} + c_2 \times \dot{E}_2 + \dot{Z}_{CC} = c_{CC,out} \times \dot{E}_{CC,out}$	
GT	$c_{CC.out} \times \dot{E}_{CC,out} + \dot{Z}_{GT} = c_{w,GT} \times \dot{W}_{GT} + c_3 \times \dot{E}_3$	$c_{w,AC} = c_{w,GT}$
ECO	$c_{10} \times \dot{E}_{10} + c_5 \times \dot{E}_5 + \dot{Z}_{ECO} = +c_6 \times \dot{E}_6 + c_{11} \times \dot{E}_{11}$	$c_6 = c_5 = c_3$
EVA	$c_4 \times \dot{E}_4 + c_{11} \times \dot{E}_{11} + \dot{Z}_{EVA} = +c_5 \times \dot{E}_5 + c_{12} \times \dot{E}_{12}$	$c_4 = c_3$
SUP	$c_{12} \times \dot{E}_{12} + c_3 \times \dot{E}_3 + \dot{Z}_{SUP} = c_{13} \times \dot{E}_{13} + c_4 \times \dot{E}_4$	
HPP	$c_9 \times \dot{E}_9 + c_{w,HPP} \times \dot{W}_{HPP} + \dot{Z}_{HPP} = c_{10} \times \dot{E}_{10}$	$c_7 = 0 \quad c_{w,HPP} = c_{w,ST}$
ST 1	$c_{13} \times \dot{E}_{13} + \dot{Z}_{ST1} = c_{14} \times \dot{E}_{14} + c_{w.ST1} \times \dot{W}_{ST1}$	$c_{14} = c_{13}$
ST 2	$c_{14} \times \dot{E}_{14} + \dot{Z}_{ST2} = c_{15} \times \dot{E}_{15} + c_{w.ST2} \times \dot{W}_{ST2}$	$c_{15} = c_{13}$
HX 2	$c_{17} \times \dot{E}_{17} + c_{25} \times \dot{E}_{25} + \dot{Z}_{HX2} = c_{18} \times \dot{E}_{18} + c_{28} \times \dot{E}_{28}$	$c_{17} = c_{18} = c_{13}$
ORCT 2	$c_{28} \times \dot{E}_{28} + \dot{Z}_{ORCT2} = c_{27} \times \dot{E}_{27} + c_{w,ORCT2} \times \dot{W}_{ORCT2}$	$c_{28} = c_{27}$
Cond 2	$c_{27} \times \dot{E}_{27} + c_{29} \times \dot{E}_{29} + \dot{Z}_{Cond2} = c_{30} \times \dot{E}_{30} + c_{26} \times \dot{E}_{26}$	$c_{27} = c_{26}$
ORCP 2	$c_{26} \times \dot{E}_{26} + c_{w,ORCP2} \times \dot{W}_{ORCP2} + \dot{Z}_{ORCP2} = c_{25} \times \dot{E}_{25}$	$c_{w,ORCP2} = c_{w,ST}$
HX 1	$c_6 \times \dot{E}_6 + c_{19} \times \dot{E}_{19} + \dot{Z}_{HX1} = c_7 \times \dot{E}_7 + c_{22} \times \dot{E}_{22}$	$c_6 = c_7 = c_3$
ORCT 1	$c_{22} \times \dot{E}_{22} + \dot{Z}_{ORCT1} = c_{21} \times \dot{E}_{21} + c_{w,ORCT1} \times \dot{W}_{ORCT1}$	$c_{22} = c_{21}$
Cond 1	$c_{23} \times \dot{E}_{23} + c_{21} \times \dot{E}_{21} + c_{38} \times \dot{E}_{38} + \dot{Z}_{\mathrm{Cond1}}$ $= c_{24} \times \dot{E}_{24} + c_{20} \times \dot{E}_{20}$	$c_{21} = c_{20}$
ORCP 1	$c_{20} \times \dot{E}_{20} + c_{w,ORCP1} \times \dot{W}_{ORCP1} + \dot{Z}_{ORCP1} = c_{19} \times \dot{E}_{19}$	$c_{w,ORCP1} = c_{w,ST}$

CO₂ capture	$c_{32} \times \dot{E}_{32}+c_7 \times \dot{E}_7+c_{16} \times \dot{E}_{16}+\dot{Z}_{CO2}$ $= c_{33} \times \dot{E}_{33} + c_{31} \times \dot{E}_{31} + c_{41} \times \dot{E}_{41}$ $+ c_8 \times \dot{E}_8$	$c_{32} = c_{31} = 0$ $c_{16} = c_{41} = c_{13}$
Solar field	$c_{44} \times \dot{E}_{44} + c_{sun} \times \dot{E}_{sun}+\dot{Z}_{Solar} = c_{45} \times \dot{E}_{45}$	$c_{sun} = 0$
SFHX	$c_{42} \times \dot{E}_{42} + c_{46} \times \dot{E}_{46} + \dot{Z}_{SFHX} = c_{43} \times \dot{E}_{43} + c_{47} \times \dot{E}_{47}$	$c_{43} = c_{46}$
SFP	$c_{43} \times \dot{E}_{43} + c_{w,SFP} \times \dot{W}_{SFP} + \dot{Z}_{SFP} = c_{44} \times \dot{E}_{44}$	$c_{w,SFP} = c_{w,ST}$
Humidifier	$c_{34} \times \dot{E}_{34} + c_{35} \times \dot{E}_{35} + \dot{Z}_{humidifier}$ $= c_{36} \times \dot{E}_{36} + c_{37} \times \dot{E}_{37}$	$c_{35} = 0$ $c_{34} = c_{18}$
Dehumidifier	$c_{36} \times \dot{E}_{36} + c_{40} \times \dot{E}_{40} + \dot{Z}_{dehumidifier}$ $= c_{38} \times \dot{E}_{38} + c_{39} \times \dot{E}_{39}$	$c_{40} = 0$

Table A.3

Purchasing cost relations for the different system components.

Component	Capital Investment Cost (US$)	Reference
AC	$Z_{AC} = 0.076 + 0.0003 \times \dot{W}_{net} \times 10^6$	*(proposed)*
CC	$Z_{CC} = 0.046 + 0.0002 \times \dot{W}_{net} \times 10^6$	*(proposed)*
GT	$Z_{GT} = (0.073 + 0.001 \times \dot{W}_{net} - 1.183 \times 10^{-7} \times \dot{W}_{net}^2) \times 10^6$	*(proposed)*
ECO	$Z_{\mathrm{ECO}} = 6570(\dot{Q}_{ECO}/\Delta T_{ECO})^{0.8} + 21276\dot{m}_w + 1184.4\dot{m}_g^{1.2}$	(Cavalcanti, 2017)
EVA	$Z_{\mathrm{EVA}} = 6570(\dot{Q}_{EVA}/\Delta T_{EVA})^{0.8} + 21276\dot{m}_w + 1184.4\dot{m}_g^{1.2}$	(Cavalcanti, 2017)
SUP	$Z_{\mathrm{SUP}} = 6570(\dot{Q}_{SUP}/\Delta T_{SUP})^{0.8} + 21276\dot{m}_w + 1184.4\dot{m}_g^{1.2}$	(Cavalcanti, 2017)
HPP	$Z_{Pump} = 3540\left(\dot{W}_{Pump}\right)^{0.7}$	(Dincer et al., 2017)
ST 1	$Z_{\mathrm{ST1}} = 2210\left(\dot{W}_{ST1}\right)^{0.7}$	(Cavalcanti, 2017)
ST 2	$Z_{\mathrm{ST2}} = 2210\left(\dot{W}_{ST2}\right)^{0.7}$	(Cavalcanti, 2017)
HX 2	$Z_{\mathrm{HX2}} = 1000(A_{HX2})^{0.65}$	(Dincer et al., 2017)
ORCT 2	$Z_{\mathrm{ORCT2}} = 4750\left(\dot{W}_{ORCT2}\right)^{0.75}$	(Dincer et al., 2017)
Cond 2	$Z_{\mathrm{Cond2}} = 1773\dot{m}_{ORC1}$	(Cavalcanti, 2017)
ORCP 2	$Z_{\mathrm{ORCP2}} = 200(\dot{W}_{ORCP2})^{0.65}$	(Dincer et al., 2017)
HX 1	$Z_{\mathrm{HX1}} = 1000(A_{HX1})^{0.65}$	(Dincer et al., 2017)
ORCT 1	$Z_{\mathrm{ORCT1}} = 4750\left(\dot{W}_{ORCT1}\right)^{0.75}$	(Dincer et al., 2017)

Cond 1	$Z_{\text{Cond1}} = 1773\dot{m}_{ORC2}$	(Cavalcanti, 2017)
ORCP 1	$Z_{\text{ORCP1}} = 200(\dot{W}_{ORCP1})^{0.65}$	(Dincer et al., 2017)
CO_2 capture	$Z_{\text{CO2}} = 74\ US\$/\text{ton CO}_2$	(Rubin et al., 2015)
Solar Field	$Z_{Solar} = 355\ \text{US\$/m}^2$ aperture area	(Cavalcanti, 2017)
SFHX	$Z_{SFHX} = 12000(A/100)^{0.6}$	(Cavalcanti, 2017)
SFP	$Z_{SFP} = 3540\left(\dot{W}_{SFP}\right)^{0.7}$	(Dincer et al., 2017)
Humidifier	$Z_{humidifier} = 746.749.\left(L_{h,in}\right)^{0.79}.(R_h)^{0.57}.(A_h)^{-0.9924}.(0.022T_{wb} + 0.39)^{2.447}$ $R_h = T_{35} - T_{36}$ $A_h = T_{35} - T_{wb}$	(Gholizadeh et al., 2020)
Dehumidifier	$Z_{dehumidifier} = 2143(A_{dehumidifier})^{0.514}$	(Gholizadeh et al., 2020)

Table A.4

Fuel-product cost rate relations for the different system components.

Component	Fuel	Product
AC	$\dot{C}_{AC}$	$\dot{C}_{AC,out} - \dot{C}_1$
CC	$\dot{C}_{fuel}$	$\dot{C}_{CC,out} - \dot{C}_{AC,out}$
GT	$\dot{C}_{CC,out} - \dot{C}_3$	$\dot{C}_{w,GT}$
ECO	$\dot{C}_5 - \dot{C}_6$	$\dot{C}_{11} - \dot{C}_{10}$
EVA	$\dot{C}_4 - \dot{C}_5$	$\dot{C}_{12} - \dot{C}_{11}$
SUP	$\dot{C}_3 - \dot{C}_4$	$\dot{C}_{13} - \dot{C}_{12}$
HPP	$\dot{C}_{w,HPP}$	$\dot{C}_{10} - \dot{C}_9$
ST 1	$\dot{C}_{13} - \dot{C}_{14}$	$\dot{C}_{w,ST1}$
ST 2	$\dot{C}_{14} - \dot{C}_{15}$	$\dot{C}_{w,ST2}$
HX 2	$\dot{C}_{17} - \dot{C}_{18}$	$\dot{C}_{28} - \dot{C}_{25}$
ORCT 2	$\dot{C}_{28} - \dot{C}_{27}$	$\dot{C}_{ORCT2}$
Cond 2	$\dot{C}_{27} - \dot{C}_{26}$	$\dot{C}_{30} - \dot{C}_{29}$
ORCP 2	$\dot{C}_{w,ORCP2}$	$\dot{C}_{25} - \dot{C}_{26}$
HX 1	$\dot{C}_6 - \dot{C}_7$	$\dot{C}_{22} - \dot{C}_{19}$
ORCT 1	$\dot{C}_{22} - \dot{C}_{21}$	$\dot{C}_{w,ORCT1}$
Cond 1	$\dot{C}_{21} - \dot{C}_{20}$	$\dot{C}_{24} - \dot{C}_{23}$
ORCP 1	$\dot{C}_{w,ORCP1}$	$\dot{C}_{19} - \dot{C}_{20}$
CO_2 Capture	$\dot{C}_7 + \dot{C}_{16} + \dot{C}_{32} + \dot{C}_{CO2} - \dot{C}_{31} - \dot{C}_{41} - \dot{C}_8$	$\dot{C}_{33}$
Solar field	$\dot{C}_{sun}$	$\dot{C}_{45} - \dot{C}_{44}$
SFHX	$\dot{C}_{46} - \dot{C}_{43}$	$\dot{C}_{47} - \dot{C}_{42}$

SFP	$\dot{C}_{w,solarPump}$	$\dot{C}_{44} - \dot{C}_{43}$
Humidifier	$\dot{C}_{34} - \dot{C}_{37}$	$\dot{C}_{36} - \dot{C}_{35}$
Dehumidifier	$\dot{C}_{36} + \dot{C}_{40} - \dot{C}_{38}$	$\dot{C}_{39}$

Table A.5
Emergoeconomic and emergoenvironmental governing equations (Aghbashlo and Rosen, 2018).

Definition	**Emergy-based Equation**
Emergy cost balance	$\sum_{i}^{N}\left(m_i\dot{E}_i\right)_k + m_{q.k}\dot{E}_{q.k} + \dot{U}_k = \sum_{e}^{N}\left(m_e\dot{E}_e\right)_k + m_{w.k}\dot{W}_{q.k}$
Component-related economic emergoeconomic	$\dot{U}_k = \dot{U}_k^{CI} + \dot{U}_k^{OM}$
Economic emergy rate associated with exergy destruction	$\dot{M}_{D.k} = m_{F.k}\dot{E}_{D.k}$
Total economic emergy rate	$\dot{M}_{TOT.k} = \dot{M}_{D.k} + \dot{U}_k$
Specific emergoeconomic values for fuel	$m_{F,k} = \frac{\dot{M}_{F,k}}{\dot{E}_{F,k}}$
Specific emergoeconomic values for product	$m_{P,k} = \frac{\dot{M}_{P,k}}{\dot{E}_{P,k}}$
Relative emergy-based cost difference	$r_{m.k} = (m_{P.k} - m_{F.k})/m_{P.k}$
Emergy-based exergoeconomic factor	$f_{m.k} = \dot{U}_k/\left(\dot{U}_k + \dot{M}_{D.k}\right)$
Emergy-based exergoenvironmental balance	$\sum_{i}^{N}\left(n_i\dot{E}_i\right)_k + n_{q.k}\dot{E}_{q.k} + \dot{V}_k = \sum_{e}^{N}\left(n_e\dot{E}_e\right)_k + n_{w.k}\dot{W}_{q.k}$
Environmental emergy rate	$\dot{V}_k = \dot{V}_k^{CO} + \dot{V}_k^{OM} + \dot{V}_k^{DI}$
Environmental impact rate associated with exergy destruction	$\dot{N}_{D.k} = n_{F.k}\dot{E}_{D.k}$
Total environmental emergy rate	$\dot{N}_{TOT.k} = \dot{N}_{D.k} + \dot{V}_k$
Specific emergoenvironmental values for fuel	$n_{F,k} = \frac{\dot{N}_{F,k}}{\dot{E}_{F,k}}$
Specific emergoenvironmental values for product	$n_{P,k} = \frac{\dot{N}_{P,k}}{\dot{E}_{P,k}}$
Relative environmental emergy difference	$r_{n.k} = (n_{P.k} - n_{F.k})/n_{P.k}$
Emergy-based exergoenvironmental factor	$f_{n.k} = \frac{\dot{V}_k}{\left(\dot{V}_k + \dot{N}_{D.k}\right)}$

Appendix B. Additional design, dynamic simulation and 6E analyses results obtained for the integrated polygeneration system

B.1 Thermodynamic Analysis

Table B.1

Thermodynamic properties of process streams for the polygeneration system configuration without solar energy field (**Fig. 1**).

	$\dot{m}$ (kg/s)			T (°C)			P (bar)		
Stream	*THFX*	*Code*	*Error (%)*	*THFX*	*Code*	*Error (%)*	*THFX*	*Code*	*Error (%)*
1	2.973	2.973	0	15	15	0	1.013	1.013	0
AC, out	2.973	2.973	0	267.3	264.4	1.08	6.92	6.92	0
2	0.043	0.043	0	25	25	0	9.79	9.79	0
CC, out	3.017	3.017	0	887.2	887.2	0	6.644	6.644	0
3	3.017	3.017	0	519.8	519.8	0	1.043	1.044	0.001
4	3.017	3.017	0	455.2	456.4	0.2	1.041	1.041	0
5	3.017	3.017	0	273.6	272.7	0.3	1.036	1.036	0
6	3.017	3.017	0	189.7	189.6	0.05	1.034	1.034	0
7	3.017	3.017	0	157.3	157.3	0	1.013	1.013	0
8	2.894	2.892	0.06	35	35	0	1.013	1.013	0
9	0.3178	0.3178	0	15	15	0	1.04	1.04	0
10	0.3178	0.3178	0	15.17	15.05	0.8	20.4	20.4	0
11	0.3178	0.3178	0	212.9.	212.9	0	20.2	20.2	0
12	0.3178	0.3178	0	212.9	212.9	0	20.2	20.2	0
13	0.3178	0.3178	0	510	510	0	20	20	0
14	0.3178	0.3178	0	228	227.2	0.3	2	2	0
15	0.3178	0.3178	0	165.6	163.6	1.2	2	2	0
16	0.159	0.159	0	165.6	163.6	1.2	2	2	0
17	0.159	0.159	0	165.6	163.6	1.2	1.034	1.034	0
18	0.159	0.159	0	80	80	0	1.014	1.014	0
19	0.454	0.429	5.5	27.63	27.72	0.3	4.08	4.08	0
20	0.454	0.429	5.5	27.46	27.46	0	1	1	0
21	0.454	0.429	5.5	74.06	73.92	0.1	1	1	0
22	0.454	0.429	5.5	108.7	108.7	0	4	4	0
23	2.287	2.159	5.6	15	15	0	1.013	1.013	0
24	2.287	2.159	5.6	24.68	24.68	0	0.994	0.994	0
25	1.708	1.72	0.7	27.61	27.7	0.3	3.512	3.514	0.06
26	1.708	1.72	0.7	27.46	27.46	0	1	1	0
27	1.708	1.72	0.7	79.42	79.27	0.2	1	1	0
28	1.708	1.72	0.7	110.1	110.1	0	3.443	3.444	0.03

29	8.771	8.825	0.6	24.68	24.68	0	1.573	1.573	0
30	8.771	8.825	0.6	15	15	0	1.542	1.525	1.1
31	21.79	21.79	0	25	25	0	2.068	2.068	0
32	21.79	21.79	0	15	15	0	3.447	3.447	0
33	0.109	0.112	0.03	35	35	0	151.7	151.7	0

Table B.2

Thermodynamic properties of process streams for the polygeneration system configuration integrated with the solar energy field (**Fig. 2**).

	***ṁ* (kg/s)**			***T* (°C)**			***P* (bar)**		
Stream	*THFX*	*Code*	*Error (%)*	*THFX*	*Code*	*Error (%)*	*THFX*	*Code*	*Error (%)*
1	2.973	2.973	0	15	15	0	1.013	1.013	0
AC, out	2.973	2.973	0	267.3	264.4	1.08	6.92	6.92	0
2	0.043	0.043	0	25	25	0	9.79	9.79	0
CC, out	3.017	3.017	0	887.2	887.2	0	6.644	6.644	0
3	3.017	3.017	0	519.8	519.8	0	1.043	1.044	0.001
4	3.017	3.017	0	455.2	456.4	0.2	1.041	1.041	0
5	3.017	3.017	0	276.4	276.3	0.04	1.036	1.036	0
6	3.017	3.017	0	259.7	260.29	0.2	1.034	1.034	0
7	3.017	3.017	0	227.8	227.8	0	1.013	1.013	0
8	2.894	2.892	0.06	35	35	0	1.013	1.013	0
9	0.3178	0.3178	0	15	15	0	1.04	1.04	0
10	0.3178	0.3178	0	15.17	15.05	0.8	20.4	20.4	0
11	0.3178	0.3178	0	212.9.	212.9	0	20.2	20.2	0
12	0.3178	0.3178	0	212.9	212.9	0	20.2	20.2	0
13	0.3178	0.3178	0	510	510	0	20	20	0
14	0.3178	0.3178	0	228	227.2	0.3	2	2	0
15	0.3178	0.3178	0	165.6	163.6	1.2	2	2	0
16	0.159	0.159	0	165.6	163.6	1.2	2	2	0
17	0.159	0.159	0	165.6	163.6	1.2	1.034	1.034	0
18	0.159	0.159	0	80	80	0	1.014	1.014	0
19	0.454	0.429	5.5	27.63	27.72	0.3	4.08	4.08	0
20	0.454	0.429	5.5	27.46	27.46	0	1	1	0
21	0.454	0.429	5.5	74.06	73.92	0.1	1	1	0
22	0.454	0.429	5.5	108.7	108.7	0	4	4	0
23	2.287	2.159	5.6	15	15	0	1.013	1.013	0
24	2.287	2.159	5.6	24.68	24.68	0	0.994	0.994	0
25	1.708	1.72	0.7	27.61	27.7	0.3	3.512	3.514	0.06
26	1.708	1.72	0.7	27.46	27.46	0	1	1	0
27	1.708	1.72	0.7	79.42	79.27	0.2	1	1	0
28	1.708	1.72	0.7	110.1	110.1	0	3.443	3.444	0.03
29	8.771	8.825	0.6	24.68	24.68	0	1.573	1.573	0

30	8.771	8.825	0.6	15	15	0	1.542	1.525	1.1
31	21.79	21.79	0	25	25	0	2.068	2.068	0
32	21.79	21.79	0	15	15	0	3.447	3.447	0
33	0.109	0.112	0.03	35	35	0	151.7	151.7	0
42	0.254	0.258	1.5	15.17	15.17	0	20.6	20.6	0
43	0.681	0.659	3.23	45.15	45.18	0.06	1.014	1.014	0
44	0.681	0.659	3.23	45.16	45.18	0.04	1.137	1.138	0.09
45	0.681	0.659	3.23	222.9	222.9	0	1.034	1.034	0
46	0.254	0.258	1.5	212.9	212.9	0	20.2	20.2	0
47	0.063	0.6	4.76	15.17	15.17	0	20.4	20.6	0.98
48	0.063	0.6	4.76	212.9	212.9	0	20.2	20.2	0

B.2 Sensitivity Analysis of HDH Desalination Unit

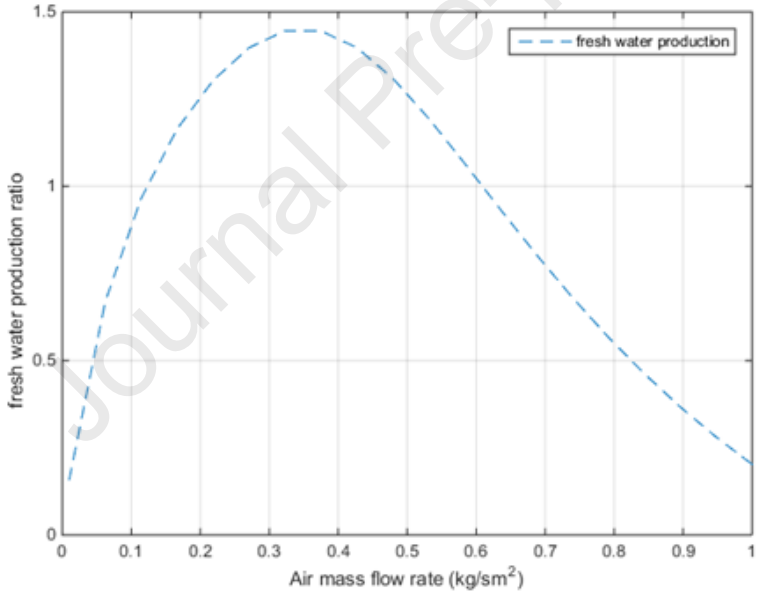

Fig. B.1. Effect of air mass flowrate on the HDH freshwater production.

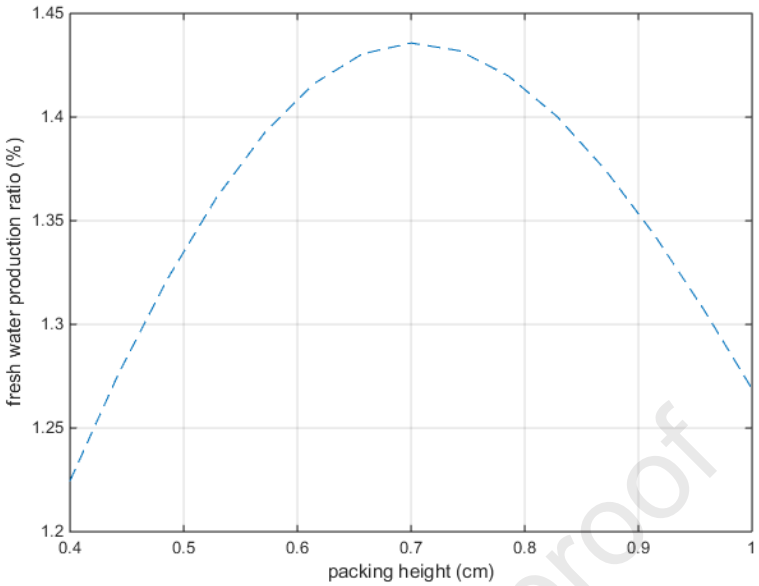

Fig. B.2. Effect of packing height on the HDH freshwater production.

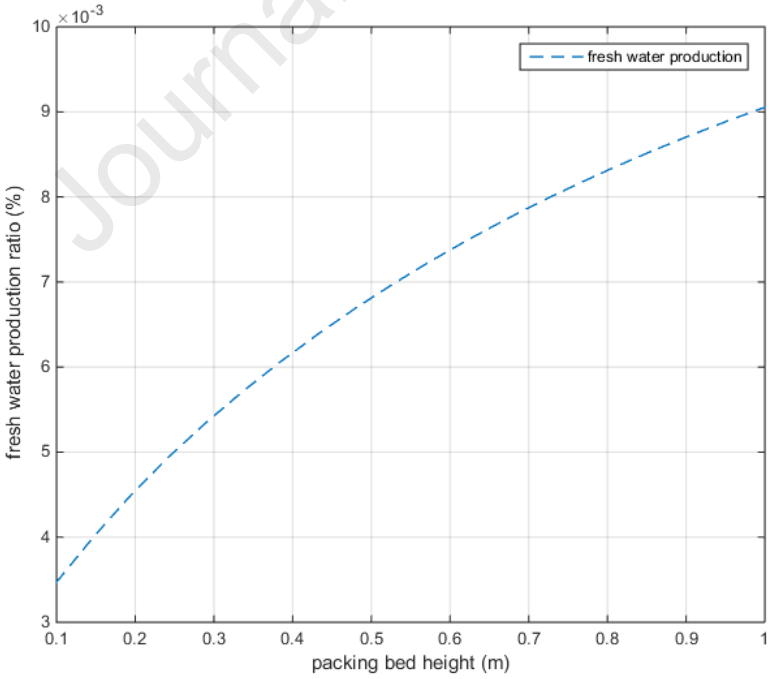

Fig. B.3. Effect of packing length on the HDH freshwater production.

B.3 Exergy Analysis

Table B.3

Exergy analysis results of the polygeneration system integrated with solar energy field.

Component	$\dot{E}_{F,k}$ (kW)	$\dot{E}_{P,k}$ (kW)	$\dot{E}_{D,k}$ (kW)	ε_k (%)
AC	796.20	680.46	115.73	85.46
CC	2936	2033.1	902.88	69.25
GT	1318	1293.5	24.08	98.17
ECO	22.63	11.93	10.69	52.74
EVA	313.85	244.18	75.01	77.8
SUP	165.6	116.62	48.98	70.42
ST 1	191.27	173.15	18.12	90.53
ST 2	42.97	38.53	4.44	90.53
HPP	0.83	0.62	0.21	74.66
ORCT 1	35.1	30.58	4.52	87.13
ORCHX 1	133.33	49.62	83.71	37.11
ORCP 1	0.29	0.29	0	100
COND 1	14.81	4.58	10.34	30.91
ORCT 2	42.4	37	5.37	87.31
ORCHX 2	91.77	58.69	31.5	63.96
ORCP 2	0.3	0.3	0	100
COND 2	19.42	5.77	14.9	29.45
CO_2 Capture	213.14	51.19	161.95	24.02
Solar Field	157.83	0.71	97.8	38.02
SFHX	60	0.22	7.5	86.28
SFP	0.01	0.001	0.01	9.48
Humidifier	0.89	0.71	0.17	80.41
Dehumidifier	0.39	0.22	0.17	56.42

Table B.4

Exergy analysis results of the polygeneration system without the solar energy field.

Component	$\dot{E}_{F,k}$ (kW)	$\dot{E}_{P,k}$ (kW)	$\dot{E}_{D,k}$ (kW)	ε_k (%)
AC	796.20	680.46	115.73	85.46
CC	2936	2033.1	902.88	69.25
GT	1318	1293.5	24.08	98.17
ECO	110.18	64.85	45.33	58.86
EVA	319.28	244.18	75.01	76.48
SUP	165.61	116.62	48.98	70.42
ST 1	193.89	179.26	14.64	92.45
ST 2	42.66	39.11	3.55	92.46
HPP	0.64	0.59	0.05	92.01
ORCT 1	10.86	9.46	1.41	87.13

ORCHX 1	40.14	15.35	25.02	38.24
ORCP 1	0.09	0.09	0	100
COND 1	4.58	1.42	3.2	30.91
ORCT 2	39.07	34.11	5	87.31
ORCHX 2	90.6	58.2	32.41	64.23
ORCP 2	0.29	0.29	0	100
COND 2	19.42	5.71	13.74	29.45
CO_2 capture	212.03	51.19	160.84	24.14
Humidifier	0.89	0.71	0.17	80.41
Dehumidifier	0.39	0.22	0.17	56.42

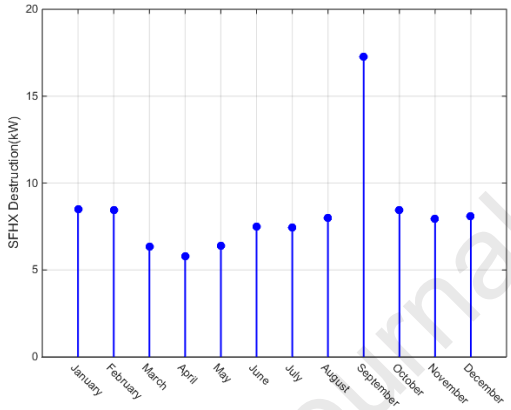

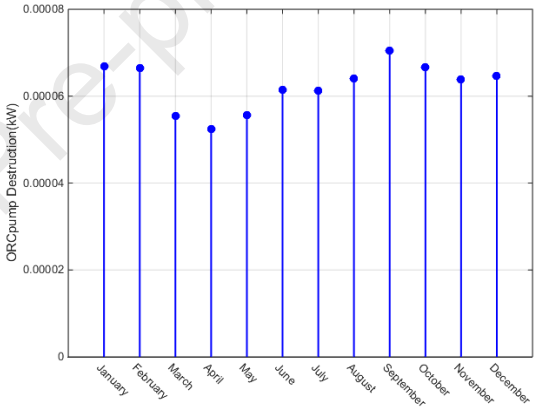

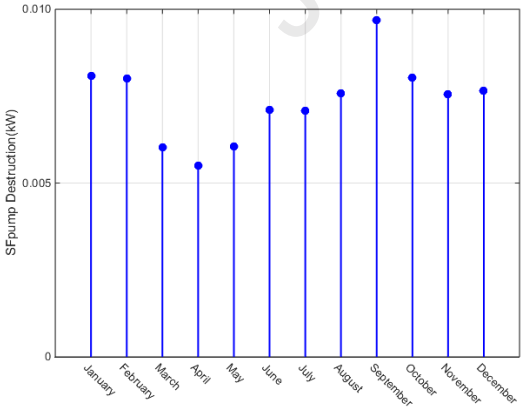

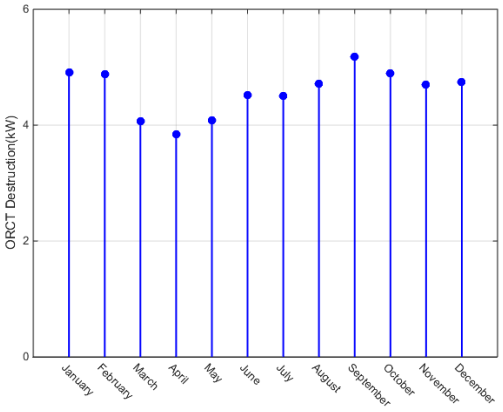

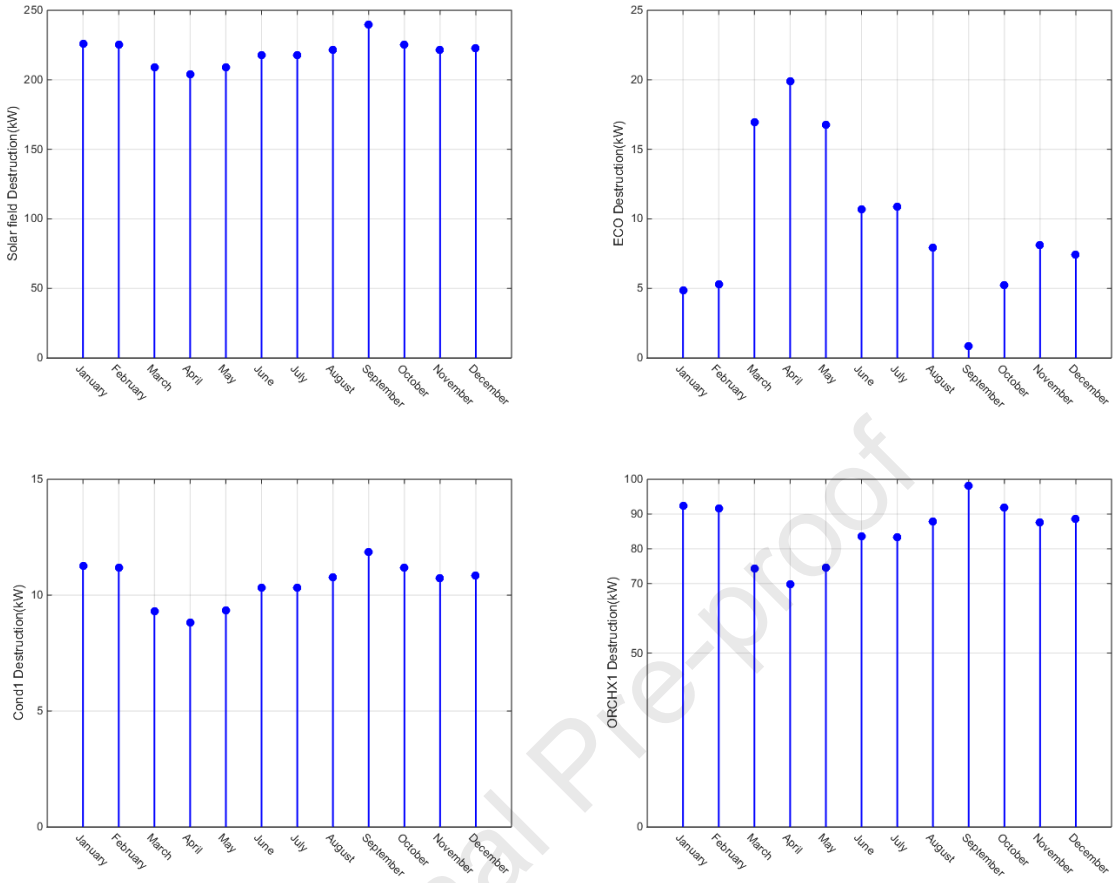

Fig. B.4. Monthly total exergy destruction of different equipment units of the integrated solar energy-driven polygeneration system.

B.4 Exergoeconomic Analysis

Table B.5

Exergoeconomic analysis results of the polygeneration system without the solar energy field.

Component	$\dot{C}_D$ (US$/h)	c_f (US$/GJ)	c_p (US$/GJ)	$\dot{Z}_k$ (US$/h)	$\dot{Z}_k + \dot{C}_D$	f_k (%)	r_k
AC	9.36	22.7	28.5	4.68	14.04	32.35	0.25
CC	37.8	11.6	17.1	2.88	40.68	7	0.48
GT	1.48	17	22.7	24.84	26.32	94.33	0.33
HPP	3×10^{-5}	0.18	0.57	0.072	0.07	99.95	2.22
SUP	3.02	17	25.4	0.49	3.51	14.04	0.49
EVA	4.68	17	23	0.5	5.18	9.68	0.34
ECO	2.77	17	31.2	0.49	3.26	15	0.82
ST 1	1.33	25	30.1	2.16	3.49	60.5	0.21
ST 2	0.33	25	32.2	0.68	1.01	68.46	0.29
ORCHX 2	2.9	25	236	10.44	13.86	93.41	2.54
ORCT 2	1.58	88.1	114.7	1.62	15.66	27.83	0.3
COND 2	4.32	88.1	309.6	0.07	3.2	0.63	2.51
ORCP 2	10^{-5}	30.7	32.7	0.002	0.002	99.75	0.06
ORCHX 1	1.51	17	598	30.6	32.11	99.03	33.96
ORCT 1	2.9	595.4	701.5	0.62	3.61	4.12	0.18
COND 1	6.84	595.4	2000	0.02	6.86	0.06	2.32
ORCP 1	1.91×10^{-7}	30.7	33.8	0.001	0.001	99.98	0.1
CO_2 Capture	14.04	24.5	704.8	112.32	126.36	88.7	27.89
Humidifier	0.03	25	37.9	0.01	0.04	26.58	0.52
Dehumidifier	0.02	31.2	41.23	0.0005	0.02	2.22	0.32

Table B.6

Exergoenvironmental analysis results of the polygeneration system integrated with the solar energy field.

Component	$\dot{C}_D$ (US$/h)	c_f (US$/GJ)	c_p (US$/GJ)	$\dot{Z}_k$ (US$/h)	$\dot{Z}_k + \dot{C}_D$	f_k (%)	r_k
AC	9.36	22.7	28.5	4.68	14.04	32.35	0.25
CC	37.8	11.6	17.1	2.88	40.68	7	0.48
GT	1.48	17	22.7	24.84	26.32	94.33	0.33
HPP	3×10^{-5}	0.18	0.57	0.072	0.07	99.95	2.22
SUP	3.02	17	25.4	0.49	3.51	14.59	0.49
EVA	4.32	17	20.3	0.5	4.82	10.48	0.18
ECO	0.648	17	44.08	0.5	1.148	43	1.57
ST 1	2.02	30.8	37.2	2.01	4.18	59.91	0.21

ST 2	0.5	30.8	39.3	0.68	1.18	58.23	0.29
ORCHX 2	3.6	30.8	101.8	4.88	8.48	92.8	2.3
ORCT 2	1.84	101.5	129.8	1.72	3.56	47.12	0.27
COND 2	5.04	101.5	356.1	0.08	5.12	1.44	2.51
ORCP 2	3×10^{-6}	37.2	39.3	0.002	0.002	99.69	0.06
ORCHX 1	5.04	17	305.6	46.4	41.04	96.81	16.85
ORCT 1	5.04	304.1	362.5	1.48	6.52	23.16	0.19
COND 1	6.84	304.1	1000	0.06	6.9	0.52	2.33
ORCP 1	1.91×10^{-7}	37.2	39.3	0.002	0.002	99.89	0.06
CO_2 Capture	15.82	27.4	717.7	112.32	128.14	87.6	25.23
Solar Field	0	0	23.1	5.04	5.04	100	-
SFHX	0.61	23.1	87.8	11.52	12.13	94.89	2.8
SFP	5.7×10^{-4}	22.7	1300	0.003	0.004	82.42	55.3
Humidifier	0.03	25	37.9	0.01	0.04	26.58	0.52
Dehumidifier	0.02	31.2	41.23	0.0005	0.02	2.22	0.32

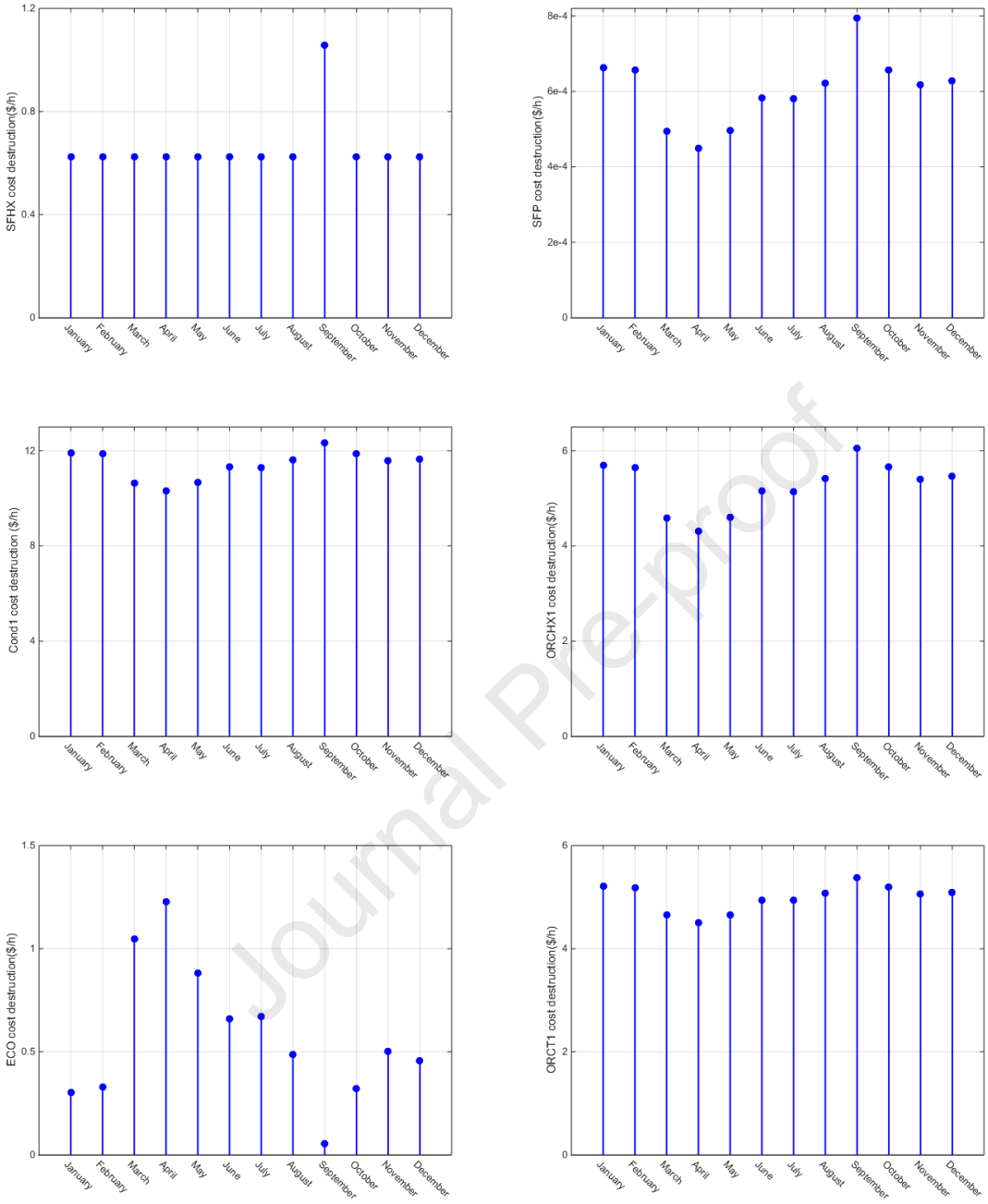

Fig. B.5. Monthly cost of exergy degradation for the different polygeneration system components.

B.5 Exergoenvironmental Analysis

Table B.7

Exergoenvironmental analysis results of the base polygeneration system without the solar energy field.

Component	$\dot{B}_D$ (mPts/h)	$\dot{Y}$ (mPts/h)	$\dot{Y}_k + \dot{B}_D$	b_f (mPts/GJ)	b_p (mPt/GJ)	f_b (%)	r_b
AC	2160	2.07	2162.07	5200	6100	0.1	0.17
CC	11556	10.4	11566.4	3500	5100	0.09	0.44
GT	432	18.4	450.4	5100	5200	3.94	0.02
HPP	1.684	0.003	1.687	9100	9900	0.19	0.09
SUP	900	9	909	5100	7300	0.98	0.42
EVA	1404	0.63	1404.63	5100	6700	0.05	0.31
ECO	836.6	0.31	836.91	5100	8800	0.04	0.71
ST 1	468	873.7	1341.7	7200	9100	69.78	0.3
ST 2	378.4	284.4	4206.4	7200	9900	75.77	0.37
ORCHX 2	837.7	24.48	862.18	7200	11300	2.82	0.57
ORCT 2	241.6	1.93	243.53	11300	12900	0.79	0.15
COND 2	569.2	0.023	569.223	11500	38300	0.004	2.32
ORCP 2	0.002	0.007	0.009	9100	31000	82.16	2.11
ORCHX 1	457.6	9.36	466.96	5100	13600	1.97	1.65
ORCT1	68.04	0.54	68.58	13500	15600	0.78	0.15
COND 1	155.8	0.02	155.82	13500	44900	0.01	2.32
ORCP 1	0.001	0.002	0.003	9300	9100	79	0.001
CO_2 Capture	3175.2	4335.8	7511	5500	50300	57.73	8.16
Humidifier	7.76	1.23×10^{-5}	7.76	7200	9900	1.59×10^{-4}	0.38
Dehumidifier	5.56	1.26×10^{-5}	5.56	8200	10700	2.27×10^{-4}	0.31

Table B.8

Exergoenvironmental analysis results of the polygeneration integrated with the solar energy field.

Component	$\dot{B}_D$ (mPts/h)	$\dot{Y}$ (mPts/h)	$\dot{Y}_k + \dot{B}_D$	b_f (mPts/GJ)	b_p (mPt/GJ)	f_b (%)	r_b
AC	2160	2.07	2162.07	5200	6100	0.1	0.17
CC	11556	10.4	11566.4	3500	5100	0.09	0.44
GT	432	18.4	450.4	5100	5200	3.94	0.02
HPP	1.684	0.003	1.687	9100	9900	0.19	0.09
SUP	900	9	909	5100	7300	0.98	0.42
EVA	1286.3	0.63	1286.93	5100	6100	0.05	0.19
ECO	197.3	0.31	197.61	5100	9700	0.16	0.89
ST 1	468	873.7	1341.7	5800	7600	69.25	0.32
ST 2	92.52	284.4	376.92	5800	8400	79.47	0.44

ORCHX 2	690.8	26	715.28	5800	9100	3.47	0.58
ORCT2	165.2	2	167.13	9100	10500	1.16	0.15
COND 2	456.8	0.023	456.823	9100	31800	0.005	2.47
ORCP 2	0.002	0.007	0.009	7600	7600	84.63	0.001
ORCHX 1	1545.1	20.9	1566	5100	13900	4.37	1.71
ORCT 1	225.4	1.73	227.13	13900	15900	0.76	0.15
COND 1	515.9	0.02	515.92	13900	45900	0.004	2.31
ORCP 1	0.001	0.007	0.008	7600	7600	93.77	0.001
CO_2 Capture	3780	4335.8	8115.8	6500	47400	53.41	6.3
Solar Field	0	0.55	0.55	0	0.003	100	-
SFHX	0.09	16.2	16.29	0.003	0.1	99.46	26.4
SFP	0.13	0.0001	0.1301	5200	56100	0.04	9.7
Humidifier	7.76	1.23×10^{-5}	7.76	7200	9900	1.59×10^{-4}	0.38
Dehumidifier	5.56	1.26×10^{-5}	5.56	8200	10700	2.27×10^{-4}	0.31

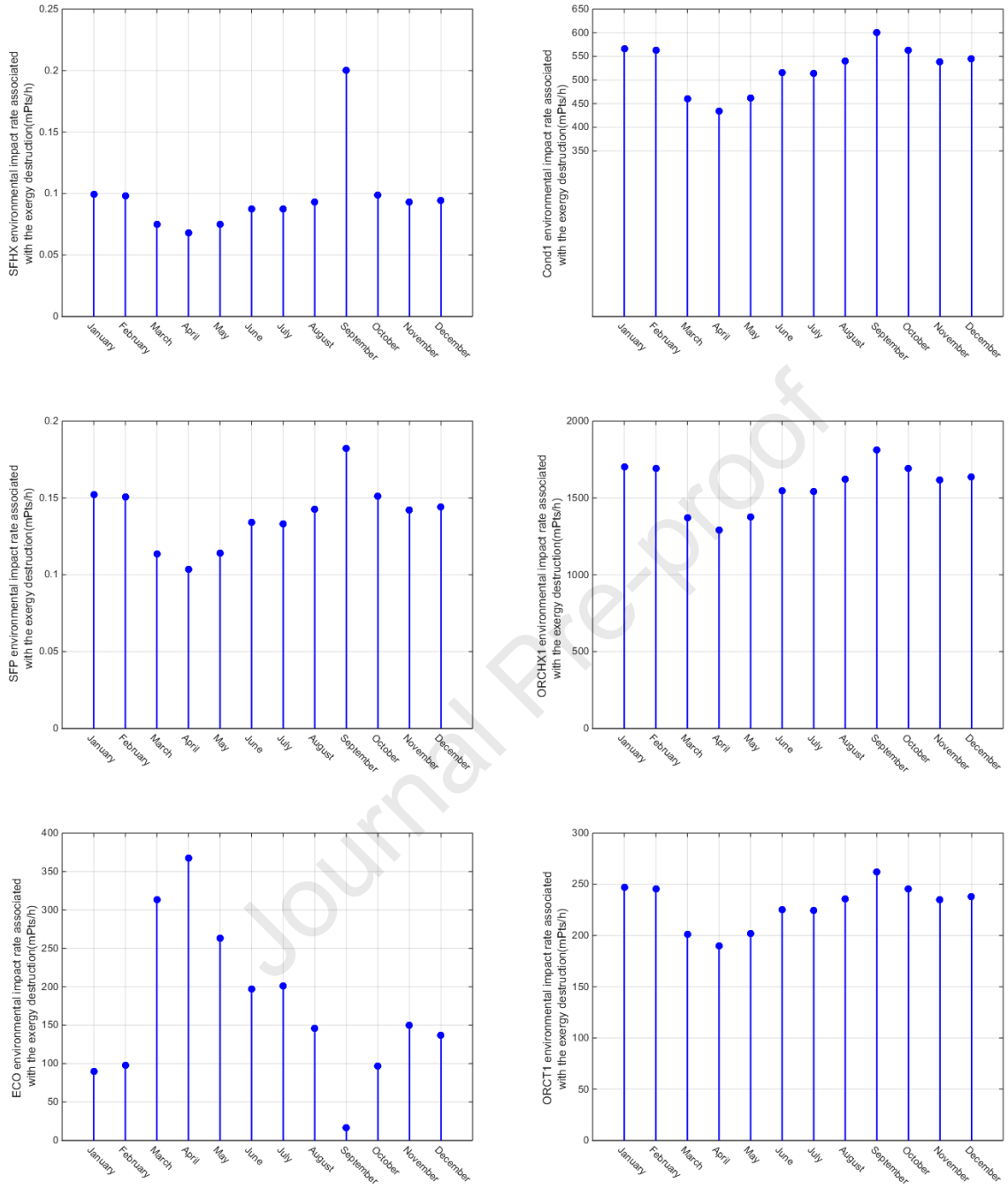

Fig. B.6. Monthly rate of destructive environmental impacts related to exergy destruction of different system components.

B.6 Emergoeconomic Analysis

Table B.9

Emergoeconomic analysis results of the based polygeneration system without the solar energy field.

Component	$\dot{M}_D$ (sej/h)	$\dot{U}$ (sej/h)	$\dot{M}_D + \dot{U}$	m_f (sej/kJ)	m_p (sej/kJ)	f_m (%)	r_m
AC	8.24×10^{12}	4.68×10^{12}	1.3×10^{13}	1.98×10^{7}	2.52×10^{7}	37.01	0.27
CC	3.03×10^{13}	3.03×10^{12}	3.34×10^{13}	9.33×10^{6}	1.39×10^{7}	9.1	0.49
GT	1.2×10^{11}	2.64×10^{13}	2.76×10^{13}	1.39×10^{7}	1.98×10^{7}	95.64	0.43
HPP	4.71×10^{9}	6.66×10^{10}	9.97×10^{10}	2.6×10^{7}	9.99×10^{7}	93.4	2.92
SUP	2.45×10^{12}	5.51×10^{11}	3×10^{12}	1.39×10^{7}	2.1×10^{7}	18.39	0.51
EVA	3.75×10^{12}	5.29×10^{11}	4.28×10^{12}	1.39×10^{7}	1.88×10^{7}	12.39	0.35
ECO	2.26×10^{12}	5.29×10^{11}	2.79×10^{12}	1.39×10^{7}	2.6×10^{7}	18.89	0.87
ST 1	1.08×10^{12}	2.16×10^{12}	3.24×10^{12}	2.05×10^{7}	2.6×10^{7}	66.59	0.24
ST 2	3.28×10^{11}	7.42×10^{11}	1.07×10^{12}	2.05×10^{7}	2.77×10^{7}	73.86	0.35
ORCHX 2	2.63×10^{12}	1.11×10^{13}	1.35×10^{13}	2.05×10^{7}	8.49×10^{7}	82.26	3.14
ORCT 2	1.5×10^{12}	1.37×10^{12}	3.24×10^{12}	8.46×10^{7}	1.11×10^{8}	53.39	0.31
COND 2	4.18×10^{12}	7.8×10^{10}	4.25×10^{12}	8.46×10^{7}	2.98×10^{8}	1.84	2.52
ORCP 2	5.15×10^{6}	2.47×10^{9}	2.33×10^{9}	2.6×10^{7}	2.77×10^{7}	98.8	0.09
ORCHX 1	1.24×10^{12}	3.28×10^{13}	3.4×10^{13}	1.39×10^{7}	6.29×10^{8}	96.36	44.3
ORCT 1	3.15×10^{12}	6.62×10^{11}	3.82×10^{12}	6.26×10^{8}	7.37×10^{8}	17.37	0.17
COND 1	7.2×10^{12}	1.96×10^{10}	7.24×10^{12}	6.25×10^{8}	2.08×10^{9}	0.27	2.32
ORCP 1	1.75×10^{6}	2.47×10^{9}	1.09×10^{9}	2.6×10^{7}	3.18×10^{8}	99.84	11.47
CO_2 Capture	1.17×10^{13}	1.2×10^{14}	1.32×10^{14}	2.02×10^{7}	7.31×10^{8}	91.16	35.32
Humidifier	7.39×10^{10}	1.04×10^{10}	8.43×10^{10}	2.05×10^{7}	3.19×10^{7}	32.09	0.56
Dehumidifier	2.21×10^{10}	5.14×10^{8}	2.26×10^{10}	2.63×10^{7}	3.48×10^{7}	2.80	0.32

Table B.10

Emergoeconomic analysis results of the polygeneration system integrated with the solar energy field.

Component	$\dot{M}_D$ (sej/h)	$\dot{U}$ (sej/h)	$\dot{M}_D + \dot{U}$	m_f (sej/kJ)	m_p (sej/kJ)	f_m (%)	r_m
AC	8.24×10^{12}	4.68×10^{12}	1.31×10^{13}	1.98×10^{7}	2.52×10^{7}	37.01	0.27
CC	3.03×10^{13}	3.03×10^{12}	6.06×10^{13}	9.33×10^{6}	1.39×10^{7}	9.1	0.49
GT	1.2×10^{11}	2.64×10^{13}	3.84×10^{13}	1.39×10^{7}	1.98×10^{7}	95.64	0.43
HPP	4.71×10^{9}	6.66×10^{10}	7.13×10^{10}	2.6×10^{7}	9.99×10^{7}	93.4	2.92
SUP	2.45×10^{12}	5.51×10^{11}	3×10^{12}	1.39×10^{7}	2.1×10^{7}	18.39	0.51
EVA	3.48×10^{12}	5.29×10^{11}	4.01×10^{12}	1.39×10^{7}	1.92×10^{7}	13.38	0.38
ECO	5.33×10^{12}	5.32×10^{11}	5.86×10^{12}	1.39×10^{7}	3.9×10^{7}	49.85	1.78
ST 1	1.56×10^{12}	2.16×10^{12}	3.72×10^{12}	2.96×10^{7}	3.53×10^{7}	66.59	0.19
ST 2	3.78×10^{11}	7.42×10^{11}	1.12×10^{12}	2.96×10^{7}	3.75×10^{7}	66.22	0.27
ORCHX 2	3.45×10^{12}	1.11×10^{13}	1.46×10^{13}	2.96×10^{7}	9.79×10^{7}	75.89	2.31

ORCT 2	1.74×10^{12}	1.37×10^{12}	3.11×10^{12}	9.76×10^{7}	1.26×10^{8}	49.84	0.28
COND 2	4.82×10^{12}	7.8×10^{10}	4.9×10^{12}	9.76×10^{7}	$3..43\times10^{8}$	1.6	2.51
ORCP 2	6.41×10^{6}	2.47×10^{9}	2.48×10^{9}	3.53×10^{7}	3.76×10^{7}	99.73	0.09
ORCHX 1	4.18×10^{12}	4.97×10^{13}	5.39×10^{13}	1.39×10^{7}	3.15×10^{8}	97.56	21.6
ORCT 1	5.11×10^{12}	1.6×10^{12}	6.71×10^{12}	3.13×10^{8}	3.74×10^{8}	23.83	0.19
COND 1	1.17×10^{13}	6.34×10^{10}	1.18×10^{13}	3.13×10^{8}	1.04×10^{9}	0.54	2.33
ORCP 1	7.8×10^{6}	2.33×10^{9}	2.34×10^{9}	3.53×10^{7}	3.76×10^{8}	99.66	0.06
CO_2 Capture	1.43×10^{13}	1.2×10^{14}	1.34×10^{14}	2.47×10^{7}	7.5×10^{8}	89.39	29.4
Solar Field	0	1.48×10^{9}	1.48×10^{9}	0	2.47×10^{7}	100	-
SFHX	6.7×10^{11}	1.24×10^{13}	1.31×10^{13}	2.48×10^{7}	9.4×10^{7}	94.89	2.8
SFP	5.08×10^{8}	2.9×10^{9}	3.41×10^{9}	1.98×10^{7}	1.32×10^{9}	85.21	65.7
Humidifier	7.39×10^{10}	1.04×10^{10}	8.43×10^{10}	2.05×10^{7}	3.19×10^{7}	32.09	0.56
Dehumidifier	2.21×10^{10}	5.14×10^{8}	2.26×10^{10}	2.63×10^{7}	3.48×10^{7}	2.80	0.32

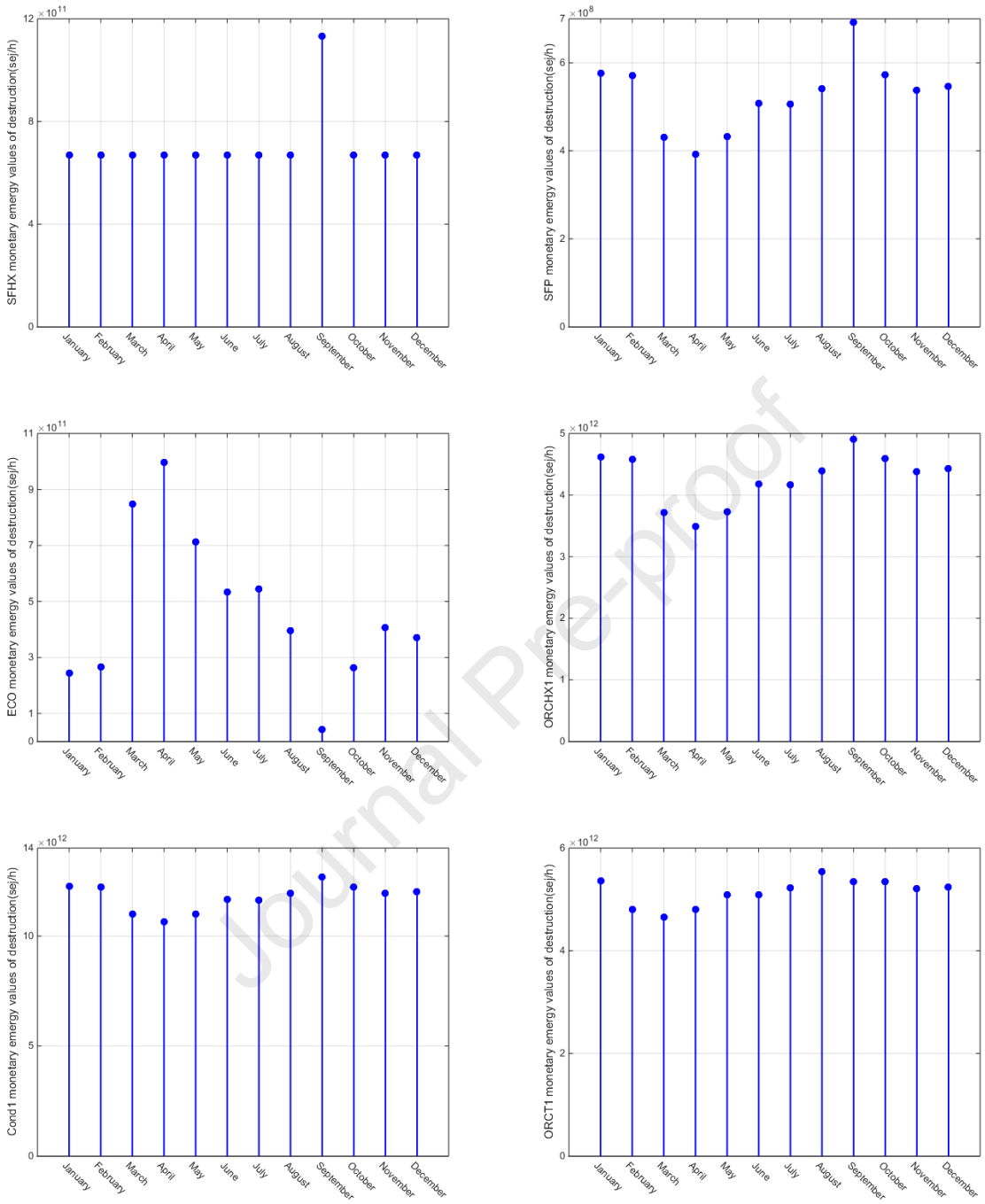

Fig. B.7. Economic emergy rate associated with exergy destruction for the different polygeneration system components.

B.7 Emergoenvironmental Analysis

Table B.11

Emergoenvironmental analysis results for the base polygeneration system without the solar energy field.

Component	$\dot{N}_D$ (sej/h)	$\dot{V}$ (sej/h)	$\dot{N}_D + \dot{V}_k$	n_f (sej/kJ)	n_p (sej/kJ)	f_n (%)	r_n
AC	3.18×10^{13}	2.46×10^{10}	3.18×10^{13}	7.62×10^{7}	8.92×10^{7}	0.07	0.17
CC	1.68×10^{14}	7.74×10^{10}	1.68×10^{14}	5.18×10^{7}	7.48×10^{7}	0.05	0.44
GT	6.48×10^{12}	2.01×10^{11}	6.5×10^{12}	7.48×10^{7}	7.62×10^{7}	3	0.02
HPP	2.37×10^{10}	1.4×10^{7}	2.37×10^{10}	1.31×10^{8}	1.39×10^{8}	0.06	0.09
SUP	1.32×10^{13}	9.86×10^{10}	1.33×10^{13}	7.48×10^{7}	1.06×10^{8}	0.74	0.42
EVA	2.02×10^{13}	1.66×10^{10}	2.02×10^{13}	7.48×10^{7}	9.78×10^{7}	0.08	0.31
ECO	1.22×10^{13}	8.21×10^{9}	1.22×10^{13}	7.48×10^{7}	1.28×10^{8}	0.07	0.7
ST 1	5.51×10^{12}	9.61×10^{12}	1.51×10^{13}	1.05×10^{8}	1.28×10^{8}	63.51	0.22
ST 2	1.34×10^{12}	3.16×10^{12}	4.5×10^{12}	1.05×10^{8}	1.37×10^{8}	70.21	0.31
ORCHX 2	1.21×10^{13}	6.34×10^{11}	1.27×10^{13}	1.05×10^{8}	1.66×10^{8}	4.94	0.59
ORCT 2	3.51×10^{11}	2.12×10^{10}	3.71×10^{11}	1.66×10^{8}	1.9×10^{8}	0.71	0.15
COND 2	8.17×10^{12}	5.98×10^{8}	8.17×10^{12}	1.66×10^{8}	5.76×10^{8}	0.01	2.47
ORCP 2	2.33×10^{7}	3.21×10^{7}	5.54×10^{7}	1.28×10^{8}	1.28×10^{8}	58	0.0004
ORCHX 1	6.7×10^{12}	2.4×10^{11}	6.94×10^{12}	7.48×10^{7}	2×10^{8}	3.47	1.67
ORCT 1	1.00×10^{12}	5.87×10^{9}	1.01×10^{12}	2×10^{8}	2.29×10^{8}	0.58	0.15
COND 1	2.29×10^{12}	5.18×10^{8}	2.29×10^{12}	2×10^{8}	6.61×10^{8}	0.02	2.32
ORCP 1	8.78×10^{6}	9.9×10^{6}	1.87×10^{7}	1.28×10^{8}	1.28×10^{8}	53	0.0004
CO_2 Capture	5.98×10^{13}	1.94×10^{13}	7.92×10^{13}	1.03×10^{8}	4.93×10^{8}	24.46	3.77
Humidifier	1.13×10^{11}	9.92×10^{3}	1.13×10^{11}	1.05×10^{8}	1.48×10^{8}	8.76×10^{-6}	0.38
Dehumidifier	8.18×10^{10}	1.01×10^{4}	8.18×10^{10}	1.2×10^{8}	1.58×10^{8}	1.24×10^{-5}	0.31

Table B.12

Emergoenvironmental analysis results for polygeneration system integrated with the solar energy field.

Component	$\dot{N}_D$ (sej/h)	$\dot{V}$ (sej/h)	$\dot{N}_D + \dot{V}_k$	n_f (sej/kJ)	n_p (sej/kJ)	f_n (%)	r_n
AC	3.18×10^{13}	2.46×10^{10}	3.18×10^{13}	7.62×10^{7}	8.92×10^{7}	0.07	0.17
CC	1.68×10^{14}	7.74×10^{10}	1.68×10^{14}	5.18×10^{7}	7.48×10^{7}	0.05	0.44
GT	6.48×10^{12}	2.01×10^{11}	6.5×10^{12}	7.48×10^{7}	7.62×10^{7}	3	0.02
HPP	2.37×10^{10}	1.4×10^{7}	2.37×10^{10}	1.31×10^{8}	1.39×10^{8}	0.06	0.09
SUP	1.32×10^{13}	9.86×10^{10}	1.33×10^{13}	7.48×10^{7}	1.06×10^{8}	0.74	0.42
EVA	2.02×10^{13}	1.66×10^{10}	2.02×10^{13}	7.48×10^{7}	8.9×10^{7}	0.09	0.19
ECO	2.88×10^{12}	8.21×10^{9}	2.89×10^{13}	7.48×10^{7}	1.42×10^{8}	0.28	0.9
ST 1	4.46×10^{12}	9.61×10^{12}	1.41×10^{13}	8.48×10^{7}	1.07×10^{8}	63.51	0.26
ST 2	1.08×10^{12}	3.16×10^{12}	4.24×10^{12}	8.48×10^{7}	1.15×10^{8}	74.43	0.36

ORCHX 2	9.9×10^{12}	6.34×10^{11}	1.05×10^{13}	8.48×10^{7}	1.35×10^{8}	6.03	0.59
ORCT 2	3.51×10^{11}	2.12×10^{10}	3.72×10^{11}	1.35×10^{8}	1.55×10^{8}	0.87	0.15
COND 2	6.66×10^{12}	5.98×10^{8}	6.66×10^{12}	1.35×10^{8}	4.68×10^{8}	0.01	2.47
ORCP 2	1.9×10^{7}	3.21×10^{7}	5.54×10^{7}	1.07×10^{8}	1.07×10^{8}	62.41	0.0005
ORCHX 1	2.25×10^{13}	5.47×10^{11}	2.3×10^{13}	7.48×10^{7}	2.04×10^{8}	7.56	1.73
ORCT 1	3.31×10^{12}	1.9×10^{10}	3.33×10^{12}	2.03×10^{8}	2.34×10^{8}	0.57	0.15
COND 1	7.56×10^{12}	5.83×10^{8}	7.56×10^{12}	2.03×10^{8}	6.74×10^{8}	0.01	2.31
ORCP 1	6.84×10^{6}	3.2×10^{7}	3.88×10^{7}	1.07×10^{8}	1.07×10^{8}	82.23	0.0003
CO_2 Capture	5.4×10^{13}	1.94×10^{13}	7.34×10^{13}	9.35×10^{7}	4.52×10^{8}	26.4	3.84
Solar Field	7.85×10^{8}	1.79×10^{10}	1.87×10^{10}	10^{3}	8.52×10^{4}	95.79	84.2
SFHX	2.57×10^{9}	4.21×10^{11}	4.24×10^{11}	9.52×10^{4}	2.34×10^{6}	99.39	23.54
SFP	1.95×10^{9}	2.13×10^{5}	1.95×10^{9}	7.62×10^{7}	8.18×10^{8}	0.0001	9.73
Humidifier	1.13×10^{11}	9.92×10^{3}	1.13×10^{11}	1.05×10^{8}	1.48×10^{8}	8.76×10^{-6}	0.38
Dehumidifier	8.18×10^{10}	1.01×10^{4}	8.18×10^{10}	1.2×10^{8}	1.58×10^{8}	1.24×10^{-5}	0.31

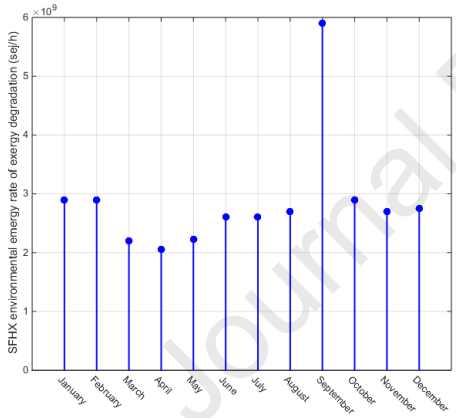

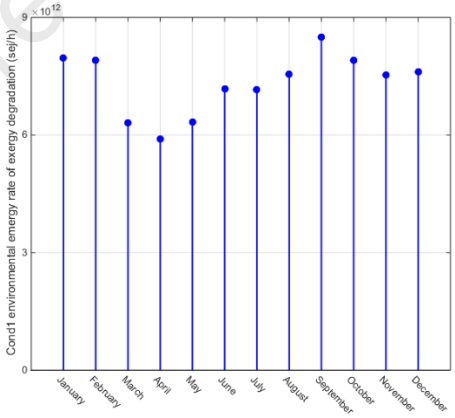

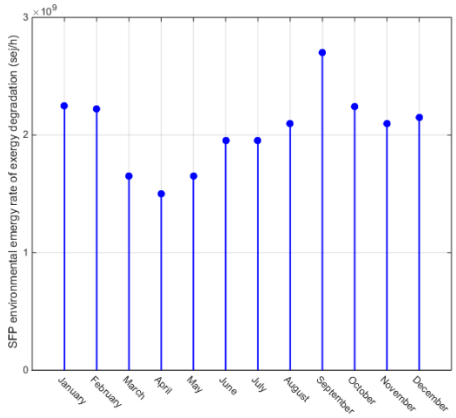

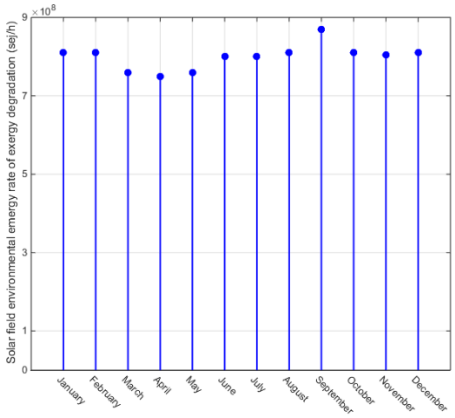

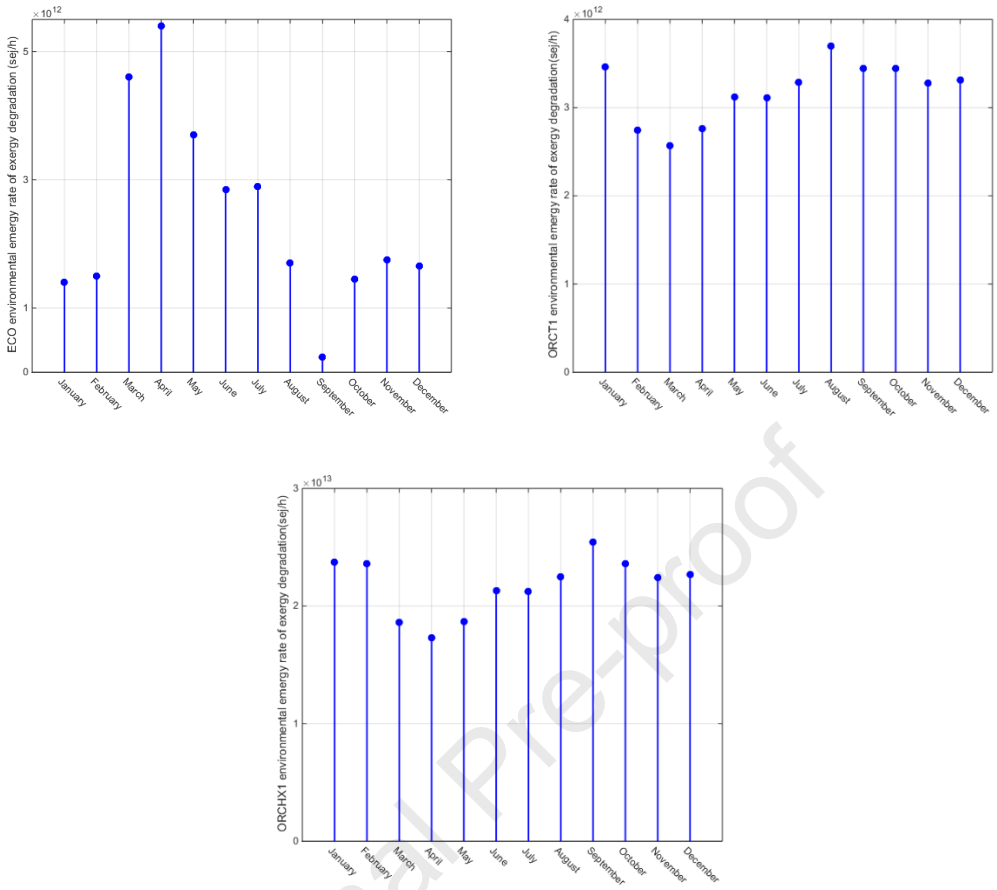

Fig. B.8. Monthly environmental emergy rate related to the exergy destruction of some dynamic system components.

References

Aghbashlo, M., Rosen, M.A., 2018. Consolidating exergoeconomic and exergoenvironmental analyses using the emergy concept for better understanding energy conversion systems. Journal of Cleaner Production 172, 696-708.

Anvari, S., Mahian, O., Taghavifar, H., Wongwises, S., Desideri, U., 2020. 4E analysis of a modified multigeneration system designed for power, heating/cooling, and water desalination. Applied Energy 270, 115107.

Ayati, E., Rahimi-Ahar, Z., Hatamipour, M.S., Ghalavand, Y., 2019. Water productivity enhancement in variable pressure humidification dehumidification (HDH) desalination systems using heat pump. Applied Thermal Engineering 160, 114114.

Bastianoni, S., Facchini, A., Susani, L., Tiezzi, E., 2007. Emergy as a function of exergy. Energy 32(7), 1158-1162.

Bejan, A., Tsatsaronis, G., Moran, M.J., 1995. Thermal design and optimization. John Wiley & Sons.

Botero, C., Finkenrath, M., Bartlett, M., Chu, R., Choi, G., Chinn, D., 2009. Redesign, optimization, and economic evaluation of a natural gas combined cycle with the best integrated technology CO2 capture. Energy Procedia 1(1), 3835-3842.

Cao, Y., Gao, Y., Zheng, Y., Dai, Y., 2016. Optimum design and thermodynamic analysis of a gas turbine and ORC combined cycle with recuperators. Energy Conversion and Management 116, 32-41.

Cavalcanti, E.J.C., 2017. Exergoeconomic and exergoenvironmental analyses of an integrated solar combined cycle system. Renewable and Sustainable Energy Reviews 67, 507-519.

Deniz, E., Çınar, S., 2016. Energy, exergy, economic and environmental (4E) analysis of a solar desalination system with humidification-dehumidification. Energy Conversion and Management 126, 12-19.

Dincer, I., Rosen, M.A., 2012. Exergy: energy, environment and sustainable development. Newnes.

Dincer, I., Rosen, M.A., Ahmadi, P., 2017. Optimization of energy systems. John Wiley & Sons.

Ehyaei, M., Baloochzadeh, S., Ahmadi, A., Abanades, S., 2021. Energy, exergy, economic, exergoenvironmental, and environmental analyses of a multigeneration system to produce electricity, cooling, potable water, hydrogen and sodium-hypochlorite. Desalination 501, 114902.

El-Emam, R.S., Dincer, I., 2018. Development and assessment of a novel solar heliostat-based multigeneration system. International Journal of Hydrogen Energy 43(5), 2610-2620.

Eslamimanesh, A., Hatamipour, M., 2010. Economical study of a small-scale direct contact humidification–dehumidification desalination plant. Desalination 250(1), 203-207.

Ghiasirad, H., Asgari, N., Saray, R.K., Mirmasoumi, S., 2021. Thermoeconomic assessment of a geothermal based combined cooling, heating, and power system, integrated with a humidification-dehumidification desalination unit and an absorption heat transformer. Energy Conversion and Management 235, 113969.

Gholizadeh, T., Vajdi, M., Rostamzadeh, H., 2020. Exergoeconomic optimization of a new trigeneration system driven by biogas for power, cooling, and freshwater production. Energy Conversion and Management 205, 112417.

Ghorbani, B., Javadi, Z., Zendehboudi, S., Amidpour, M., 2020a. Energy, exergy, and economic analyses of a new integrated system for generation of power and liquid fuels using liquefied natural gas regasification and solar collectors. Energy Conversion and Management 219, 112915.

Ghorbani, B., Mehrpooya, M., Sadeghzadeh, M., 2020b. Process development of a solar-assisted multi-production plant: Power, cooling, and hydrogen. International Journal of Hydrogen Energy 45(55), 30056-30079.

Jadidi, E., Khoshgoftar Manesh, M.H., Delpisheh, M., Onishi, V.C., 2021. Advanced exergy, exergoeconomic, and exergoenvironmental analyses of integrated solar-assisted gasification cycle for producing power and steam from heavy refinery fuels. Energies 14(24), 8409.
Kabiri, S., Manesh, M.K., Yazdi, M., Amidpour, M., 2020. Dynamic and economical procedure for solar parallel feedwater heating repowering of steam power plants. Applied Thermal Engineering 181, 115970.
Khoshgoftar Manesh, M.H., Onishi, V.C., 2021. Energy, Exergy, and Thermo-Economic Analysis of Renewable Energy-Driven Polygeneration Systems for Sustainable Desalination. Processes 9(2), 210.
Lazzaretto, A., Tsatsaronis, G., 2006. SPECO: a systematic and general methodology for calculating efficiencies and costs in thermal systems. Energy 31(8-9), 1257-1289.
Liu, X., Yang, X., Yu, M., Zhang, W., Wang, Y., Cui, P., Zhu, Z., Ma, Y., Gao, J., 2020. Energy, exergy, economic and environmental (4E) analysis of an integrated process combining CO2 capture and storage, an organic Rankine cycle and an absorption refrigeration cycle. Energy Conversion and Management 210, 112738.
Lozano, M., Valero, A., 1993. Theory of the exergetic cost. Energy 18(9), 939-960.
Lüpfert, E., Zarza, E., Geyer, M., Nava, P., Langenkamp, J., Schiel, W., Esteban, A., Osuna, R., Mandelberg, E., 2003. Euro Trough collector qualification complete-performance test results from PSA, ISES Solar World Congress 2001 & 2003 Proceedings.
Manesh, M.H.K., Amidpour, M., 2020. Cogeneration and Polygeneration Systems. Academic Press.
Manesh, M.K., Firouzi, P., Kabiri, S., Blanco-Marigorta, A., 2021a. Evaluation of power and freshwater production based on integrated gas turbine, S-CO2, and ORC cycles with RO desalination unit. Energy Conversion and Management 228, 113607.
Manesh, M.K., Firouzi, P., Kabiri, S., Blanco-Marigorta, A.M., 2021b. Evaluation of power and freshwater production based on integrated gas turbine, S-CO2, and ORC cycles with RO desalination unit. Energy Conversion and Management 228, 113607.
Méndez, C., Bicer, Y., 2021. Integrated system based on solar chimney and wind energy for hybrid desalination via reverse osmosis and multi-stage flash with brine recovery. Sustainable Energy Technologies and Assessments 44, 101080.
Meyer, L., Tsatsaronis, G., Buchgeister, J., Schebek, L., 2009. Exergoenvironmental analysis for evaluation of the environmental impact of energy conversion systems. Energy 34(1), 75-89.
Miyoshi, Y., Hidaka, K., Okayasu, T., Yasutake, D., Kitano, M., 2017. Effects of local CO2 enrichment on strawberry cultivation during the winter season. Environmental Control in Biology 55(4), 165-170.
Modabber, H.V., Manesh, M.H.K., 2021. Optimal exergetic, exergoeconomic and exergoenvironmental design of polygeneration system based on gas Turbine-Absorption Chiller-Solar parabolic trough collector units integrated with multi-effect desalination-thermal vapor compressor-reverse osmosis desalination systems. Renewable Energy 165, 533-552.
Mouaky, A., Rachek, A., 2020. Thermodynamic and thermo-economic assessment of a hybrid solar/biomass polygeneration system under the semi-arid climate conditions. Renewable Energy 156, 14-30.
Nami, H., Ertesvåg, I.S., Agromayor, R., Riboldi, L., Nord, L.O., 2018. Gas turbine exhaust gas heat recovery by organic Rankine cycles (ORC) for offshore combined heat and power applications-Energy and exergy analysis. Energy 165, 1060-1071.
Nouri, M., Miansari, M., Ghorbani, B., 2020. Exergy and economic analyses of a novel hybrid structure for simultaneous production of liquid hydrogen and carbon dioxide using photovoltaic and electrolyzer systems. Journal of cleaner production 259, 120862.
Nourpour, M., Khoshgoftar Manesh, M.H., 2021. Modeling and 6E analysis of a novel quadruple combined cycle with turbocompressor gas station. Journal of Thermal Analysis and Calorimetry 147, 5165–5197.
Olaleye, A.K., Wang, M., 2017. Conventional and advanced exergy analysis of post-combustion CO2 capture based on chemical absorption integrated with supercritical coal-fired power plant. International Journal of Greenhouse Gas Control 64, 246-256.

Patiño, G.G.E., Rivera, F.N., 2019. Global warming potential and net power output analysis of natural gas combined cycle power plants coupled with CO2 capture systems and organic Rankine cycles. Journal of Cleaner Production 208, 11-18.
Petrakopoulou, F., 2011. Comparative evaluation of power plants with CO2 capture: thermodynamic, economic and environmental performance.
Petrakopoulou, F., Tsatsaronis, G., Boyano, A., Morosuk, T., 2012a. Post-combustion CO2 capture with monoethanolamine in a combined-cycle power plant: exergetic, economic and environmental assessment, Greenhouse Gases–Emission, Measurement and Management. InTech–Open Access Company.
Petrakopoulou, F., Tsatsaronis, G., Morosuk, T., Paitazoglou, C., 2012b. Environmental evaluation of a power plant using conventional and advanced exergy-based methods. Energy 45(1), 23-30.
Rubin, E.S., Davison, J.E., Herzog, H.J., 2015. The cost of CO2 capture and storage. International Journal of Greenhouse gas control 40, 378-400.
Smith, R., 2005. Chemical process: design and integration. John Wiley & Sons.
Sun, W., Yue, X., Wang, Y., 2017. Exergy efficiency analysis of ORC (Organic Rankine Cycle) and ORC-based combined cycles driven by low-temperature waste heat. Energy Conversion and Management 135, 63-73.
Tukenmez, N., Koc, M., Ozturk, M., 2021. A novel combined biomass and solar energy conversion-based multigeneration system with hydrogen and ammonia generation. International Journal of Hydrogen Energy 46(30), 16319-16343.
Tzivanidis, C., Bellos, E., Antonopoulos, K.A., 2016. Energetic and financial investigation of a stand-alone solar-thermal Organic Rankine Cycle power plant. Energy conversion and management 126, 421-433.
Zamen, M., Amidpour, M., 2013. Modeling of Humidification and Dehumidification Process and design of HD desalinator for production of fresh water in greenhouse and analysis of the combined system.
Zamen, M., Amidpour, M., Firoozjaei, M.R., 2013. A novel integrated system for fresh water production in greenhouse: Dynamic simulation. Desalination 322, 52-59.
Zubair, M.I., Al-Sulaiman, F.A., Antar, M., Al-Dini, S.A., Ibrahim, N.I., 2017. Performance and cost assessment of solar driven humidification dehumidification desalination system. Energy Conversion and Management 132, 28-39.

HIGHLIGHTS

- New solar-driven polygeneration system coupling ORC, CO_2 capture and HDH desalination
- Dynamic simulations of polygeneration system for producing power, freshwater and CO_2
- Comprehensive 6E analyses performed for scenarios with/without the solar energy field
- New system weight functions developed for enhancing environmental impact assessment
- Solar energy integration improves power generation, energy and exergy efficiencies

Declaration of interests

☒ The authors declare that they have no known competing financial interests or personal relationships that could have appeared to influence the work reported in this paper.

☐The authors declare the following financial interests/personal relationships which may be considered as potential competing interests: